Ole Martin Brende

Reverberation suppression with dual band imaging in medical ultrasound

Doctoral thesis
for the degree of Philosophiae Doctor

Trondheim, June 2016

Norwegian University of Science and Technology
Faculty of Medicine
Department of Circulation and Medical Imaging

NTNU
Innovation and Creativity

NTNU

Norwegian University of Science and Technology

Doctoral thesis
for the degree of Philosophiae Doctor

Faculty of Medicine
Department of Circulation and Medical Imaging

ISBN 978-82-326-1726-5 (printed version)
ISBN 978-82-326-1727-2 (electronic version)
ISSN 1503-8181

Doctoral theses at NTNU, 2016:194

Printed by NTNU-trykk

Undertrykkelse av reverberasjonsstøy med to-frekvent medisinsk ultralyd

Ultralyd er en velkjent og velbrukt metode for avbildning i medisin. Det er mange grunner til dette. Ultralydutstyr er billig å kjøpe og bruke, det går raskt å samle inn bilder og billedraten er høy. Det er veldig sikkert for pasient og lege, og utstyret som trengs tar relativt lite plass. Men, ultralyd er ikke like enkelt å bruke på alle typer pasienter. I noen tilfeller vil multiple refleksjoner av lydbølgen skape støy i bildet. Dette, enten diffuse eller markante støyet, kan gjøre det vanskelig å stille en diagnose basert på bildene.

I arbeidet som er presentert i denne avhandlingen har målet vært å redusere denne støyen slik at bildet får bedre kontrastforhold og det blir lettere å bruke bildene til å stille en diagnose. For å gjøre dette har kandidaten sett på to-frekvent ultralyd hvor det i tillegg til den konvensjonelle høyfrekvente ultralydbølgen (HF) sendes en lavfrekvent bølge (LF). Frekvensforholdet mellom HF og LF er en faktor 10, og HF bølgen er enten på toppen eller bunnen av LF bølgen. Den lavfrekvente bølgen endrer så bølgehastigheten i mediet som observert av bildepulsen (HF). Denne endringen er avhengig av posisjonen til HF på LF. Hovedpoenget er at måten LF bølgen påvirker HF bølgen på er forskjellig for det "ekte" signalet og støysignalet. Ved å estimere tidsforsinkelsen som kommer ut av endret bølgehastighet er målet å separere det ekte signalet fra støysignalet og undertrykke støyen. Denne metoden kalles forsinkelse korrigert subtraksjon (delay corrected subtraction, DCS) og hele prosesseringen kalles også for SURF avbildning.

Den første artikkelen i avhandlingen beskriver de underliggende fenomenene som gir støy i ulineær bølgeforplantning når både en HF og en LF bølge benyttes. Artikkelen diskuterer også hva som vil være beste tilfellet for støyundertrykkelse, mulige hindringer og kvantisering av disse. Den andre artikkelen ser på hvordan tidsforsinkelsen til støysignalet kan estimeres. Den nye estimeringsmetoden som er presentert her viser å gi en bedre undertrykkelse av støyen enn fra tidligere metoder. Også inkludert i avhandlingen er en diskusjon på hvordan tidsforsinkelsen til det ekte signalet kan estimeres, samt hvordan en kan bruke SURF for å avbilde ulineære spredere.

Abstract

Ultrasound for medical imaging is in widespread use. The reasons for this are many and include the possibility of lightweight instruments, low cost, fast acquisition times, high safety and ease of use to both the operator and the patient. However, ultrasound is not as easy to use on all patients. In some cases multiple scattering of the ultrasound wave can result in reverberation noise in the image. This noise can be diffuse or a direct replica of another structure in the tissue. The common factor is that the noise makes images more difficult to use for diagnosing the patient.

In this work the main goal has been to understand and counter this multiple scattering, or reverberation, noise in order to make clearer images with better contrast ratio than in conventional ultrasound imaging. Here, dual band imaging (DBI) was utilized, where, in addition to a conventional high frequency imaging pulse (HF), a low frequency manipulation pulse (LF) has been added to the transmitted wave. To do this the candidate has utilized dual band imaging (DBI), where, in addition to a conventional high frequency imaging pulse (HF), a low frequency manipulation pulse (LF) has been added to the transmitted wave. The pulses are separated by a factor 10 in frequency and the HF imaging pulse is positioned on either a crest or a trough of the LF wave. This positioning alters the observed propagation delay of the HF and creates nonlinear propagation delays between the different acquired signals. The main idea is that this nonlinear propagation delay is different for the first order (true) signal and the reverberation noise. By estimating the nonlinear propagation delays the aim is to suppress the reverberations trough a method called delay corrected subtraction (DCS). The combination of DBI and DCS processing is commonly referred to as SURF processing.

The first paper included in this thesis discusses the underlying physics of the problem and analyses the best case scenario possible for SURF processing. Various obstacles for reverberation suppression are presented and quantized. The second paper presents a method to adaptively estimate the nonlinear propagation delay of the reverberation components which shows to give better suppression of the reverberation noise compared to earlier methods. Also included in this thesis is a discussion on estimation of the first order delay and an initial study of using SURF processing for detection of nonlinear scatterers.

Preface

This thesis is submitted in partial fulfillment of the requirements for the degree of *Philosophiae Doctor* (Ph.D.) at the Faculty of Medicine at the Norwegian University of Science and technology (NTNU). The work was funded through an SO (Strategisk Omsetningsmidler) scholarship from NTNU, and was carried out at the Department of Circulation and Medical Imaging. The main supervisor was Professor Bjørn A. J. Angelsen from the same department.

Acknowledgements

I would not have been able to complete this thesis without the guidance and help of others. Firstly I want to thank my main supervisor Bjørn A. J. Angelsen. He always saw opportunities where I saw problems. Quotes such as "When you get something you don't understand you have the opportunity to understand something new!" represents his positive attitude. I would also like to thank the SURF research group as a whole. I have felt included in a group of people where each has contributed to a good work environment. First of these I would like to thank Johannes Kvam. We started working with Bjørn around the same time and have shared our ups and downs. Johannes has helped me with the key pulse simulations I have used. I would also like to thank Ola Finneng Myhre. I always left our conversations with a deeper and clearer knowledge of the subjects we discussed than when we started. Previous Master student Tollef Jahren also deserves my thanks. His hard work on our shared problems not only increased my understanding but also motivated me to work just as hard as he did. In addition to the SURF group I would also like to thank Professor Anne C. Elster for including me in the High Performance Computing group, and supplying me with hardware to run simulations on.

Lastly a big thanks to friends and family for their interest in my work and supporting me when my motivation was low.

Contents

Abbreviations and variables

Abbreviations

DBI	Dual Band Imaging.
DCS	Delay Corrected Subtraction.
HF	High Frequency (pulse).
LF	Low Frequency (wave).
ND	Noise Distortion (reverberations), $L(\omega)$.
NPD	Nonlinear Propagation Delay.
NSD	Nonlinear Self Distortion.
TGC	Time Gain Compensation.
THI	Tissue Harmonic Imaging.
PFD	Pulse Form Distortion, $V(\omega)$.
PI	Pulse Inversion.
SRR	Signal to Reverberation noise Ratio.

Variables

Nonlinear propagation delays (NPDs, τ) are listed in another table.

β_{n}	Nonlinearity parameter of medium.
κ	Compressibility of medium.
$L(\omega)$	Reverberation filter.*
$\widetilde{L}(\omega)$	Noise Distortion (reverberations).*
$N(\omega)$, $n(t)$	Reverberation signal.*
ν	Gradient of linear NPD, $\tau_{\mathrm{x}}(z) = \nu z$.
p	LF-wave configuration (polarity).
$V(\omega)$	First order signal filter.*
$\widetilde{V}(\omega)$	Pulse Form Distortion.*
$X(\omega)$, $x(t)$	First order signal.*
$Y(\omega)$, $y(t)$	Total signal.*

*Additional Subscripts exist. See other table.

NPDs, τ

Delays are defined between a non-zero polarity signal and the zero-polarity signal. Delays are between corresponding components of the two signals. Superscripts are Y and subscripts are Z, such that the final notation is $\tau_{\mathrm{Z}}^{\mathrm{Y}}$. Additional subscripts are listed in the table below this.

Z	Y	Description
n		Reverberation (component) delay.
n	e$\langle\rangle$	Mean phasor reverberation delay. Equation (2.65)
n	$\langle\rangle$	Arithmetic mean reverberation delay. Equation (2.66)
n	h	Fixed-relation reverberation delay. Equation (B.10)
n	hv	Half value reverberation delay. Equation (2.67)
n	RR	Adaptive reverberation delay. Equation (B.16)
x		First order (component) delay.
y		Total signal delay.

Subscripts

$+$	Positive polarity of the LF pulse, $p = 1$.
$-$	Negative polarity of the LF pulse, $p = -1$.
i	The variable/filter is constant within an interval, i.
p	Polarity of the LF pulse.

Word usage

Unless explicitly stated the word “noise” is used for *reverberation* noise. The total received signal consists of two components (or sometimes referred to as signals), the first order and reverberation component. Unless explicitly stated the word “signal” is reserved for the total signal. The dual band imaging method utilizes multiple transmits of combinations of high frequency (HF) and low frequency (LF) pulses. A combination of one HF and one LF transmitted simultaneously is called a pulse complex. The structure of the LF pulse is referred to as the “polarity”. The polarity is defined as a number and generally takes any real value. In this work the polarity is limited to three values, $+1$, 0, or -1. These three polarities are referred to as the “plus”, “zero”, and “minus” polarity. Using this, a “zero polarity signal” is the combined received first order and reverberation signals of a transmitted pulse complex where the LF polarity is zero. A zero polarity LF is defined to be equivalent to no LF. A “zero polarity signal” therefore corresponds to a received total signal from transmit of only the HF pulse. Note that in paper A the LF component is referred to as a “wave” instead of a pulse.

The reverberation component of the total signal consists of many pairs. A reverberation pair consists of a CIa and a CIb (defined later) component.

Nonlinear propagation delays, or often simply “delays”, define the delay of a signal component to it’s corresponding component in the zero-polarity-signal. The terms “first order delay”, “reverberation/noise delay”, and “total delay” are used to refer to the delays of the first order, reverberation, and total signal components respectively.

Part I

Thesis

Introduction

I expect that everyone doing a PhD at one point or another has had to explain to friends and family what it is they “do”. I also expect that more often than not it was difficult to explain in a non-technical manner what the core idea of their PhD was. The solution might not be to hand out a copy of a recent paper, but rather to give a softer introduction to the work. Such a softer introduction is the goal of this chapter, where, in addition to explaining core ultrasound concepts, the extension towards dual band imaging is made. An overview of the included articles and additional chapters is given, and the main results are discussed.

1.1 Conventional medical ultrasound

Ultrasound is sound waves with frequencies above the upper limit of human hearing at 20 kHz. Ultrasound imaging is the process of emitting such sound waves and utilizing the received signals to generate an image of the scattering medium based on certain assumptions of the underlying physics. Typically the transmit and receive system is located at the same position, and in most conventional systems the same system is used for both transmit and receive. This system is referred to as the *transducer*. The three main assumptions used to create an image of the received sound is:

(1) the emitted sound field is only scattered once before it returns to the transducer,
(2) the speed of sound, c_0, is constant, and
(3) the sound waves only travel straight ahead from the transducer hitting scatterers on a straight line.

Under these assumptions the transmission of one sound pulse can be used to determine the distance to a set of scatterers from the transducer. But first, what is a scatterer? A scatterer, or *reflector*, is not a physical entity but rather a change in the material where the sound wave propagates. The interface determined by this change is called a scatterer. For sound waves a change in the density or compressibility of the medium causes a fraction of the incoming wave to be reflected back. The amount of energy reflected is determined by this relative change. By transmitting an ultrasound pulse into a heterogeneous medium, the medium will reflect back pulses at each interface where the density changes. Knowing the mean propagation velocity, c_0, of the medium and keeping in line with assumptions (1) and (2), one can calculate the depth of the interfaces through

$$z = \frac{c_0 t}{2}, \tag{1.1}$$

where t is the time between transmit of the pulse and the receive of a reflected pulse. The intensity of the received pulse gives information about the relative change in the density of the medium, referred to as the strength of a scatterer. The result is what is called an M-mode image. Which, following assumption (3) is a one dimensional image of the structure on a straight line from the transducer. To generate a full 2D image the transducer (or start pulse) can be moved mechanically (or electronically) to sweep over an area and the line images from each position can be combined. It is also possible to sweep in two dimensions to generate a 3D image.

The direct use of the received signal strength as a measure of scatterer strength is not completely accurate. As a wave propagates some of the energy is absorbed and lost due to non-adiabatic contraction and expansion of the medium.[1] Diffraction of the sound field also causes energy to travel out to the sides and not just straight forward. The spread of the wave in addition to absorption in the medium leads to an attenuation of the wave with depth. In biological soft tissue the absorption is in the order of 0.5 dB/MHz per centimeter of propagation.[1, p. 1.24] Note the frequency dependence of the resulting attenuation. Higher frequency waves are attenuated more than lower frequency waves. A fourth assumption of no attenuation is not included above as the attenuation can be compensated for by a priori knowledge of the mean attenuation of the medium at hand. This depth variable attenuation correction is referred to as Time Gain Compensation (TGC).

Higher attenuation for higher frequencies seems to favor the lower frequencies. But as the name of the technology indicates, *ultrasound* is the use of relatively high frequencies. So why use high frequencies? A useful analogy is to think of the transmitted pulse as the “brush” used to paint the image of the structure one want to study. By having a smaller brush, corresponding to transmission of a higher frequency and shorter pulse, one can paint a finer image. There is therefore a trade-off between imaging depth and imaging resolution. Frequencies used in medical ultrasound typically vary from 1 to 15 MHz, depending on the needed imaging depth. To image deep organs and the hearth in adults typical frequencies are between 2.5 and 5 MHz. Imaging of e.g. the common carotid artery (in the neck) needs lower penetration and a higher frequency can be used. Typically around 8 MHz. It is also possible with imaging directly inside blood vessels, or otherwise during operation. Here, frequencies up to 40 MHz has been used.[1, p. 1.6]

1.1.1 Breakdown of the general assumptions

There is a reason for why the three assumptions in the previous section are called just that, and not physical laws. They are wrong. Material dependent propagation velocity leads to a breakdown of assumption (2) and when the propagation velocity varies laterally over the wave field the result is a distortion of the received pulse. This effect is called aberration. Change in the propagation velocity with depth results in a stretching of the resulting image compared to the real medium. The width of the wave field, or ultrasound beam, as well as the presence of side lobes creates received pulses from scatterers on the sides of the direction the pulse was sent out. This breaks assumption (3).

The main goal of the work in this thesis is to combat the destructive effects resulting from the breakdown of assumption (1). As described above, changes in the density of the medium will split an incoming pulse into one forward- and one backward propagating pulse. Thus, a reflected pulse will work as an incoming one on another interface and be split again. For soft tissue interfaces the change in density is relatively small and only a small fraction of the pulse is reflected. Thus, pulses only reflected once before their return to the transducer, denoted the first order component (or first order *signal*), has an overall higher amplitude than signals created by multiple scatterings in the medium. The signal generated by multiple reflections of the pulse is called the reverberation component (or reverberation *signal*). The amplitude and time of arrival of the reverberation component cannot be directly related to structures in the medium through Eq. (1.1), and this component of the received signal is therefore referred to as noise. The extra propagation path caused by the change in propagation direction causes the signal to arrive back to the transducer at a later time than the first order component originating from the same set of scatterers. In low echogenic areas, meaning that the change in density is low, the first order component will be low. However, as the reverberation component is created by scatterers at shallower depths this signal component can give signal in this low echogenic area and the reverberation noise can be dominant.

1.1.2 Nonlinear effects and nonlinear imaging methods

Linear models are seen throughout physics. Linearization of the underlying physics typically leads to a simpler mathematical solution and can, within a certain range of the given variables, yield accurate results. However, linearization is often just a useful tool rather than an accurate representation of the real phenomena. This is also the case in wave physics. A nonlinear relation between an applied pressure and the resulting displacement of the medium yields a pressure, and material, dependent propagation speed. It can be shown through derivation of the wave equation[2] that a more precise second order propagation speed can be given as

$$c_1 = \frac{c_0}{1 - \beta_n \kappa p} \approx c_0(1 + \beta_n \kappa p). \tag{1.2}$$

Here, κ is the compressibility of the medium and β_n is the nonlinearity parameter which relates the adiabatic volume compression, δV of a small volume ΔV through $\delta V/\Delta V = (1 - \beta_n \kappa p)\kappa p$. (See also paper A.)

The pressure dependent propagation speed makes the crests propagate faster than the troughs of a wave. The result is generation of higher order frequency components, harmonics, and a distortion of the pulse. Loss of energy from the main frequency band of the pulse due to this nonlinear propagation is called nonlinear attenuation. Note also that as the attenuation increases with frequency, the generation of harmonics results in overall less wave energy and more dissipation in the medium.

Another source for nonlinearity in the received signal is nonlinear scatterers. Microbubbles is a prime example of a nonlinear scatterer.[3] As the detection of microbubbles can be advantageous in medicine, ultrasound imaging modalities have been developed to image such nonlinear scatterers. A main example is Tissue Harmonic Imaging (THI). In THI the received signal is filtered around the second harmonic component. The result is an image of the nonlinear propagation and scattering effects of the medium.[4] Another well known method is Pulse Inversion (PI).[5, 6] In PI two pulses are transmitted where one is the inverse of the other. By summing the received signals the even harmonic components add up and all other cancel out.

A key point ties nonlinear propagation to reverberations, the drop in amplitude after scattering. Often referred to as the Born approximation this assumption is used to exclude reverberations from the theory (assumption (3)). Taking the model up to the second order, both in regards to multiple scatterings of the wave and second order propagation, the Born approximation can be used to tie the nonlinearity of a wave to the position of the first scattering event. After the first scattering the amplitude of the returning wave drops so much that nonlinear effects of further propagation can be neglected. The nonlinear properties of the wave then contains information of the depth of the first scattering event. This can be used to suppress the reverberation component of the total signal.

As the first order component is the part of the signal at a given depth that has the longest propagation before the first scattering, this signal component will have the highest influence of nonlinear propagation and will be favored by THI. THI is thus a method not only for imaging of nonlinear scatterers but also a method for suppressing reverberation noise.[7] However, as shall be evident in Sec. 1.3 this only works for one part of the reverberation noise. To suppress more of the reverberation noise Dual Band Imaging (DBI) is needed.[8, paper D]

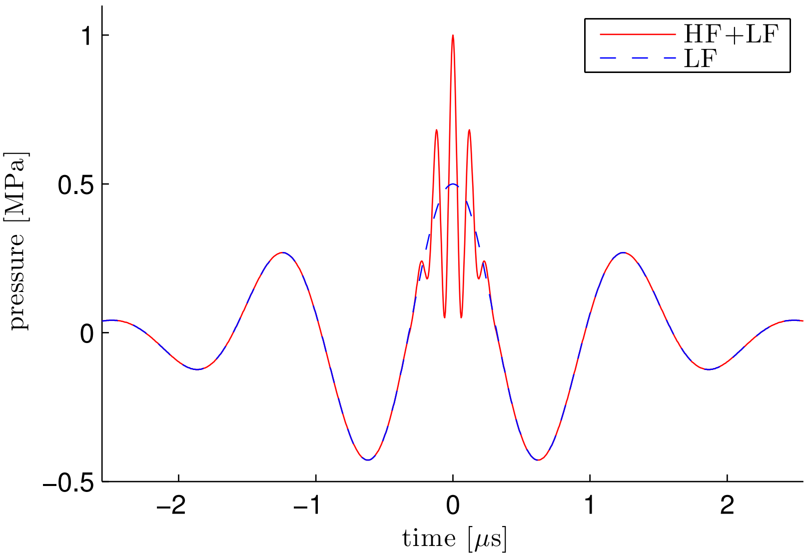

Figure 1.1: Dual band transmit pulse. The high frequency (HF, 8 MHz) and low frequency (LF, 0.78 MHz) pulses both have a pulse length of 2.5 oscillations and max amplitude of 0.5 MPa. This positioning of the HF on the LF is called plus polarity.

1.2 Dual band imaging

Dual band imaging (DBI) as described in this work is developed at the Department of Circulation and Medical Imaging at the Norwegian University of Science and Technology under Bjørn Angelsen and also goes under the name of SURF imaging.[2, 9–14] The main idea is to transmit a modifying low frequency (LF) wave alongside a conventional high frequency (HF) imaging pulse. The LF wave is used to modify the nonlinearity of the medium as observed by the imaging pulse. A method similar to pulse inversion can be used to extract information created by the nonlinear propagation. But instead of inverting the whole pulse complex only the LF pulse is flipped. This change in the polarity of the LF pulse is kept track of by a variable, p. Positioning the HF pulse on a crest of the LF is denoted a positive, or plus, polarity transmit ($p = 1$) and positioning the HF on the trough of the LF is denoted as a negative, or minus, polarity transmit ($p = -1$). The received signals are referred to as the positive (polarity) and negative (polarity) signals respectively. Transmitting only the HF imaging pulse is referred to as a zero polarity transmit ($p = 0$). An example of a transmit pulse with positive polarity is shown in Fig. 1.1.

Going back to Eq. (1.2), we see that an increase in the pressure creates a higher propagation speed. The presence of a positive polarity LF pulse thus increases the propagation velocity of the HF. The result is a nonlinear propagation delay

(NPD) between a zero polarity signal and a positive, or negative, polarity signal. The NPD increases with depth as long as the LF pulse is present. Following the Born approximation, the amplitude of both the HF and the LF will drop at the first scattering event. The NPD thus contains information about the depth of the first scattering event, whereas the time of flight only tells us the total propagation path. Multiple scatterings will cause pulses to reach the transducer at a later time than corresponding first order components of the same set of scatterers. However, the NPD would be the same for the reverberation components and corresponding first order scatterers. By extracting the NPD of a received plus or minus polarity signal compared to a zero polarity signal it is therefore possible to distinguish first order from reverberation components. It is shown below how signals of different polarities can be delayed and subtracted to suppress the reverberation components.

1.3 Reverberation noise and reverberation suppression

Reverberations are generally lower in magnitude than first order components from the same set of scatterers. With this in mind it makes sense to only study the strongest kind of reverberations, as it is these that will have the most damaging effect on the final image. As scattering of planar interfaces are generally stronger than scattering of a point particle, since a larger reflector reflects more energy, special interest is given to reverberations of planes in this thesis. A further specialization is on planes which are parallel to the transducer and body wall. This can for example be planar scatterers due to fatty layers or arteries. Of special interest was study of plaque in the common carotid artery where the blood vessel and fatty layers create such planes. As each planar reflector reverses the direction of the wave, reverberations will be combinations of an odd number of scatterers; which would be required for the reverberations to return to the transducer. Scattering of one single plane would, of course, correspond to the first order component. Three or more planes would correspond to reverberations. As the amplitude of the pulse drops with each scattering the work here is on combinations of only three scatterers.

1.3.1 Classification of reverberations

A special case is made for the scenario when the transducer is one of the scattering planes. This is not only due to the simpler mathematics this assumption poses, but also due to the fact that the transducer-body interface generally acts as a strong reflector. In this thesis this scenario is said to generate Class I reverberation noise. Reverberations where the second scatterer is not on the transducer-body interface is called Class II. A third class, Class III, is used when all three scatterers are deep in the tissue. Class III scattering is not treated explicitly here, but is mentioned as it appears in the referenced literature.

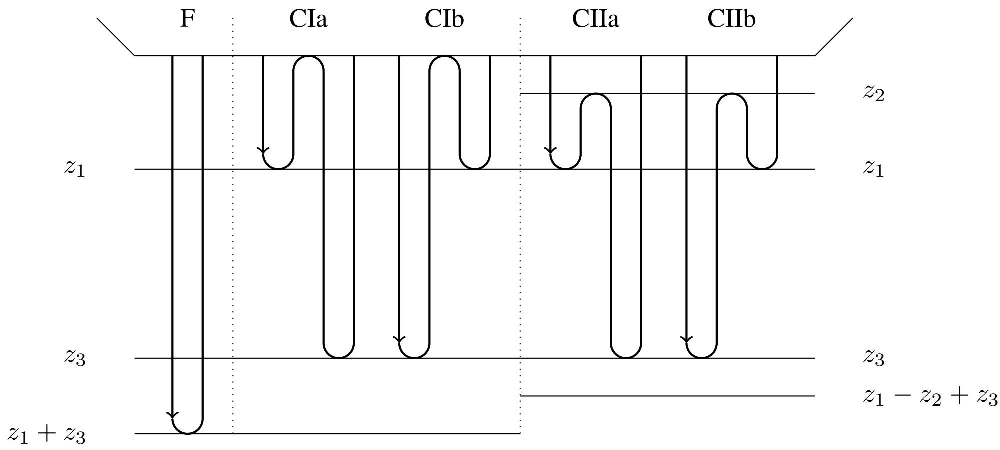

Figure 1.2: Classification scheme for third order reverberations. The prefix "C" to the reverberation components is short for "Class" and is meant to make the notation more distinguishable from other text. "F" is the first order signal.

Table 1.1: Reverberation classification scheme comparison to other literature. Note how the meaning of Greek and alpha numbering is switched between this work and the work by Høilund-Kaupang.

Brende	Høilund-Kaupang	Näsholm
Ia	Ia	II
Ib	IIa	III
IIa	Ib	-
IIb	IIb	-
III	III	I

Høilund-Kaupang *et al.* demonstrated that reverberation noise from a given set of scatters always act in pairs. This is illustrated by considering three scatterers, one at z_1, one at a shallower depth (often the transducer surface) at z_2, and the deepest at z_3 (see Fig. 1.2 for an illustration). The emitted pulse can take two possible paths. One, denoted "a", when it is reflected off the shallow scatterer first, $z_1 \to z_2 \to z_3$, and another, "b", when it is reflected off the deepest scatterer first, $z_3 \to z_2 \to z_1$. Both these propagation paths give reverberation noise at a depth, z, given by $z = z_1 - z_2 + z_3$. For a comparison to reverberation classification schemes of other authors see Table 1.1. As mentioned above, this thesis focuses mainly on Class I reverberations as this is believed to be the strongest. A note on Class II reverberation is included in Sec. 2.14.

The different reverberation classes are often referred to through abbreviations, ie. CIa referring to Class I type “a”. Often also written out as Class Ia. A capital “C” is used to make the notation stand out from other text.

1.3.2 Nonlinear propagation delay of reverberations

As discussed above, the NPD of a signal is dependent on the propagation path up to the first scattering of the pulse. This makes Class a and b reverberation components have different NPDs. The NPD of the combined pulse is referred to as the reverberation NPD, or simply “reverberation delay”, and is denoted τ_{n}. An additional subscript is often used to indicate the polarity of the LF wave used in the transmit.

The signal received at a given time (corresponding to a depth through Eq. (1.1)) is generally a combination of a first order component and a reverberation component. The first order component will always have a higher NPD than the combined reverberation component since the first order component has the maximum propagation path before scattering. This is illustrated in Fig. 1.3 which shows the time versus depth plot of a first order component and reverberations of Class Ia and Ib which arrive at the same time under a zero polarity transmit (or conventional ultrasound imaging). By altering the propagation speed up to the first scattering through the addition of a LF pulse in transmit, the received components are separated in time. This separation is greatly exaggerated here in order to make a clear figure. In reality the induced propagation delay is below 40 ns which is well below a typical HF pulse period of $1/(8\ \mathrm{MHz}) = 125$ ns.

How the different signal components overlap is illustrated in Fig. 1.4. Here the pulses are illustrated by their envelope rather than as rf-signals for a clearer figure. Notice how Class a of the minus polarity signal comes before Class b, and the opposite for the plus polarity. Longer propagation before reflection makes the Class b component more influenced by the nonlinearity of the medium than Class a. Nonlinear attenuation also makes Class b lower in amplitude compared to Class a. The difference between Class a and b, and their different relative arrival time for different polarities, makes the interference of the reverberation components different between the plus and minus polarity signals.

In the example of Fig. 1.4 the first order component at the given depth is larger than the reverberation component. Here, when estimating the total NPD between e.g. the total plus and minus signals, the resulting NPD will be closer to the NPD of the first order component than of the combined reverberation components. If there at a given depth was no reverberation noise, the total NPD between a plus and zero polarity signal would be equal to the first order NPD as the signal would only consist of the first order component. In the same way, the NPD of the total signal would be equal to the reverberation NPD if the total signal was fully consisting of reverberation noise.

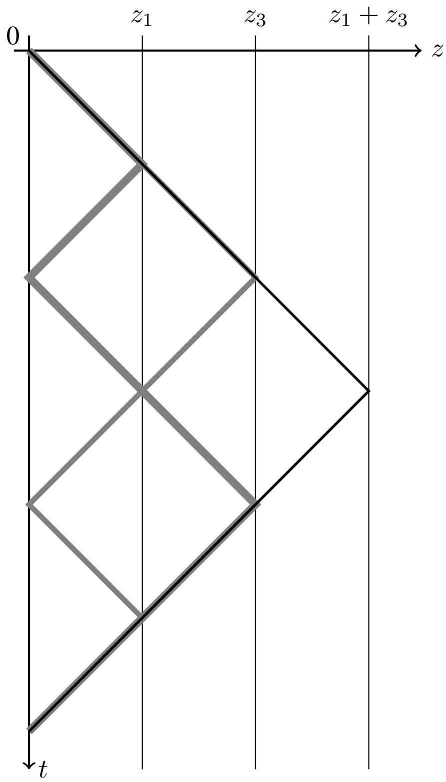

(a) HF pulse.

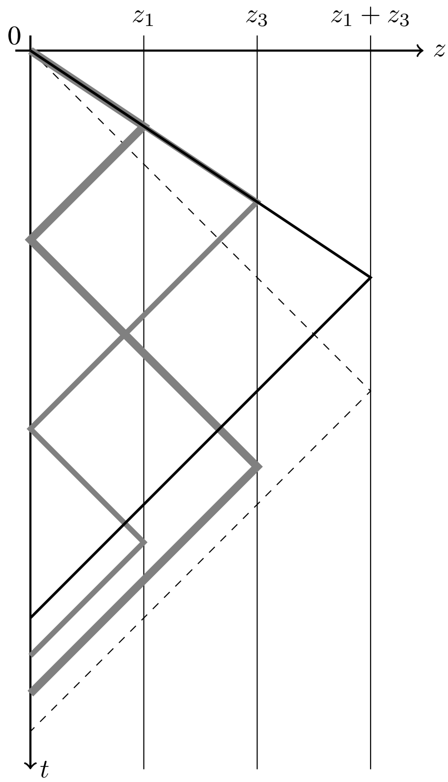

(b) HF and LF pulse.

Figure 1.3: Arrival time map of different signal components without (a) and with (b) modifying LF pulse. The first order component path from (a) is shown as a dotted line in (b).

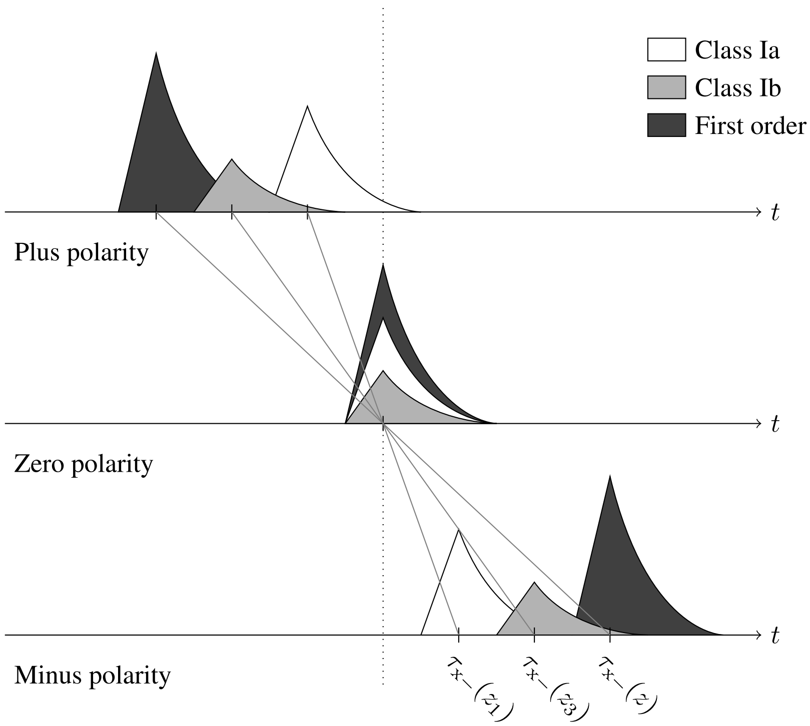

Figure 1.4: Behaviour of classes under DBI.

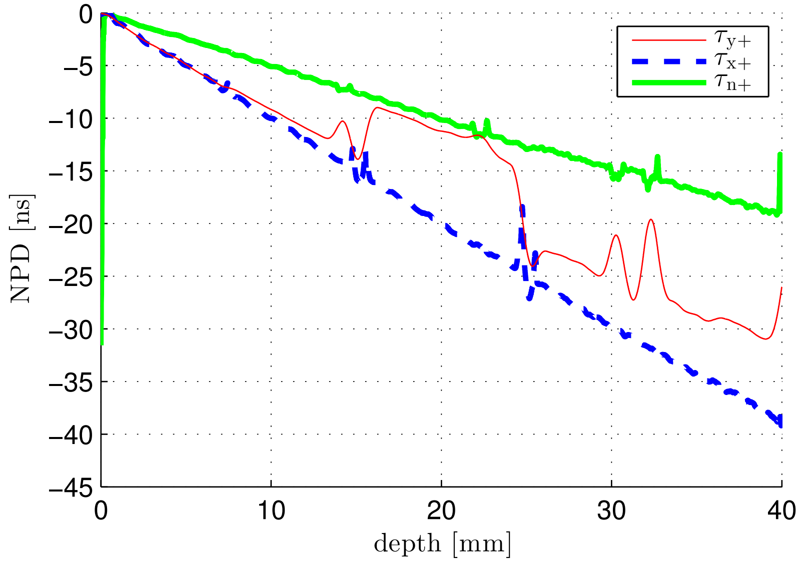

Figure 1.5: Nonlinear propagation delays (NPDs) of the total signal, τ_y, the first order component, τ_x, and the reverberation components, τ_n. The example is the medium of case VI from paper B, with a synthetic linear first order delay applied to simulated pulses used to create the rf-signal. The plot shows the average of 300 runs of the simulations where weak background scatterers varied randomly. Strong scatterers are introduced at 7, 15 and 25 mm. And a low echogene section is introduced between 15 and 25 mm where the scattering strength is 20 % compared to the rest of the image. The spike in the reverberation NPD in the beginning is caused by a breakdown of the delay estimation algorithm as the reverberation component is close to zero here.

Figure 1.5 shows how the NPD of the total signal, τ_y, relates to the NPD of the first order component, τ_x, and the reverberation component, τ_n. The example here is of the NPD between a plus polarity and zero polarity signal which is defined to yield a negative delay. Observe that the delay of the total signal is close to the first order NPD up to around 15 mm. This would mean that the total signal here is dominated by first order scattering. Between 15 and 25 mm the NPD of the total signal is close to the reverberation NPD which indicates that the signal here is dominated by reverberation noise. After 25 mm there seems to be a combination of first order and reverberation components. The ripples in the delay curves in Fig. 1.5 are due to the presence of strong signals, first order or reverberations, at the given depths.

1.3.3 Reverberation suppression

The difference in NPD between first order and reverberation components of the total signal can be utilized to suppress the reverberation noise. The idea is to align the total reverberation components of the plus and minus polarity signals by applying an appropriate reverberation delay and then subtract the signals. The resulting signal is a subtraction of two shifted, but otherwise equal, first order signal components. The gain in the signal introduced by this shifted subtraction can be calculated and corrected for. The result is an estimation of the first order component in a noisy total signal. This method is called Delay Corrected Subtraction (DCS) and was introduced by Näsholm *et al.*[14] The combination of using DCS with DBI is commonly referred to as SURF processing.

Bibliography

[1] Bjørn A. J. Angelsen. *Ultrasound imaging : waves, signals, and signal processing*, volume I. Emantec, 2000.

[2] Rune Hansen, Svein-Eirik Måsøy, Tonni F. Johansen, and Bjørn A. J. Angelsen. Utilizing dual frequency band transmit pulse complexes in medical ultrasound imaging. *J. Acoust. Soc. Am.*, 127(1):579–587, January 2010.

[3] D. L. Miller. Ultrasonic detection of resonant cavitation bubbles in a flow tube by their second-harmonic emissions. *IEEE Ultrasonics Symposium*, pages 217–224, September 1981.

[4] Michalakis A. Averkiou, David N. Roundhill, and Jeffrey E. Powers. A new imaging technique based on the nonlinear properties of tissues. *ULTRASON*, pages 1561–1566, 1997.

[5] D. H. Simpson, Chien Ting Chin, and P. N. Burns. Pulse inversion doppler: a new method for detecting nonlinear echoes from microbubble contrast agents. *IEEE Trans. Ultrason., Ferroelect., Freq. Control*, 46(2):372–382, March 1999.

[6] P. Jiang, Z. Mao, and J. Lazenby. A new tissue harmonic imaging scheme with better fundamental frequency cancellation and higher signal-to-noise ratio. *Proc IEEE Ultrason Symp*, 2:1589–1594, 1998.

[7] Michalakis A. Averkiou. Tissue harmonic imaging. *ULTRASON*, pages 1563–1572, 2000.

[8] Jochen Matthias Rau. *Dual frequency band ultrasound for suppression of multiple scattering*. PhD thesis, NTNU, 2013.

[9] Rune Hansen and Bjørn. A. J. Angelsen. SURF imaging for contrast agent detection. *IEEE Trans. Ultrason., Ferroelect., Freq. Control*, 56(2):280–290, February 2009.

[10] Svein-Eirik Måsøy, Øvind Standal, Sven Peter Näsholm, Tonni F. Johansen, Bjørn Angelsen, and Rune Hansen. SURF imaging: In vivo demonstration of an ultrasound contrast agent detection technique. *IEEE Trans. Ultrason., Ferroelect., Freq. Control*, 55(5):1112–1121, May 2008.

[11] Rune Hansen, Svein-Erik Måsøy, Tor Andreas Tangen, and Bjørn A. J. Angelsen. Nonlinear propagation delay and pulse distortion resulting from dual frequency band transmit pulse complexes. *J. Acoust. Soc. Am.*, 129(2):1117–1127, February 2011.

[12] Sven Peter Näsholm, Rune Hansen, and Bjørn A. J. Angelsen. Post-processing enhancement of reverberation-noise suppression in dual frequency surf imaging. *IEEE Trans. Ultrason., Ferroelect., Freq. Control*, 58(2):338–348, February 2011.

[13] Jochen Matthias Rau, Svein-Erik Måsøy, Rune Hansen, Bjørn Angelsen, and Thor Andreas Tangen. Methods for reverberation suppression utilizing dual frequency band imaging. *J. Acoust. Soc. Am.*, 134(3):2313–2325, 2013.

[14] Sven Peter Näsholm, Rune Hansen, Svein-Eirik Måsøy, Tonni F. Johansen, and Bjørn A. J. Angelsen. Transmit beams adapted to reverberation noise suppression using dual-frequency surf imaging. *IEEE Trans. Ultrason., Ferroelect., Freq. Control*, 56(10):2124–2133, October 2009.

Chapter 2

Extended theory and results

2.1 Overview of work submitted for publication

This thesis includes two papers submitted for peer review enclosed in part II of this document. The theory laid out in this chapter is not otherwise published. This format, with a rather extensive unpublished theory section, was chosen as the theory in this chapter closely follows the submitted papers, and thus serves more as of a companion to the published work rather than one, or a set of, standalone publications.

This chapter begins with a summary of the work submitted for journal publication and then extends upon this work with additional theories and numerical experiments. After reading the introductory parts on the submitted papers the writer suggest reading part II of this thesis before continuing in this chapter. However, the train of thought is not broken by reading this thesis cover to cover.

The first paper in the thesis, paper A, was originally written last of the two. The order is changed in the thesis as paper A can be seen as more general than paper B and is thus more well suited as an introduction to the rest of the work presented here.

Paper A: Limiting factors in reverberation suppression through delay corrected subtraction methods in dual band ultrasound imaging

This paper explores the theoretical limit of delay corrected subtraction based reverberation suppression under dual band imaging. The paper explains the behavior of reverberation noise in dual band imaging through general theory of nonlinear propagation. This theory is used as basis for the discussion of how various aspects of nonlinear propagation, such as the presence of nonlinear propagation delays and pulse form distortions affect the possible suppression of the reverberation components. Other effects include: heterogeneity of nonlinearity in the medium, nonlinear self distortion, differences in nonlinear propagation delay between transmits of different polarities of the low frequency pulse, statistics of reverberation pairs, errors in delay estimations, and the length of the high frequency pulse. The paper concludes that the shape of the first order nonlinear propagation delay, as an effect of heterogeneity of the nonlinearity of the medium, seems to have the biggest effect on the theoretical maximum reverberation suppression under the delay corrected subtraction method.

Pulse simulation tool and text on Abersim attributed to Johannes Kvam. Theory development, simulation setup, analysis, discussion, conclusions, and text editing done by the candidate. Background theory attributed to Bjørn Angelsen.

This work is submitted to IEEE Transactions on Ultrasonics, Ferroelectrics and Frequency Control. It is awaiting the second stage of review.

Paper B: Adaptive reverberation noise delay estimation for reverberation suppression in dual band ultrasound imaging

Here, a method to estimate the nonlinear propagation delay of the reverberation components based on the statistics of the signal is introduced. The paper reintroduces the theory and definitions behind reverberations and nonlinear propagation and, with this as basis, presents a simulation scheme to generate a complete rf-signal with Class I reverberations. The background theory is also utilized in the derivation of an adaptive estimation algorithm for the nonlinear propagation delay of the combined reverberation components. A key element in the paper is the importance of how different scatterer combinations can generate different reverberation components. The adaptive delay estimation algorithm aims to extract information from the received total signal and use this as a basis for estimating how the reverberation noise is realized in the medium. Five different test scenarios are introduced and delay corrected subtraction suppression of the reverberation components are tested based on the presented delay estimation algorithm. The proposed delay estimation algorithm showed improved increase in the Signal to Reverberation noise Ratio (SRR) after delay corrected subtraction suppression compared to earlier methods. The proposed reverberation delay estimation method proved especially better in the situation where the nonlinearity of the medium was emulated to vary with depth.

Pulse simulation tool attributed to Johannes Kvam. Theory development, simulation setup, analysis, discussion, conclusions, and text editing done by the candidate. Background theory attributed to Bjørn Angelsen.

This paper was published by the Journal of the Acoustical Society of America, 25. November 2015. `http://dx.doi.org/10.1121/1.4935555`

2.2 Overview of extended theory

First order delay estimation

When paper B is concerned with estimating the NPD of the reverberation components, this work illustrates how the NPD of the first order component can be estimated. The first order delay is important for the estimation of the reverberation delay but has been assumed to be known otherwise in the thesis. The method discussed here is the same as that mentioned by Rau[1]. In addition to a general presentation various problems with this estimation scheme is presented and possible solutions are presented.

This work is included in Sec. 2.5.

Extensions on reverberation delay estimation

Assumptions are done in paper B which are not fully backed by simulations and mathematical derivation in the paper. Such backing is given here (Secs. 2.7 to 2.9). In addition, additional reverberation delay estimation schemes are presented. Some simpler than the one presented in paper B (Sec. 2.11), and one iterative scheme which increases the complexity of noise suppression algorithm (Sec. 2.13)

This work is included in Secs. 2.7 to 2.9, 2.11 and 2.13.

Discussion on pulse shape and pulse simulations

Paper B and A use symmetrical Gaussian pulses as basis. This was chosen to ease reproduceability of the results. Here, simulations with more realistic pulses are examined and compared to the results from the papers. A discussion around the change in the signal generation algorithm based on simulated pulses from paper A to paper B is also discussed.

This work is included in Secs. 2.10 and 2.12.

Other kinds of reverberation noise

This part is about Class II reverberations. This type of reverberations is excluded from the discussion in other parts of the thesis as it is assumed to be much weaker than Class I. A brief discussion of the behavior of this type of reverberation is, however, included for completeness. The expected mean Class II reverberation delay is derived, and the adaptive reverberation delay estimation from paper B is extended to also include this type of reverberation noise.

This work is included in Sec. 2.14.

Estimation of nonlinear scatterers

Nonlinear scatterers are scatterers that depend on the polarity of the LF pulse. It has been shown that microbubbles exhibit this property.[2] This section discusses initial simulations on a proposed estimation scheme for detection of nonlinear scatterers as well as suppression of reverberation noise. The proposed method highlights nonlinear scatterers over linear scattering, but fails in suppressing reverberations adequately.

This work is included in Sec. 2.15.

2.3 Signal model

In the previous chapter the signals and delays were discussed with plain words rather than with mathematical formulas. Here, a more thorough discussion is given and it is therefore beneficial with a more mathematical description.

For now, the discussion is limited to first order linear scattering and reverberations. A total signal for a conventional imaging pulse with no modifying low frequency (LF) wave is written

$$y_0(t) = x_0(t) + n_0(t). \tag{2.1a}$$

Here, $x_0(t)$ is the first order component and $n_0(t)$ is the reverberation component. The subscript 0 indicates no LF, or a "zero-polarity" LF wave. When an LF wave is added this subscript is changed to +/- depending on the polarity of the LF wave,

$$y_+(t) = x_+(t) + n_+(t), \quad \text{or} \tag{2.1b}$$
$$y_-(t) = x_-(t) + n_-(t). \tag{2.1c}$$

To generalize, the parameter p is used for the polarity of the LF wave. In this work p can take the values, $+1, 0$, and -1. This enables the notation of Eq. (2.1) as

$$y_p(t) = x_p(t) + n_p(t). \tag{2.2}$$

In the previous chapter a delay difference between the x_p and n_p components was introduced. The introduction of the LF wave also introduces other nonlinear propagation effects. The total effect of the LF wave is contained in the filter $V_p(\omega)$ for the first order components and $L_p(\omega)$ for the reverberation components. In Fourier space this gives

$$X_{ip}(\omega) = V_{ip}(\omega)X_{i0}(\omega), \quad \text{and} \tag{2.3}$$
$$N_{ip}(\omega) = L_{ip}(\omega)N_{i0}(\omega). \tag{2.4}$$

The subscript i denotes an interval in time. The modification filters are divided into two parts. The first is the linear phase of the filters which give a delay in the time domain. The other part is the pulse form distortion (PFD) for the first order components and noise distortion (ND) for the reverberation components. In mathematical form

$$V_{ip}(\omega) = \widetilde{V}_{ip}(\omega)\mathrm{e}^{-i\omega\tau_{\mathrm{x}ip}}, \text{ and} \tag{PFD, 2.5a}$$

$$L_{ip}(\omega) = \widetilde{L}_{ip}(\omega)\mathrm{e}^{-i\omega\tau_{\mathrm{n}ip}}. \tag{ND, 2.5b}$$

In this form the delays are assumed constant in the interval i. Neglecting the PFD and ND, $V_{ip} = L_{ip} = 1$, gives a pure delay and Eq. (2.2) can be written

$$y_p(t) = x_0(t - \tau_{\mathrm{x}}(t)) + n_0(t - \tau_{\mathrm{n}}(t)). \tag{2.6}$$

The delays are now allowed to vary freely.

2.4 Delay corrected subtraction

As discussed in the previous chapter (Sec. 1.3.3), delay corrected subtraction works by aligning the reverberation components of two signals and subtracting. The difference in propagation delay between first order and reverberation components then makes sure that the first order signal can be retained by applying an appropriate gain correction.

Write Eq. (2.2) in Fourier space for the plus and minus polarity LF

$$\begin{pmatrix} Y_+ \\ Y_- \end{pmatrix} = \begin{pmatrix} V_+ & L_+ \\ V_- & L_- \end{pmatrix} \cdot \begin{pmatrix} X \\ N \end{pmatrix}. \tag{2.7}$$

The interval subscript i, as well as the frequency has been omitted for a simpler notation. Solving Eq. (2.7) for the signal X yields

$$X = \frac{Y_+ L_+^{-1} - Y_- L_-^{-1}}{V_+ L_+^{-1} - V_- L_-^{-1}}. \tag{2.8}$$

Utilizing Eq. (2.5) and assuming no PFD or ND simplifies to

$$X = \frac{Y_+ \mathrm{e}^{i\omega\tau_{\mathrm{n}+}} - Y_- \mathrm{e}^{i\omega\tau_{\mathrm{n}-}}}{\mathrm{e}^{-i\omega(\tau_{\mathrm{x}+} - \tau_{\mathrm{n}+})} - \mathrm{e}^{-i\omega(\tau_{\mathrm{x}-} - \tau_{\mathrm{n}-})}}. \tag{2.9}$$

Note that in order to suppress the reverberation noise only the delays of the reverberation components (reverberation delays) are needed. The delays of the first order signal components, or first order delays for short, only appear in the gain factor used to lift the signal amplitude of the estimated first order signal. One could therefore argue that the reverberation delay is the most important. However, the first order delay is important for estimating the reverberation delay. A good estimate for the first order delay is therefore also important for the DCS method.

2.5 Estimating the first order delay

The first order delay is used in all current estimation methods of the reverberation delay. As the reverberation delay is the core input of the DCS method utilized to suppress reverberation noise, a proper estimation scheme for the first order delay is needed.

Estimation of the first order delay has not been included in the two papers included in this thesis. Assumptions have been made, as in earlier work, that this delay is known. The aim of this section is to explain the first order delay as presented by Rau[1] and highlight positives and negatives of this estimation method. Effects of electronic noise and saturation of the received signals are also considered in the estimation scheme. But first, an introduction to estimating the total delay, τ_y, which is used as basis for the first order delay estimation.

2.5.1 Delay estimation

There are multiple methods available to estimate the delay between two similar signals. The one explained here is the one developed by Standal *et al.* [5] as this method was developed by the group previously working on the same problems as the author and aimed to estimate delays of the same kind of signal as is of interest here.

The following procedure differs from the description published by Standal *et al.* [5] in that it concerns continuous signals and not sampled signals. The minimum square error approach presented in the paper by Standal *et al.* is not included here as this was not implemented in the code used in this work.

Consider two analytical signals $y_0(t)$ and $y_p(t)$ separated by a delay, τ, such that $y_p(t) = y_0(t-\tau)$,

$$y_p(t) = a(t-\tau)\mathrm{e}^{i\omega_\mathrm{c}\cdot(t-\tau)+i\phi(t-\tau)}, \tag{2.10a}$$

$$y_0(t) = a(t)\mathrm{e}^{i\omega_\mathrm{c}t+i\phi(t)}. \tag{2.10b}$$

The center frequency is represented by ω_c, a general phase as $\phi(t)$, and the amplitude as $a(t)$. The interest lies in the phase difference between these signals. More precisely, in the delay τ. Compute the phase difference between the two signals,

$$\begin{aligned}\angle\left\{y_0(t)y_p^*(t)\right\} &= \omega_\mathrm{c}t + \phi(t) - \omega_\mathrm{c}\cdot(t-\tau) - \phi(t-\tau),\\ &= \omega_\mathrm{c}\tau + \phi(t) - \phi(t-\tau),\\ &= \Big(\omega_\mathrm{c} + \dot{\phi}(t-\tau/2)\Big)\,\tau. \end{aligned} \tag{2.11}$$

Observe that the phase difference is proportional to the delay, τ. The change in phase over an interval $[t-\delta_t, t+\delta_t]$ for one of the signals along with Eq. (2.11) can be used to extract the delay between the two signals. Compute the change in phase for the $y_0(t)$ signal,

$$\begin{aligned}\angle\left\{y_0(t+\delta_t)y_0^*(t-\delta_t)\right\} = &\quad \omega_\mathrm{c}\cdot(t+\delta_t)+\phi(t+\delta_t)\\ &-\omega_\mathrm{c}\cdot(t-\delta_t)-\phi(t-\delta_t),\\ &= 2\omega_\mathrm{c}\delta_t+\phi(t+\delta_t)-\phi(t-\delta_t),\\ &= \left(\omega_\mathrm{c}+\dot{\phi}(t)\right)2\delta_t, \end{aligned} \tag{2.12}$$

and for $y_p(t)$,

$$\begin{aligned}\angle\left\{y_p(t+\delta_t)y_p^*(t-\delta_t)\right\} = &\quad \omega_\mathrm{c}\cdot(t+\delta_t-\tau)+\phi(t+\delta_t-\tau)\\ &-\omega_\mathrm{c}\cdot(t-\delta_t-\tau)-\phi(t-\delta_t-\tau),\\ &= 2\omega_\mathrm{c}\delta_t+\phi(t+\delta_t-\tau)-\phi(t-\delta_t-\tau),\\ &= \left(\omega_\mathrm{c}+\dot{\phi}(t-\tau)\right)2\delta_t. \end{aligned} \tag{2.13}$$

Averaged, the change in phase for $y_0(t)$ and $y_p(t)$ can be used to estimate the proportionality factor to τ in Eq. (2.11),

$$\frac{1}{4\delta_t}\left(\left(\omega_\mathrm{c}+\dot{\phi}(t)\right)2\delta_t+\left(\omega_\mathrm{c}+\dot{\phi}(t-\tau)\right)2\delta_t\right)\approx\left(\omega_\mathrm{c}+\dot{\phi}(t-\tau/2)\right), \tag{2.14}$$

or simplified,

$$\frac{1}{2}\left(\dot{\phi}(t)+\dot{\phi}(t-\tau)\right)\approx\dot{\phi}(t-\tau/2). \tag{2.15}$$

Which seems like a reasonable assumption. A method to estimate the delay, τ, could then be

$$\tau\approx\frac{4\delta_t\angle\left\{y_0(t)y_p^*(t)\right\}}{\angle\left\{y_0(t+\delta_t)y_0^*(t-\delta_t)\right\}+\angle\left\{y_p(t+\delta_t)y_p^*(t-\delta_t)\right\}}. \tag{2.16}$$

In the computer code used in this work the step size is $\delta_t = 1$ sample, and the nominator and denominator of Eq. (2.16) are lowpass filtered separately to reduce rapid fluctuations due to electronic noise in the signals.

2.5.2 Shortest path method

First it should be noted that no extensive research of the estimation of the first order NPD was found in current literature or was conducted by the author. Presented here are arguments for why the shortest path method is a reasonable estimation scheme.

As briefly mentioned by Rau[1] a robust estimation scheme of the first order NPD, τ_x, is found by calculating the shortest path above (for a positive delay, negative polarity) or below (for a negative delay, plus polarity) the total NPD curve, τ_y. This method yields a first order NPD curve with a decreasing absolute value of the derivative with depth. However, as shown in paper A, the derivative of the first order NPD along the propagation path, s, follows

$$\frac{\mathrm{d}\tau_\mathrm{x}(z)}{\mathrm{d}s} = \beta_\mathrm{n}(z)\kappa(z)p_\mathrm{LF}(z). \tag{2.17}$$

As there are no inherent restrictions on the material, and as such on the parameters $\beta_\mathrm{n}(z)$ and $\kappa(z)$, it seems that one is erroneous in assuming a reduction of the gradient with depth. Note also that the LF pressure *increases* up to the diffraction focus.[3] Why is this assumption on the gradient then done?

The main argument lies in the monotonic increase in the value of the first order NPD. The derivative (Eq. (2.17)) has the same sign throughout the propagation when assuming that the HF pulse stays in the same peak of the LF as when it was transmitted (see Fig. 1.1). Ie. a HF pulse initially experiencing a positive LF pressure at transmit does not at some depth move to a negative LF pressure. This increase with depth is true for both the first order NPD and the reverberation NPD.

Consider a strong first order signal at some given depth. The total NPD, τ_y, at this depth is close to the first order NPD, τ_x. The question is then to find the further development of the first order NPD curve from this point. The delays are increasing in value with depth so one can limit oneself to considering peaks of higher value than the one used as a starting point. It might be alluring to chose the next higher-value peak as the continuation of the τ_x line. However, considering that as all NPDs increase in value with depth, this new peak, as it is found at a higher depth, could just as well be a delay of a total signal composed of a relatively equal strength first order and reverberation signals. Remember that the total NPD of a signal τ_y takes values between the first order and reverberation delays at a given depth (see Fig. 1.5). The question is then if one should select this new peak, or rather find an even higher peak further down giving a higher gradient of τ_x. The choice with the shortest path estimation scheme is to always find the highest possible gradient following the peaks in the total NPD. The idea is that this would give a result less dependent on small variations in the first order to reverberation signal ratio. The result is also a smoother development of the first order NPD. One might argue that the first order NPD might not be smooth, as the material might vary rapidly along the propagation path. The counter argument here is that this large variation is hard to estimate when the estimation scheme is dependent on the SRR (Signal to Reverberation Noise Ratio) which is unknown.

2.5.3 Saturation and electronic noise

At high depths electronic noise can result in signals of different polarities differing so much it is not possible to find a suitable delay between them. As discussed in

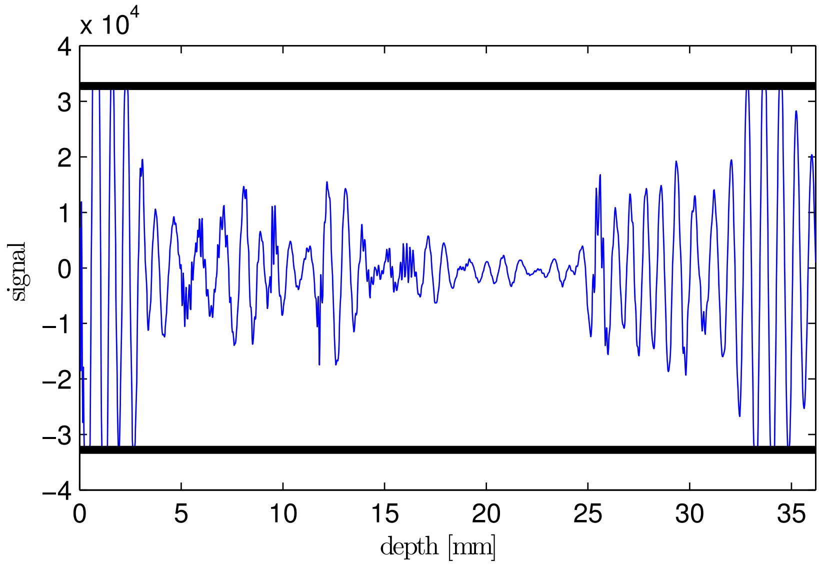

Figure 2.1: Clipping of the received signal due to presence of strong LF components. Thick lines represent the limits for what can be represented in a 16 bit integer which is the data type used in the scanner. Signal is at a lateral position of 19.8 mm of the same medium as shown Fig. 2.2. The signal is generated with transmit of a HF pulse on the peak of a LF wave (positive polarity).

paper B, this estimated nonlinear propagation delay (τ_{y}) is used to estimate the NPD of the first order component of the signal (τ_{x}) and in turn the NPD of the reverberation component (τ_{n}) which is used in the Delay Corrected Subtraction (DCS) algorithm to suppress the noise. Without knowing which parts of the total NPD is noisy or well estimated it is hard to give a proper estimation of the other delays and a good suppression of the noise.

Another destructive effect is saturation, or clipping, of the received signal. This can typically happen if large LF components are received by the transducer. As opposed to electronic noise this is something that can happen at shallow depths. If generation of the LF pulse is fine tuned in the hardware to give a short frequency response, the result is a longer LF pulse, or a longer ringing down of the LF. If this ringing has not stopped when the HF piezo elements are switched from transmit to receive, this ringing is picked up in the circuit. The result is saturation in the received signal. See Fig. 2.1 which shows the rf-signal from a scanline in an in vivo scan with corresponding B-mode image in Fig. 2.2. To combat saturation due to strong LF components the author would suggest adding a high-pass filter somewhere early in the receive electronics as also suggested by Rau[1]. Note, however, that this clipping effect can not only occur at the beginning of the signal

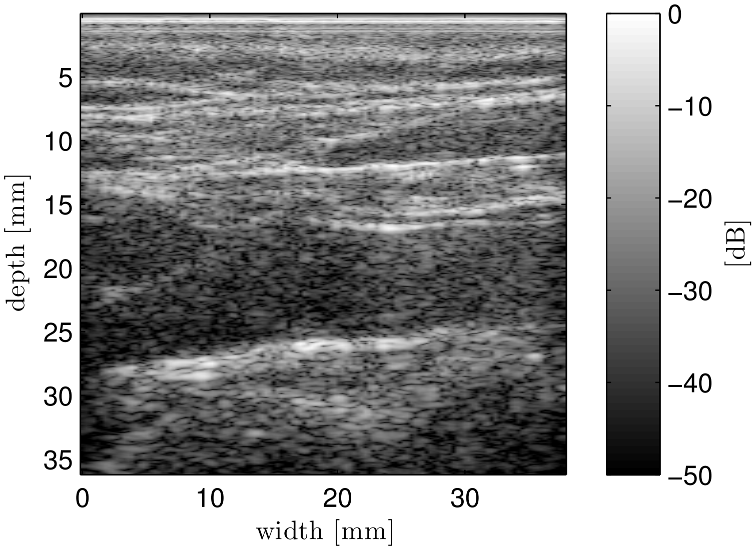

Figure 2.2: Regular B mode image. Envelope detected and log compressed. Based on transmit of a pure HF pulse (zero polarity). (Some of the dynamic range is lost in the printed version.)

but might also be present with a strong LF reflector in the medium. See again Fig. 2.1.

As mentioned above the first order NPD is found by taking the shortest path around the total NPD starting at $\tau_\mathrm{y}(0) = 0$ and ending at $\tau_\mathrm{y}(z_\mathrm{max}) =$ *some value*. A large error in τ_y at any point in the curve will therefore damage the total estimation of the first order NPD. This effect is demonstrated in Fig. 2.3, where clipping of the rf-signal (Fig. 2.1) makes delay estimation difficult (Fig. 2.4) and results in poor performance of the reverberation suppression through DCS. To combat an erroneous estimation of the first order NPD due to electronic noise, or signal saturation, at high depths one can introduce a hard limit for the maximum depth one wants to estimate the nonlinear propagation delay of the total signal, τ_y. To combat saturation of the signal at shallow depths one could likewise introduce a lower hard limit for the total NPD used in the first order NPD estimation. This would in the case of Fig. 2.3 give a more correct first order NPD as seen in Fig. 2.4.

Two new parameters have been introduced. Hard limits in the minimum and maximum depths used when estimation propagation delays. How should these be determined? One solution is to have these adjustable in the imaging software on the scanner. Assuming that the error in the total NPD estimation at the start of the signal is due to ringing down of the LF elements and that this effect is known a priori, one only needs to further consider modification of the maximum allowed

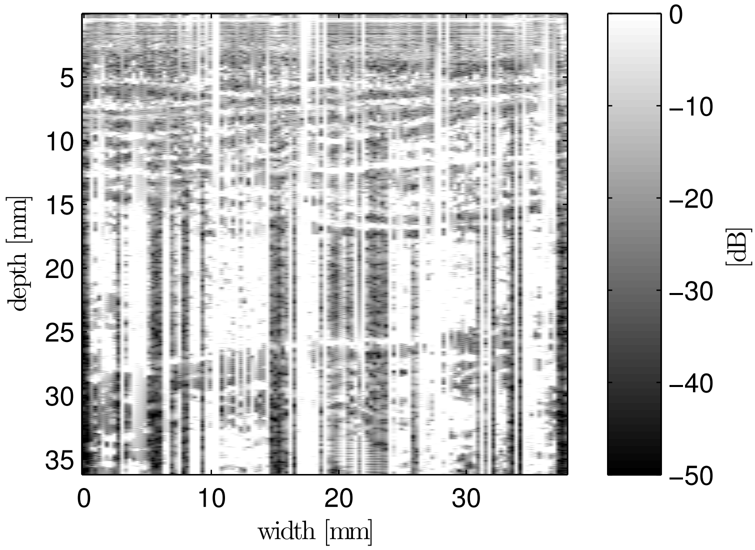

Figure 2.3: Failure of the first order delay estimation leading to poor processing of the B-mode image of Fig. 2.2. Errors in estimation of the first order NPD results in a breakdown of the reverberation NPD estimation and the DCS algorithm. Correction is done with delays corresponding to the thick dotted line of Fig. 2.4.

depth to use in the first order NPD estimation. If there are large errors in the estimation of the NPDs due to electronic noise the reverberation suppression algorithm will fail for the scanlines where this is the case. As the electronic noise can be seen as random, there will be high variance between scanlines. This will, in turn, result in very different estimations of the NPDs for different scanlines. Looking at the B-mode image the result is vertical lines in the image. See Fig. 2.5. Presence of such vertical lines would indicate that a lower value for the maximum depth allowed in NPD estimation should be used. If a too high value for the maximum allowed depth is used the estimation of the first order NPD will lose useful information. Depending on the implementation of the first order NPD estimation beyond the hard maximum limit this would lead to an erroneous estimation of the reverberation NPD. The result is poor reverberation suppression after DCS. As the true areas with high reverberation noise is not known a priori this error could be harder to notice. For reference (and completeness) see Fig. 2.6 where DCS processing is done on the same image as from Fig. 2.2 (with addition of two dual band transmits). The diffuse structure at around 35 mm depth an lateral position of around 20 mm is an artifact caused by the clipping of received rf-signal when a co-propagating LF pulse was transmitted. Delay estimation is done for each non-zero polarity transmit independently relative to the zero-polarity transmit.

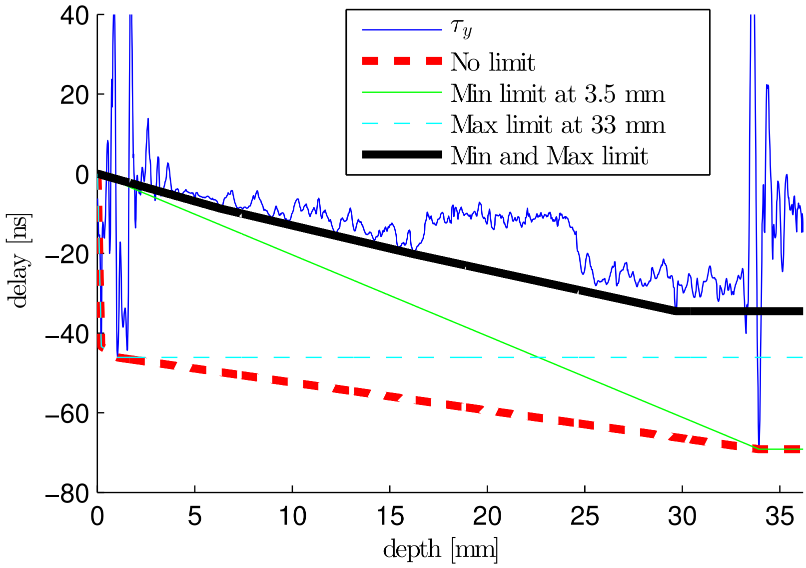

Figure 2.4: Estimation of the first order delay, τ_{x}. Medium is the same as displayed in Fig. 2.2, and calculations are done at a lateral position of 19.8 mm on a laterally smoothed version of the total NPD, τ_{y}. Different limits have been introduced on what parts of the total NPD (τ_{y}) to use in estimating the first order NPD (τ_{x}).

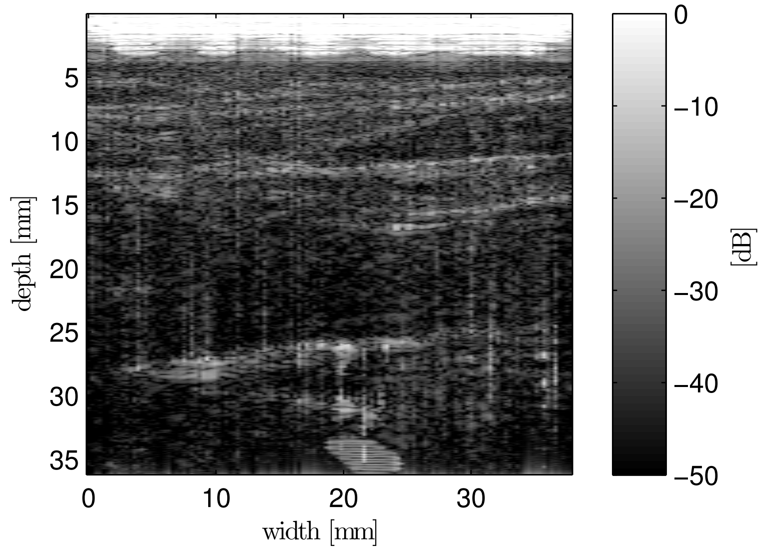

Figure 2.5: Failure of the first order delay estimation leading to poor processing of the B-mode image of Fig. 2.2. Errors in estimation of the total NPD at high depths leads to erroneous first order NPD and a breakdown of the reverberation NPD estimation and the DCS algorithm. Correction is done with delays corresponding to the thin line of Fig. 2.4.

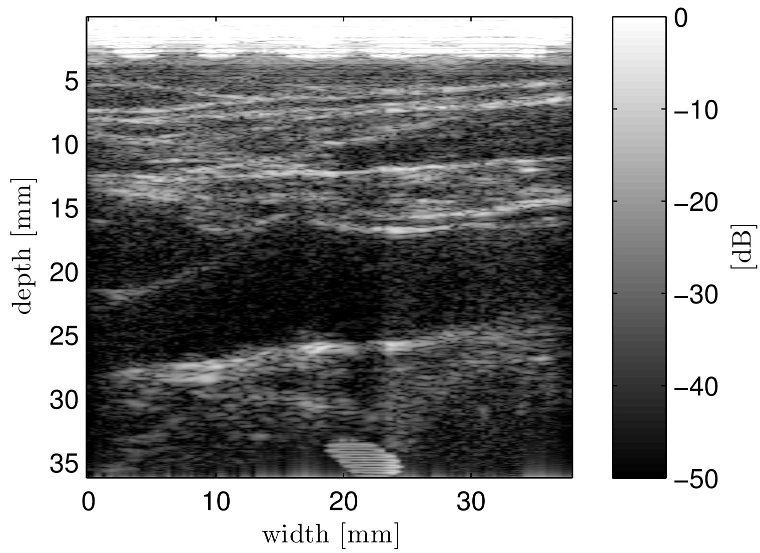

Figure 2.6: B mode image created with DCS processing of two DBI pulses and one regular pulse (Fig. 2.2). (Some of the dynamic range is lost in the printed version.)

2.5.4 Automatic adjustment of estimation regions

Manual adjustment of two (or one) extra parameters seems tedious and not user friendly. In a polished software package this adjustment should be automatic. One way to achieve this is by looking at the correlation between the signals of different polarities. When the correlation drops below a set correlation limit (CL) the signals differ so wildly that it can be assumed that electronic noise or saturation represents the strongest component of the signal. The depths where the correlation is below the set limit can then be excluded from the estimation of the first order NPD and in turn the reverberation NPD. One can either determine a hard minimum and maximum depth allowed, or simply remove areas with low correlation from the NPD estimation. The latter method would allow for low correlation areas at intermediate depths not destroying delay estimation if the correlation improves at higher depths. Note that by looking at the correlation between signals of different transmits there can be different depths allowed for different scanlines.

The correlation between two signals y_1 and y_2 within an interval i is calculated through

$$C_i(y_1, y_2) = \frac{\langle y_1 \cdot y_2 \rangle_i}{\sqrt{\langle y_1 \rangle_i^2 \cdot \langle y_2 \rangle_i^2}}. \tag{2.18}$$

The received signals from transmits of different polarities can be divided up in intervals in depth and a correlation map can be generated to determine areas with destructive effects such as saturation and/or electronic noise. See Fig. 2.7 for an example of a correlation calculation of an in vivo image, based on a plus polarity and zero polarity transmit. The image is based on the same data as the other figures in this section. Note the appearance of the clipping effects at the start and for the structure at 35 mm depth around a lateral position of 20 mm. Note also that the correlation seems to drop with depth. This can be due to increasing electronic noise and increasing pulse form distortion differences. The example used here had little dominant electronic noise as the signal strength was high even at high depths which is visible in Fig. 2.2.

For an already resource heavy imaging modality, the extra computations of correlations to set the limits for delay estimations is not ideal. A solution could be to only do the calculation for certain scanlines and make a max depth limit based on these. Note also that it might not be necessary to calculate the correlations at all depths. For instance one could pre-program a hard limit for the minimum depth allowed and only calculate the correlation between signals at depths over a certain limit, where electronic noise is to be expected.

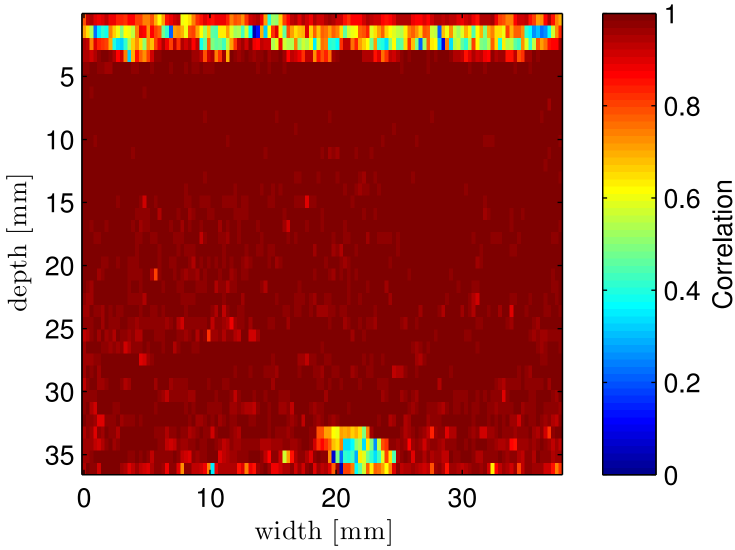

Figure 2.7: Correlation between a received plus polarity signal and zero polarity signal. The result can be used to estimate valid areas for delay estimation. The medium is shown as a regular B mode image in Fig. 2.2.

2.6 Reverberation delay estimation

As discussed in the introduction chapter the nonlinear propagation delay of any signal component is dependent on the path up to the first scattering event where the amplitude is assumed to drop so much that any further nonlinear effects can be neglected.

Scatterers at depths z_1 and z_3 gives reverberation noise at $z = z_1 + z_3$ according to Sec. 1.3.1. The reverberation component with scattering at z_1 first (Class a) gets a propagation delay as would a first order signal with scattering at z_1. This delay is denoted $\tau_{\mathrm{x}}(z_1)$. The other component (Class b) get a delay $\tau_{\mathrm{x}}(z_3)$. The observant reader will observe a potential problem. In Sec. 2.3 the reverberation delay was given by a single value for each time, $\tau_{\mathrm{n}}(t)$. However, the delay is low, 20 ns (see paper B), compared to the HF pulse period of $1/8$ MHz $= 125$ ns. The delay of the reverberation components can therefore be considered as an average delay. To calculate this average delay the signals can be assumed to be single band and infinite length giving (removing the RF oscillations)

$$n_p(t)\mathrm{e}^{-i\omega t} = \mathrm{e}^{-i\omega\tau_\mathrm{x}(z_1)} + \mathrm{e}^{-i\omega\tau_\mathrm{x}(z_3)}, \tag{2.19}$$

$$= \mathrm{e}^{-i\omega\frac{\tau_\mathrm{x}(z_1)+\tau_\mathrm{x}(z_3)}{2}} \cdot \left(\mathrm{e}^{-i\omega\frac{\tau_\mathrm{x}(z_1)-\tau_\mathrm{x}(z_3)}{2}} + \mathrm{e}^{+i\omega\frac{\tau_\mathrm{x}(z_1)-\tau_\mathrm{x}(z_3)}{2}}\right), \tag{2.20}$$

$$= \mathrm{e}^{-i\omega\frac{\tau_\mathrm{x}(z_1)+\tau_\mathrm{x}(z_3)}{2}} 2i\sin\left(\omega\frac{\tau_\mathrm{x}(z_1)-\tau_\mathrm{x}(z_3)}{2}\right). \tag{2.21}$$

The last term is just an amplitude so the end delay of the total pulse is (perhaps unsurprisingly) the arithmetic average of the delay of the two components.

2.6.1 Simple estimator

With a linear shape of the first order nonlinear propagation delay, $\tau_\mathrm{x}(z) = \nu z$ the reverberation delay becomes equal to the first order propagation delay at half depth

$$\tau_\mathrm{n}(z) = \frac{\tau_\mathrm{x}(z_1)+\tau_\mathrm{x}(z_3)}{2}, \tag{2.22a}$$

$$= \nu(z_1+z_3)/2, \tag{2.22b}$$

$$= \nu z/2, \tag{2.22c}$$

$$= \tau_\mathrm{x}(z/2). \tag{2.22d}$$

The last result defines the simple fixed-relation estimator,

$$\tau_\mathrm{n}^\mathrm{h}(z) \triangleq \tau_\mathrm{x}(z/2). \tag{2.23}$$

2.6.2 Adaptive estimator

The simple fixed-relation reverberation delay estimator of Eq. (2.23) includes a set of assumptions: 1) The first order delay is linear; and 2) Class a and b reverberation components have equal strength. Breakdown of any of these two assumptions would lead to a scatterer dependent reverberation delay. In other words it would be necessary to write $\tau_\mathrm{n}(z) \to \tau_\mathrm{n}(z; z_1)$. This is the main result presented in paper B. In this paper a solution is given by development of a signal adaptive reverberation delay estimation. A short summary is presented in this section.

When the imaging pulse (HF) propagates nonlinearly, energy is moved from the base band up to higher harmonic bands. This is utilized in for example tissue harmonic imaging (THI), but here, this energy is lost as the received pulse is subjected to a bandpass filter around the transmitted frequency. The loss of energy due to nonlinear propagation is here called *nonlinear attenuation*. After the pulse is scattered, the amplitude is assumed to drop so much that further nonlinear attenuation loss can be neglected. Let α^{z_1} be the nonlinear attenuation of the imaging pulse at depth z_1, where z_1 is the depth of the first scattering event. Note that this gives a pulse amplitude difference between Class a and b reverberations. Check Fig. B.8 to see how a value for α was found in paper B.

Let $R(z)$ be the estimated scatterer strength at depth z. This estimate is based on the envelope of the received signal and is used to adapt the reverberation delay to the estimated position, and origin, of the scatterers in the medium. It would be beneficial to steer the estimated reverberation delay towards the delay of the strongest reverberations as these are the most damaging to the resulting image. A parameter, γ is therefore introduced as an exponent to $R(z)$ making the strongest reflections stand out more. The estimated scatterer strength used in the adaptive reverberation delay estimation is thus $R^\gamma(z)$ for a depth z. See Sec. B.8.4 in paper B for a more in depth discussion around the choice of γ.

Introducing the modifications presented by nonlinear attenuation and the specificity towards strong scatterers to the estimated reverberation signal from a set of scatterers, Eq. (2.19), yields

$$\tau_{\mathrm{n}}(z_1, z_3) = \frac{-1}{\omega} \angle \Big\{ R^\gamma(z_1) R^\gamma(z_3) \alpha^{z_1} \mathrm{e}^{-i\omega\tau_{\mathrm{x}}(z_1)} \tag{2.24}$$

$$+ R^\gamma(z_3) R^\gamma(z_1) \alpha^{z_3} \mathrm{e}^{-i\omega\tau_{\mathrm{x}}(z_3)} \Big\}, \tag{2.25}$$

where the phase has been extracted and divided by the frequency to give the delay of the signal. Note how both Class a (z_1) and b (z_3) interact with the same scatterers in the medium and get the same total scattering strength. The difference between Class a and b comes from the difference in nonlinear attenuation, α^z. The scatterer strength comes into play when more than one pair of scatterers contribute to reverberation noise at a given depth. An integration of all possible scatterers is made in paper B which results in the integral (similar to Eq. (B.16))

$$\tau_{\mathrm{n}p}^{\mathrm{RR}}(z; \alpha, \omega_{\mathrm{c}}, \gamma)c \triangleq \frac{-1}{\omega_{\mathrm{c}}} \angle \int_0^z \mathrm{d}z_1 \; R^\gamma(z_1) R^\gamma(z - z_1) \alpha^{z_1} \mathrm{e}^{-i\omega_{\mathrm{c}}\tau_{\mathrm{x}p}(z_1)}. \tag{2.26}$$

Here the integration is done not over Class a and b pairs but over individual reverberation components. The frequency ω_{c} is the center frequency of the imaging pulse which is assumed to be constant.

2.7 Effect of center frequency tracking

With a nonzero width of the imaging frequency band and an attenuation that increases with frequency the center frequency of the imaging band will drop with propagation length.[4, p. 86] This is accounted for in the estimation of the total NPD, τ_{y} as described by Standal *et al.* [5] (see Sec. 2.5.1), but it is not accounted for in the reverberation delay estimation, τ_{n}, presented in paper B (and above in Eq. (2.26)) where a single constant center frequency is used throughout the signal. In this section the error of this assumption is evaluated.

2.7.1 Estimation of center frequency shift with depth

Firstly, how large is the drop in center frequency? A derivation loosely following that of Szabo[4, p. 87] is presented here. Assume a Gaussian band centered at ω_c and an attenuation as $\exp\left\{-\eta z \omega^\gamma\right\}$. The energy band then has the form

$$\left|U(\omega-\omega_\mathrm{c},z)\right|^2 = \left|U_0(\omega-\omega_\mathrm{c})\mathrm{e}^{-\eta z \omega^\gamma}\right|^2 \tag{2.27}$$

$$= \mathrm{e}^{-2\xi(\omega-\omega_\mathrm{c})^2-2\eta z \omega^\gamma}. \tag{2.28}$$

The parameter γ defines the dependence of frequency on the attenuation and, according to F. A. Duck, lies in the range of 1.0 to 1.5 for most soft tissue and biological fluids.[6, p. 112] From here and forward $\gamma = 1$ is assumed to ease the calculations. The bandwidth is defined by ξ and η is the attenuation coefficient. Allowing the attenuation do be depth dependent results in a z dependence of the attenuation coefficient, $\eta \to \eta(z)$. However, this dependence is omitted further on.

By finding the derivative of the energy band and setting it to zero the frequency corresponding to the peak energy can be found.

$$\left.\frac{\partial \left|U(\omega-\omega_\mathrm{c},z)\right|^2}{\partial \omega}\right|_{\omega=\omega_\mathrm{peak}} = 0, \tag{2.29}$$

$$\Downarrow$$

$$-4\xi(\omega_\mathrm{peak}-\omega_\mathrm{c}) - 2\eta z = 0, \tag{2.30}$$

$$\Downarrow$$

$$\omega_\mathrm{peak} = \omega_\mathrm{c} - \frac{\eta z}{2\xi}. \tag{2.31}$$

For the simulations in paper B the envelope of the pulses is defined as

$$u(t) = \mathrm{e}^{-\frac{2t^2}{T_\mathrm{p}}}. \tag{2.32}$$

Taking the Fourier transform of $u(t)$ an expression for ξ can be found.

$$\mathfrak{F}\left\{u(t)\right\} = \frac{\sqrt{\pi}}{2} T_\mathrm{p} \mathrm{e}^{-\frac{\omega^2 T_\mathrm{p}^2}{16}}, \tag{2.33}$$

Which, comparing to Eq. (2.28), gives $\xi = \left(\frac{T_\mathrm{p}}{4}\right)^2$, inserting this into the expression for the peak frequency (Eq. (2.31)) and rewriting to Hz yields

$$f_\mathrm{peak} = f_\mathrm{c} - 4\frac{\eta z}{\pi T_\mathrm{p}^2}. \tag{2.34}$$

The attenuation is generally given in units of dB/cmMHz. Represent this number by β such that

$$20\log_{10}\left(\exp\left(-\eta z\omega\right)\right) = -\beta. \tag{2.35}$$

Letting $z = 1$ cm, and $\omega = 2\pi 10^6$ gives

$$-\eta \cdot 10^{-2} \cdot 2\pi 10^6 = -\frac{\beta}{20}\ln\left(10\right), \tag{2.36}$$

and further

$$\eta = \frac{\beta}{4\pi} \cdot 10^{-5}\ln\left(10\right). \tag{2.37}$$

Setting $\beta = 0.5$ dB/cmMHz gives $\eta = 9.1617 \cdot 10^{-7}$. Inserting this and a pulse with 1.5 oscillations at 8 MHz, or $T_\mathrm{p} = 1.5/(8 \cdot 10^6)$, yields a drop of

$$\Delta f = -4\frac{\eta z}{\pi T_\mathrm{p}^2} = -0.03318 \ \text{MHz/mm}. \tag{2.38}$$

Propagation to 20 mm and back to the transducer gives a drop of $40 \cdot 0.03318 \approx 1.33$ MHz. And twice that, 2.65 MHz, for imaging at a depth of 40 mm. Increasing the length of the pulse reduces the shift in frequency. For comparison the shift when transmitting a pulse of pulse length of 2.5 oscillations leads to a modification of this result by a factor $(1.5/2.5)^2 = 0.36$.

2.7.2 Effect of erroneous center frequency in delay estimation

The center frequency of the signal changes with propagation depth, and the reverberation delay estimation uses the center frequency as input. But, does the change of the center frequency with depth significantly alter the reverberation delay estimation?

Introducing a depth dependent center frequency in the adaptive reverberation delay estimation, $\tau_\mathrm{n}^\mathrm{RR}$, from paper B yields

$$\tau_{\mathrm{n}p}^\mathrm{RR}(z) = \frac{-1}{\omega_\mathrm{peak}(z)}\angle\int_0^z \mathrm{d}z_1\, R^\gamma(z_1)\alpha^{z_1}\mathrm{e}^{i\omega_\mathrm{peak}(z)\tau_{\mathrm{x}p}(z_1)}R^\gamma(z-z_1). \tag{2.39}$$

The effect of this complication of the equation is readily checked by calculating the delay, $\tau_{\mathrm{n}p}^\mathrm{RR}$, using different, constant, center frequencies. In addition to a center frequency of 8 MHz as used in paper B, center frequencies of 5, 6 and 7 MHz are also computed. The relative change, calculated as

$$\frac{\tau_{\mathrm{n}p}^\mathrm{RR}(z;\mathrm{X\ MHz}) - \tau_{\mathrm{n}p}^\mathrm{RR}(z;8\ \mathrm{MHz})}{\tau_{\mathrm{n}p}^\mathrm{RR}(z;8\ \mathrm{MHz})}, \tag{2.40}$$

is plotted in Fig. 2.8. The result is a relative change in the order of 0.1 %. It is therefore possible to say with confidence that a depth depended center frequency does not change the estimated reverberation delay significantly.

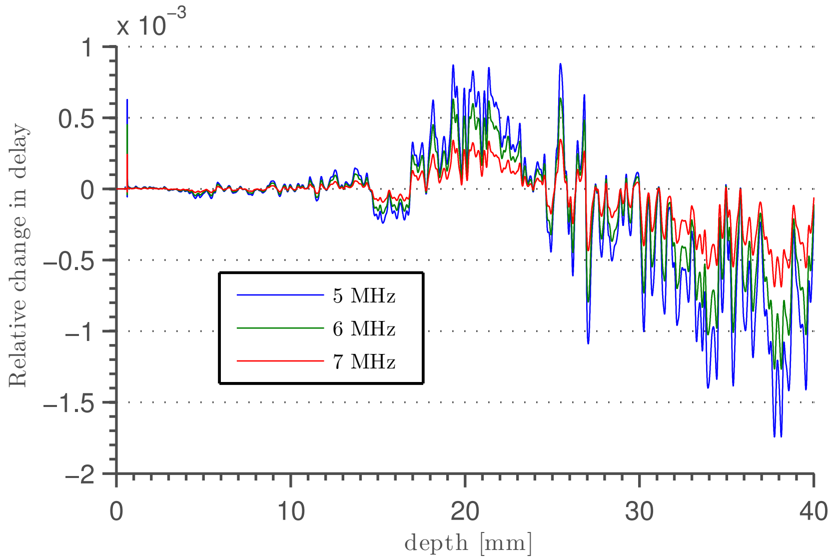

Figure 2.8: The effect of changing the center frequency used in the estimation of the reverberation delay using the adaptive method Eq. (B.16).

2.7.3 Effect on gain factor in correction

The gain factor in the DCS method is frequency dependent. Altering this gain does not change the SRR as this gain is equal for both the signal and the reverberation noise. However, an error in this gain would result in an uneven signal strength with depth in the image. Here, this effect is evaluated by calculating the gain under different center frequencies.

From paper B the gain factor is calculated as

$$G = \left| \mathrm{e}^{i\omega_{\mathrm{c}}(\tau_{\mathrm{x}+} - \tau_{\mathrm{n}+})} - \mathrm{e}^{i\omega_{\mathrm{c}}(\tau_{\mathrm{x}-} - \tau_{\mathrm{n}-})} \right|, \tag{2.41}$$

where the time (depth) dependence of the delays have been omitted. To get a clear and simple estimation assume now that the sign of the delays are flipped when flipping the sign of the polarity of the LF pulse. As makes sense from Eq. (B.16),

$$\tau_{\mathrm{x}+} = -\tau_{\mathrm{x}-} \quad \text{and} \tag{2.42a}$$

$$\tau_{\mathrm{n}+} = -\tau_{\mathrm{n}-}. \tag{2.42b}$$

This yields

$$G = 2\cos\left(\omega_{\mathrm{c}} \frac{\tau_{\mathrm{x}+} - \tau_{\mathrm{n}+}}{2}\right). \tag{2.43}$$

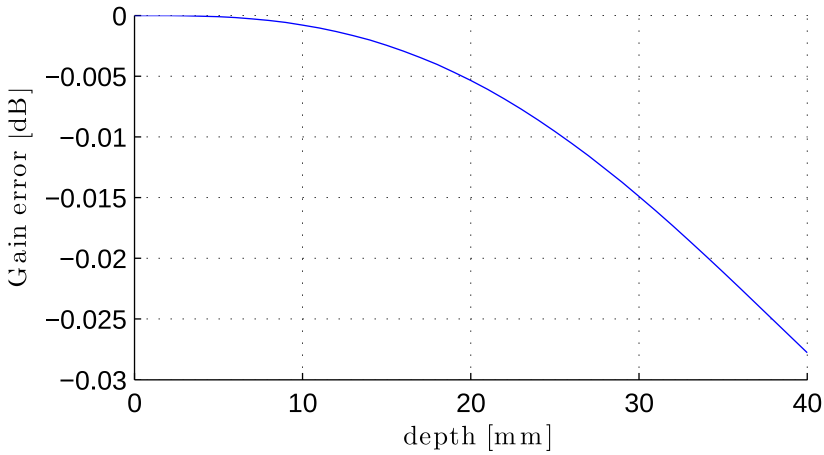

Figure 2.9: Error in DCS gain with constant compared to varying center frequency with depth.

Assume that the first order delay and reverberation delay are linear, $\tau_{x+} = \nu z$ and $\tau_{n+} = \nu z/2$, and define $\delta\omega = 2\pi\Delta f(z)/z$. The error in gain with depth can then be estimated as

$$20\log_{10}\left(\frac{\cos\left(\omega_c \nu z/4\right)}{\cos\left((\omega_c + \delta\omega z)\nu z/4\right)}\right) \tag{2.44}$$

The result is shown in Fig. 2.9 assuming $\nu = 1$ ns/mm and $\Delta f/z = -0.03318$ MHz/mm as in Sec. 2.7.1 and shows a depth varying frequency gain error of 0.03 dB at 40 mm. The added complexity of adding a center frequency shift in the gain correction of the DCS method does therefore not seem necessary as the error in the gain is extremely low.

2.7.4 Conclusion

The effect of tracking the center frequency with the processing in paper B is negligible. The effect on the reverberation delay estimation is in the order or 0.1 % and the effect on the depth varying gain factor in the delay corrected subtraction correction is below 0.04 dB.

2.8 Time shift invariance

The zero polarity signal is defined as the reference signal from which all nonlinear propagation delays are based. In this section the mathematics are laid out for the case when the reference signal is given an arbitrary time varying delay. It might already be clear to the reader that such a time shift of the defined reference should have no apparent effect on the result after DCS suppression as the only concern for DCS is the time *difference* between signal components. One would, however, expect a time shift of the estimated first order signal in the end.

The time shift can be made general by first assuming a different error on the NPD of all signal components. Written out the transformation is defined,

$$\hat{\tau}_{\mathrm{x}+}(t) = \tau_{\mathrm{x}+}(t) + \epsilon_{\mathrm{x}+}(t), \quad \text{and} \tag{2.45a}$$
$$\hat{\tau}_{\mathrm{x}-}(t) = \tau_{\mathrm{x}-}(t) + \epsilon_{\mathrm{x}-}(t), \tag{2.45b}$$

and for the reverberation delays

$$\hat{\tau}_{\mathrm{n}+}(t) = \tau_{\mathrm{n}+}(t) + \epsilon_{\mathrm{n}+}(t), \quad \text{and} \tag{2.46a}$$
$$\hat{\tau}_{\mathrm{n}-}(t) = \tau_{\mathrm{n}-}(t) + \epsilon_{\mathrm{n}-}(t). \tag{2.46b}$$

For a simpler notation the time dependence of the delays and errors in delays are not explicitly written out further on. As before, no PFD or speckle variations is assumed and the only difference between the first order and reverberation components between different polarities is a delay in time,

$$y_{+}(t) = x_0(t - \tau_{\mathrm{x}+}) + n_0(t - \tau_{\mathrm{n}+}) \quad \text{and} \tag{2.47a}$$
$$y_{-}(t) = x_0(t - \tau_{\mathrm{x}-}) + n_0(t - \tau_{\mathrm{n}-}). \tag{2.47b}$$

The DCS correction can be done with erroneous delays which gives

$$\begin{aligned}\hat{x}_0(t) &= y_{+}(t + \hat{\tau}_{\mathrm{n}+}) - y_{-}(t + \hat{\tau}_{\mathrm{n}-}),\\ &= \quad x_0(t - \tau_{\mathrm{x}+} + \hat{\tau}_{\mathrm{n}+}) - x_0(t - \tau_{\mathrm{x}-} + \hat{\tau}_{\mathrm{n}-})\\ &\quad + n_0(t - \tau_{\mathrm{n}+} + \hat{\tau}_{\mathrm{n}+}) - n_0(t - \tau_{\mathrm{n}-} + \hat{\tau}_{\mathrm{n}-}).\end{aligned}$$

And by inserting Eqs. (2.45a) and (2.45b) in the reverberation noise components,

$$\begin{aligned}\hat{x}_0(t) = x_0(t - \tau_{\mathrm{x}+} + \hat{\tau}_{\mathrm{n}+}) - x_0(t - \tau_{\mathrm{x}-} + \hat{\tau}_{\mathrm{n}-})\\ + n_0(t + \epsilon_{\mathrm{n}+}) - n_0(t + \epsilon_{\mathrm{n}-}),\end{aligned} \tag{2.48}$$

it is observed that under the condition

$$\epsilon_{\mathrm{n}+}(t) = \epsilon_{\mathrm{n}-}(t), \tag{2.49}$$

the reverberation noise is canceled. An equal time shift of the estimated reverberation NPDs thus has no effect on the reverberation suppression. This would be expected as the DCS method is only concerned with the relative delay between the signals.

The first order component can be estimated through Eq. (2.48) by first converting to the Fourier domain and assuming that Eq. (2.49) holds. The procedure is equal to that in paper B and yields

$$\hat{X}_{i0}(\omega) = Y_{i+}(\omega)\mathrm{e}^{-i\omega\hat{\tau}_{\mathrm{n}+}(t)} - Y_{i-}(\omega)\mathrm{e}^{i\omega\hat{\tau}_{\mathrm{n}-}(t)} \tag{2.50}$$

$$= X_{i0}(\omega)\left(\mathrm{e}^{i\omega(\tau_{\mathrm{x}+}(t)-\hat{\tau}_{\mathrm{n}+}(t))} - \mathrm{e}^{i\omega(\tau_{\mathrm{x}-}(t)-\hat{\tau}_{\mathrm{n}-}(t))}\right). \tag{2.51}$$

The result is a gain to the first order signal. Correcting for this with an errourous first order delay estimation yields

$$\hat{X}_{i0}(\omega) = X_{i0}(\omega)\frac{\mathrm{e}^{i\omega(\tau_{\mathrm{x}+}-\hat{\tau}_{\mathrm{n}+})} - \mathrm{e}^{i\omega(\tau_{\mathrm{x}-}-\hat{\tau}_{\mathrm{n}-})}}{\mathrm{e}^{i\omega(\hat{\tau}_{\mathrm{x}+}-\hat{\tau}_{\mathrm{n}+})} - \mathrm{e}^{i\omega(\hat{\tau}_{\mathrm{x}-}-\hat{\tau}_{\mathrm{n}-})}} \tag{2.52}$$

$$= X_{i0}(\omega)\frac{\mathrm{e}^{i\omega(\tau_{\mathrm{x}+}-\hat{\tau}_{\mathrm{n}+})} - \mathrm{e}^{i\omega(\tau_{\mathrm{x}-}-\hat{\tau}_{\mathrm{n}-})}}{\mathrm{e}^{i\omega\epsilon_{\mathrm{x}+}}\mathrm{e}^{i\omega(\tau_{\mathrm{x}+}-\hat{\tau}_{\mathrm{n}+})} - \mathrm{e}^{i\omega\epsilon_{\mathrm{x}-}}\mathrm{e}^{i\omega(\tau_{\mathrm{x}-}-\hat{\tau}_{\mathrm{n}-})}}. \tag{2.53}$$

Assuming equal errors for the first order NPDs,

$$\epsilon_{\mathrm{x}+}(t) = \epsilon_{\mathrm{x}-}(t), \tag{2.54}$$

enables a major simplification of Eq. (2.53),

$$\hat{X}_{i0}(\omega) = X_{i0}(\omega)\mathrm{e}^{-i\omega\epsilon_{\mathrm{x}+}}. \tag{2.55}$$

The result is a time shift when converted to the time domain,

$$\hat{x}_0(t) = x_0(t - \epsilon_{\mathrm{x}+}(t)). \tag{2.56}$$

As the correction algorithm is designed to find the first order signal with zero delay, shifting the defined zero point with $\epsilon_{\mathrm{x}+}$ also shifts the result of the algorithm with the same amount. In other words it is possible to define the zero delay signal however wanted and the result of the DCS correction will be an estimated first order signal positioned at this zero point. However, the result presented here is even less strict as it doesn't require any dependence between $\epsilon_{\mathrm{x}+}, \epsilon_{\mathrm{x}-}$ and $\epsilon_{\mathrm{n}+}, \epsilon_{\mathrm{n}-}$ as would be the case with a coordinate substitution in time.

2.8.1 Direct plus-minus delay estimation

It has been shown that one can define a shift in the definition of the NPDs without affecting the reverberation suppression. This makes it possible to handle one of the non-zero polarity signals as the reference signal used when computing the nonlinear propagation delays. One question which quickly arises is if the reverberation delay can be estimated the same was as before under this coordinate substitution in time. The problem can be formulated mathematically through the definitions above. Let

$$\epsilon_{\mathrm{x}+} = \epsilon_{\mathrm{x}-} = -\tau_{\mathrm{x}-}, \quad \text{and} \tag{2.57a}$$

$$\epsilon_{\mathrm{n}+} = \epsilon_{\mathrm{n}-} = -\tau_{\mathrm{n}-}. \tag{2.57b}$$

This holds the assumptions of Eqs. (2.49) and (2.54) giving the result in Eq. (2.56). Written out the new NPDs become

$$\tau_{\mathrm{x}+} \rightarrow \tau_{\mathrm{x}+} - \tau_{\mathrm{x}-}, \tag{2.58a}$$

$$\tau_{\mathrm{x}-} \rightarrow 0, \tag{2.58b}$$

$$\tau_{\mathrm{n}+} \rightarrow \tau_{\mathrm{n}+} - \tau_{\mathrm{n}-}, \quad \text{and} \tag{2.58c}$$

$$\tau_{\mathrm{n}-} \rightarrow 0. \tag{2.58d}$$

It is straightforward to show that the direct-relation reverberation delay estimator $\tau_{\mathrm{n}}^{\mathrm{h}}(z) = \tau_{\mathrm{x}}(z/2)$ holds under this time shift. If $\tau_{\mathrm{x}}(z/2) = \tau_{\mathrm{n}}(z)$ holds for both the plus and minus polarity then it should also hold for the sum of the delays, $\tau_{\mathrm{x}+}(z/2) + \tau_{\mathrm{x}-}(z/2) = \tau_{\mathrm{n}+}(z) + \tau_{\mathrm{n}-}(z)$. When this simple estimator is used it is thus possible to do the delay estimation directly between the plus and minus signals without going through the zero polarity signal. The small time shift in the resulting estimated first order signal can be ignored or corrected for by $\left(\tau_{\mathrm{x}+}(z) + \tau_{\mathrm{x}-}(z)\right)/2$.

A direct delay estimation between the plus and minus polarity signals is not as straight forward when the adaptive reverberation delay estimator, $\tau_{\mathrm{n}}^{\mathrm{RR}}$, is utilized. For a simpler discussion assume that the magnitude of the delays are equal between polarities, $|\tau_{\mathrm{x}+}| = |\tau_{\mathrm{x}-}|$ and $|\tau_{\mathrm{n}+}| = |\tau_{\mathrm{n}-}|$. Following the transformation in Eq. (2.58a) the result is a doubling of the first order delay

$$\tau_{\mathrm{x}+} \rightarrow 2\tau_{\mathrm{x}+}. \tag{2.59}$$

Following the definition of $\tau_{\mathrm{n}}^{\mathrm{RR}}$ in paper B this represents a doubling of the center frequency used in the estimation,

$$\tau_{\mathrm{n}+}^{\mathrm{RR}}(z; \omega_{\mathrm{c}}, 2\tau_{\mathrm{x}+}) = \frac{-1}{\omega_{\mathrm{c}}} \angle \int_0^z \mathrm{d}z_1 \, R^{\gamma}(z_1) \alpha^{z_1} \mathrm{e}^{-i\omega_{\mathrm{c}} 2\tau_{\mathrm{x}+}(z_1)} R^{\gamma}(z - z_1), \tag{2.60}$$

or,

$$\tau_{\mathrm{n}+}^{\mathrm{RR}}(z; 2\omega_{\mathrm{c}}, \tau_{\mathrm{x}+}) = \frac{-1}{2\omega_{\mathrm{c}}} \angle \int_0^z \mathrm{d}z_1 \, R^{\gamma}(z_1) \alpha^{z_1} \mathrm{e}^{-i2\omega_{\mathrm{c}} \tau_{\mathrm{x}+}(z_1)} R^{\gamma}(z - z_1). \tag{2.61}$$

This shows that

$$2\tau_{\mathrm{n}+}^{\mathrm{RR}}(z; 2\omega_{\mathrm{c}}, \tau_{\mathrm{x}+}) = \tau_{\mathrm{n}+}^{\mathrm{RR}}(z; \omega_{\mathrm{c}}, 2\tau_{\mathrm{x}+}). \tag{2.62}$$

However, here we are interested to see if

$$\tau_{\mathrm{n+}}^{\mathrm{RR}}(z;\omega_{\mathrm{c}},2\tau_{\mathrm{x+}}) \stackrel{?}{=} 2\tau_{\mathrm{n+}}^{\mathrm{RR}}(z;\omega_{\mathrm{c}},\tau_{\mathrm{x+}}). \tag{2.63}$$

Which would make Eq. (2.57) and the result from the previous section hold. Using Eq. (2.62) this is equivalent to prove that

$$\tau_{\mathrm{n+}}^{\mathrm{RR}}(z,2\omega_{\mathrm{c}},\tau_{\mathrm{x+}}) \stackrel{?}{=} \tau_{\mathrm{n+}}^{\mathrm{RR}}(z,\omega_{\mathrm{c}},\tau_{\mathrm{x+}}). \tag{2.64}$$

Equation (2.64) implies a frequency invariance of the reverberation delay estimation. This was already tested above in Sec. 2.7. The result was that there indeed was a center-frequency dependence. It was shown to be small, but it still disproves Eq. (2.64) and by extension Eq. (2.63). The conclusion is that it is not mathematically sound to estimate the reverberation delay directly based on only the non-zero polarity signals through the adaptive estimator presented in paper B. For a practical application however, it seems reasonable as the center frequency dependence is so low.

2.9 Is a polarity specific nonlinear attenuation parameter needed in the reverberation delay estimation?

In paper B it was mentioned that the plus, minus and zero polarity pulses exhibited different nonlinear attenuation. However, in the estimation of the reverberation NPD, the same parameter for nonlinear attenuation was used for both the plus and minus polarity signals. A discussion follows here for why this simplification is justifiable.

The most direct approach to see if a better suppression would have been possible by finding an optimal nonlinearity parameter for the reverberation NPD estimation for both the plus and minus polarity signals, is to do a numerical study and look at the results. DCS processing was carried out with 46 different values for the nonlinearity parameter, α, in the $\tau_{\mathrm{n}}^{\mathrm{RR}}$ estimation. All $46 \cdot 46$ permutations where then DCS processed 300 times on sets of random scatterers corresponding to "case I" from paper B. The SRR gain was evaluated and averaged between 5 and 39 mm and is plotted in Fig. 2.10. The plot shows that there are relatively no gain to be found in tailoring the nonlinearity parameter to each polarity. The simplification in paper B seems reasonable.

The effect of the nonlinearity parameter, α in the reverberation NPD estimation can shed some light on why just one parameter is needed. A higher value for α would put more weight on the NPD of the Class Ia reverberation component. As this component has a lover NPD than Class Ib the result is a lowering of the estimated reverberation NPD. Thus, by having an undershoot of the parameter on

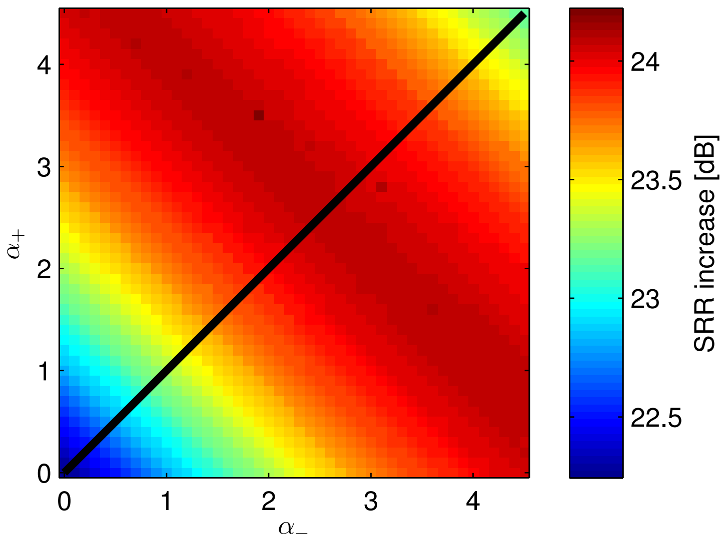

Figure 2.10: Signal to Reverberation noise Ratio (SRR) improvement for the case I medium from paper B with varying values for the nonlinear attenuation parameter α in the reverberation delay estimation $\tau_{\mathrm{n}}^{\mathrm{RR}}$. 46 values for α is used for the plus, α_+, and minus, α_-, polarity signals. The corrections for each parameter set is run on 300 sets of random scatterers totaling to 634'800 scan lines. The black line through the plot shows where $\alpha_+ = \alpha_-$. The values on the axes show dB drop at 40 mm ($20\log_{10}(\alpha^{40\text{ mm}})$).

both the plus and minus polarity delay estimation would result in an erroneous estimated separation between the reverberation components. As discussed earlier the main idea behind the delay corrected subtraction method to suppress reverberation is to align the reverberation components of different signal on top of each other and then subtract. However, with an overshoot on one polarity and an undershoot on the other the relative shift between the reverberation components can still be zero. The end result is a time shift, which discussed in Sec. 2.8 has no impact on the reverberation suppression.

As an undershoot, or overshoot, on the nonlinearity parameters used in *both* polarities is damaging, but the suppression is not destroyed by an overshoot on one polarity and a corresponding undershoot on the other, it is possible to find a common suitable nonlinearity parameter, α. However, the effect of α is determined by the shape of the first order NPD and this nonlinear dependence leaves the author uncertain if the argument used here also holds mathematically looking at the definition of $\tau_{\mathrm{n}}^{\mathrm{RR}}$. Figure 2.10 does indeed show small variations, and it seems that a better combination of nonlinearity parameters are found with α_- at around 2 dB at 40 mm and α_+ at around 3.5 dB at 40 mm. However, this effect seems very small and the author does not believe this should be a main area of focus for future study.

2.10 Simulations with realistic pulses and true NPD

The simulations in paper B were done with Gaussian pulses. This choice was made so that the simulations would be easier to reproduce by other researchers. It also introduced less parameters in the setup as true ultrasound pulses would be dependent on the hardware used to generate the pulses. However, to study if the results in the paper would hold up with more realistic pulses some of the simulations were re-done. Pulses generated in Xtrans[7] were provided by Ola Finneng Myhre and were based after the "Vora-2" probe used in other DBI experiments within the research group (see Fig. 2.11). The generated pulses exhibit more ringing than the Gaussian pulses. This is countered by using 1.5 oscillations instead of 2.5 as used for the Gaussian pulses. Otherwise the maximum amplitudes of the Xtrans HF and LF pulses are normalized to 0.5 MPa to correspond to the Gaussian pulses used in paper B.

With the point of this section being to see if the results from paper B holds up when moving towards a real world scenario the reverberation suppression was also tested with the real NPDs from the pulse simulations. Figure 2.12 shows the SRR increase in a medium corresponding to "case I" and "case II" from paper B where the scatterer strengths are following a Gaussian distribution with a Poisson distributed distance between them. Figure 2.12(b) corresponds to "case I" where the first order NPD is synthetically set to being linear and Fig. 2.12(c) corresponds

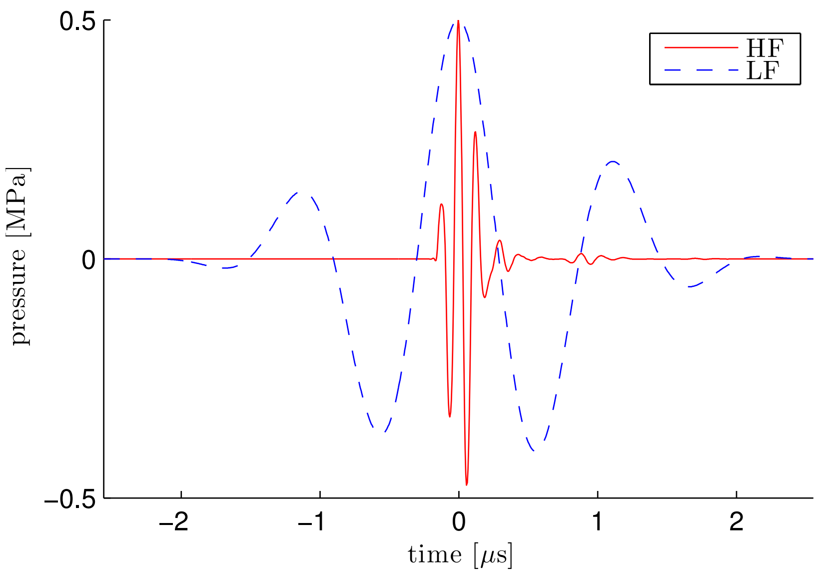

Figure 2.11: HF and LF pulses generated in Xtrans based on the Vora-2 probe design. The LF wave is the plus polarity.

Table 2.1: Correspondence between figures in Sec. 2.10 and tissue cases in paper B

Figure in Sec. 2.10	Case from paper B	Figure in paper B
2.12(a)	-	-
2.12(b)	I	B.3
2.12(c)	II	B.4
2.13(a)	-	-
2.13(b)	III	B.5
2.13(c)	IV	B.6

to "case II" where the first order NPD is piecewise linear with a 50 % reduction in the gradient between 15 and 25 mm. Figure 2.12(a) shows the result with the same scatterers but with a first order NPD determined by the simulation of the pulses. Figure 2.13 shows the same set of graphs for a medium where the scatterer strength is reduced between 15 and 25 mm corresponding to case III and IV in paper B. Table 2.1 gives an overview of how the subfigures in Figs. 2.12 and 2.13 correspond to figures in paper B.

The discussion around the SRR result of the different tissue cases will not be repeated here, but what is noted is that the results with the Xtrans based pulse exhibit the same trends as the results from the Gaussian pulses. The author is

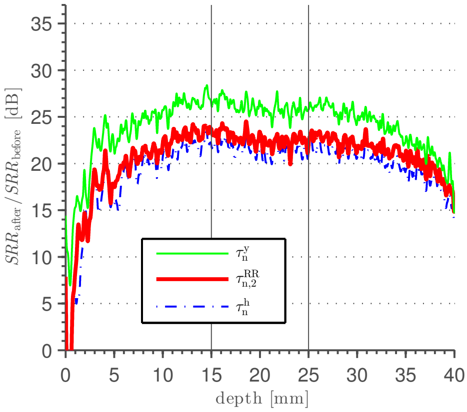

(a) True delay

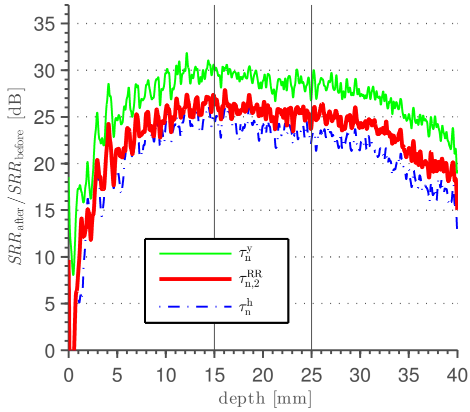

(b) Linear delay (Case I).

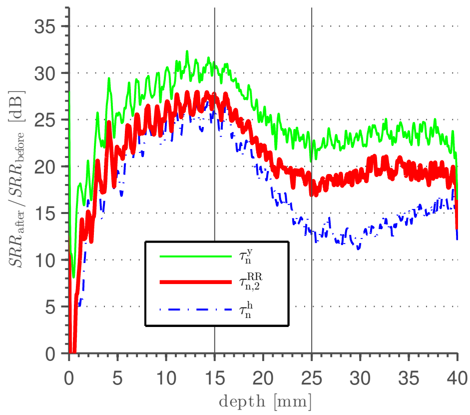

(c) Piecewise linear delay (Case II).

Figure 2.12: Signal to reverberation noise ratio increase after SURF processing on signals with Xtrans generated pulses. Uniform mean scattering strength throughout plots.

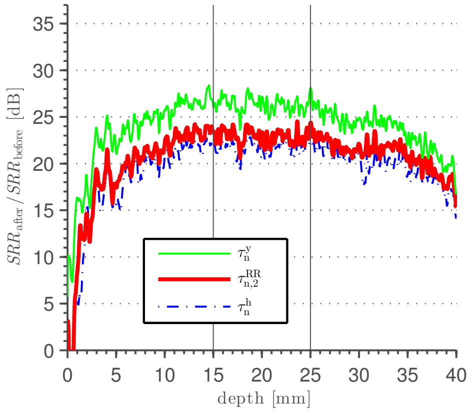

(a) True delay

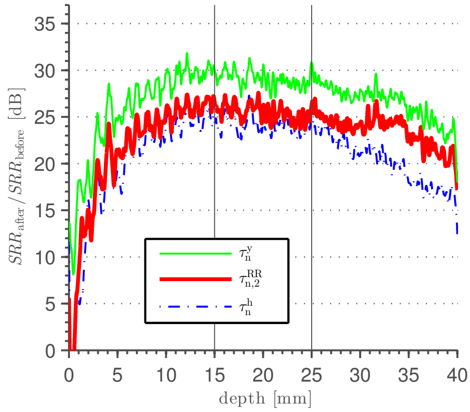

(b) Linear delay (Case III).

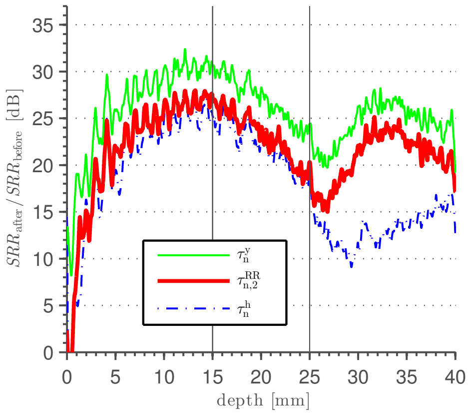

(c) Piecewise linear delay (Case IV).

Figure 2.13: Signal to reverberation noise ratio increase after SURF processing on signals with Xtrans generated pulses. Mean Gaussian scattering strength reduced to 20 % between 15 and 25 mm.

therefore confident that the results from paper B can be readily extended to hold for more realistic pulse shapes as well.

The simulations where the real simulated NPD is used instead of a synthetically applied one seems to support the claim in paper B that the shape of the first order NPD plays a large role in the possible SRR increase. The first order NPD of the Xtrans pulses, as shown in Fig. 2.14, is not optimized for a linear development of the first order NPD. The effect of this first order NPD shape is seen by comparing Figs. 2.12(a) and 2.12(b) (and Figs. 2.13(a) and 2.13(b)). The drop in SRR due to the irregular first order NPD is between 2 and 5 dB for the entire plot.

2.11 Alternative reverberation delay estimates

2.11.1 Mean based estimators

The adaptive delay estimate $\tau_{\mathrm{n}}^{\mathrm{RR}}$ integrates all possible reverberation components to give a mean value at a given depth. First order delays used as input is weighted with the assumed strength of each component, $\hat{R}(z_1)\hat{R}(z - z_1)$, where $\hat{R}(z)$ is the scatterer strength at depth z. A first step simplification of this estimator could be to assume uniform scatterer strength throughout the medium resulting in a unweighted mean first order delay as the estimated reverberation delay.

Phaser mean

The phaser mean, $\tau_{\mathrm{n}p}^{\mathrm{e}\langle\rangle}$ is derived by simply removing the scatterer weights in the adaptive estimator $\tau_{\mathrm{n}p}^{\mathrm{RR}}$. It still treats the sum of reverberation component delays as complex phases and is as such still frequency dependent. But only slightly, as discussed in Sec. 2.7.2. The estimator is defined as

$$\tau_{\mathrm{n}p}^{\mathrm{e}\langle\rangle}(z) \triangleq \frac{-1}{\omega_{\mathrm{c}}} \angle \int_0^z \mathrm{d}z_1 \, \mathrm{e}^{-i\omega_{\mathrm{c}}\tau_{\mathrm{x}p}(z_1)}. \tag{2.65}$$

Arithmetic mean

Realizing that the center frequency plays little to no role in the estimation of the reverberation delay (see Sec. 2.7.2) a further simplification from Eq. (2.65) is achieved by simply taking the arithmetic mean of the first order delays up to the imaging depth z,

$$\tau_{\mathrm{n}p}^{\langle\rangle}(z) \triangleq \frac{1}{z} \int_0^z \mathrm{d}z_1 \, \tau_{\mathrm{x}p}(z_1) \tag{2.66}$$

2.11.2 Half value estimator

Following the same assumptions as for the fixed-relation simple estimator $\tau_{\mathrm{n}}^{\mathrm{h}}(z) = \tau_{\mathrm{x}}(x)$, namely a linear first order delay development and equal strengths of Class a

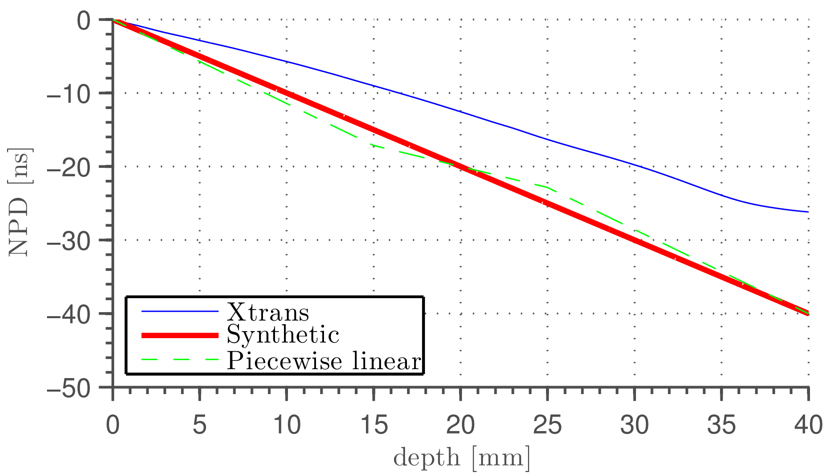

(a) First order NPD development with depth.

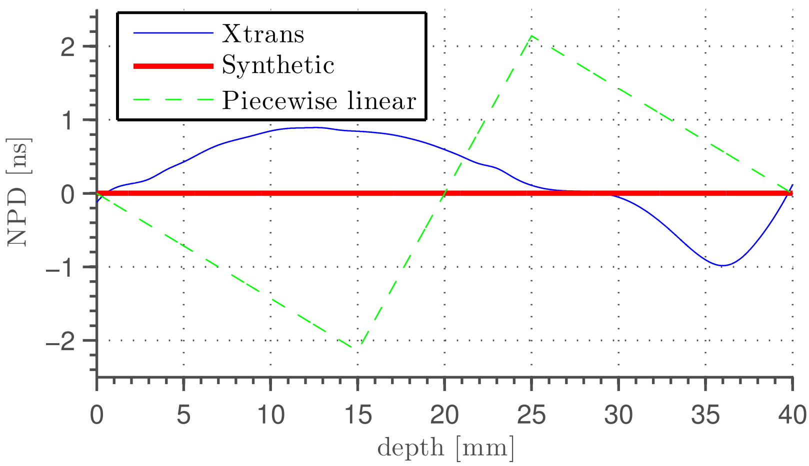

(b) De-trended version of **(a)**.

Figure 2.14: First order NPD comparison between the real delay based on simulation of Xtrans pulses and the synthetic delays used in paper B.

and b scattering one could as easily arrive at

$$\tau_{\mathrm{n}p}^{\mathrm{hv}}(z) \triangleq \tau_{\mathrm{x}}(z)/2. \tag{2.67}$$

With $\tau_{\mathrm{x}p}(z) = \nu z$, the result is the same for

$$\tau_{\mathrm{n}p}^{\mathrm{hv}}(z) = \tau_{\mathrm{x}p}(z)/2 = \nu/2 \text{ and} \tag{2.68}$$

$$\tau_{\mathrm{n}p}^{\mathrm{h}}(z) = \tau_{\mathrm{x}p}(z/2) = \nu/2. \tag{2.69}$$

2.11.3 Bias as quality measure

As is shown in paper B the position of the scatterers in the medium changes the mean reverberation delay. For the comparison of different reverberation delay estimators uniformly distributed scatterers are therefore assumed. The phaser mean, $\tau_{\mathrm{n}p}^{\mathrm{e}\langle\rangle}(z)$, is used as a guide as to where the "proper" delay might lie. However, note that in some scatterer realizations, any of the other estimated might give a more correct answer than this guide. The aim here is not to find the best gain for a given scatterer realization, but rather the bias introduced by each of the estimation schemes. A uniform distribution of scatterers is defined to represent zero bias.

Assuming a fully linear first order delay, $\tau_{\mathrm{x}}(z) = \nu z$, leads to all reverberation delays estimators being equal. Examples with change in the gradient of the first order propagation delay will therefore be discussed.

2.11.4 Special case of convex or concave τ_{x}

Here the special case of convex or concave propagation delays are discussed. As the sign on the propagation delay depends on the polarity of the LF pulse and thus makes a convex propagation delay for a positive polarity a concave propagation delay for a negative polarity, let the definition of a "concave propagation delay" be based on a positive polarity LF pulse giving a negative value for the propagation delay, $\mathrm{sgn}(\tau_{\mathrm{x}+}) = -\mathrm{sgn}(\tau_{\mathrm{x}-}) = -1$.

A function, $\tau_{\mathrm{x}}(z)$, is defined as *midway concave* at the interval C if it follows

$$\tau_{\mathrm{x}}\left(\frac{z_1 + z_2}{2}\right) \geq \frac{\tau_{\mathrm{x}}(z_1) + \tau_{\mathrm{x}}(z_2)}{2}, \tag{2.70}$$

for a given set of coordinates $[z_1, z_2] \in C$. This is a weaker constraint than on true concave function. Defining $z_1 = 0$ is a further weakening of the criterion, which yields

$$\tau_{\mathrm{x}}\left(\frac{z}{2}\right) \geq \frac{\tau_{\mathrm{x}}(z)}{2}. \tag{2.71}$$

This again can readily be rewritten to

$$\tau_{\mathrm{n}p}^{\mathrm{h}}(z) \geq \tau_{\mathrm{n}p}^{\mathrm{hv}}(z). \tag{2.72}$$

A first order delay curve concave on the interval $[0, z]$ therefore leads to a higher reverberation delay estimate value from $\tau_{\mathrm{n}p}^{\mathrm{h}}$ compared to $\tau_{\mathrm{n}p}^{\mathrm{hv}}$. And vice versa for a convex first order delay development with depth. Further assuming a concave $\tau_{\mathrm{x}}(z)$ it can be shown that

$$\begin{aligned} \tau_{\mathrm{x}}(z/2) \geq \quad & \frac{1}{z}\int_0^z \tau_{\mathrm{x}}(z_1)\,\mathrm{d}z_1 \geq \quad \tau_{\mathrm{x}}(z)/2 \;\text{ or} \\ \tau_{\mathrm{n}p}^{\mathrm{h}}(z) \geq \quad & \quad \tau_{\mathrm{n}p}^{\langle\rangle}(z) \quad\quad \geq \quad\quad \tau_{\mathrm{n}p}^{\mathrm{hv}}(z), \end{aligned} \tag{2.73}$$

holds.

Proof of Eq. (2.73)

Start by proving the left side of Eq. (2.73) by rewriting to

$$\frac{z}{2}\tau_{\mathrm{x}}(z/2) - \int_0^{z/2} \tau_{\mathrm{x}}(z_1)\,\mathrm{d}z_1 \geq \int_{z/2}^{z} \tau_{\mathrm{x}}(z_1)\,\mathrm{d}z_1 - \frac{z}{2}\tau_{\mathrm{x}}(z/2). \tag{2.74}$$

Which can be contracted to

$$\int_0^{z/2} \mathrm{d}z_1 \int_{z_1}^{z/2} \mathrm{d}\xi\; \tau_{\mathrm{x}}'(\xi) \geq \int_{z/2}^{z} \mathrm{d}z_1 \int_{z/2}^{z_1} \mathrm{d}\xi\; \tau_{\mathrm{x}}'(\xi). \tag{2.75}$$

The integration regions are of equal size but the left side is over lower values of z_1 than the right. As $\tau_{\mathrm{x}}'(z_1)$ is higher at lower z_1 when τ_{x} is concave the inequality holds. For the right side of Eq. (2.73) use that $\tau_{\mathrm{x}}(0) = 0$ and write

$$\int_0^{z/2} \tau_{\mathrm{x}}(z_1)\,\mathrm{d}z_1 - \frac{z}{2}\tau_{\mathrm{x}}(0) \geq \frac{z}{2}\tau_{\mathrm{x}}(z) - \int_{z/2}^{z} \tau_{\mathrm{x}}(z_1)\,\mathrm{d}z_1. \tag{2.76}$$

In a similar fashion as Eq. (2.75) contract this to

$$\int_0^{z/2} \mathrm{d}z_1 \int_0^{z_1} \mathrm{d}\xi\; \tau_{\mathrm{x}}'(\xi) \geq \int_{z/2}^{z} \mathrm{d}z_1 \int_{z_1}^{z} \mathrm{d}\xi\; \tau_{\mathrm{x}}'(\xi). \tag{2.77}$$

The integrals again span the same length but over different values of z_1. The left side of the inequality integrates over lower values of z_1 where $\tau_{\mathrm{x}}'(z)$ is higher than at higher given that $\tau_{\mathrm{x}}(z)$ is concave. This proves the inequality Eq. (2.73). By changing the signs of the inequalities the same is proved for a convex function.

Discussion

As the final reverberation delay depends on the set of scatterers used, and other factors such as nonlinear attenuation, it is not possible to say a priori which of the estimates $\tau_{\mathrm{n}p}^{\mathrm{h}}$, $\tau_{\mathrm{n}p}^{\langle\rangle}$, or $\tau_{\mathrm{n}p}^{\mathrm{hv}}$ produce the most correct reverberation delay.

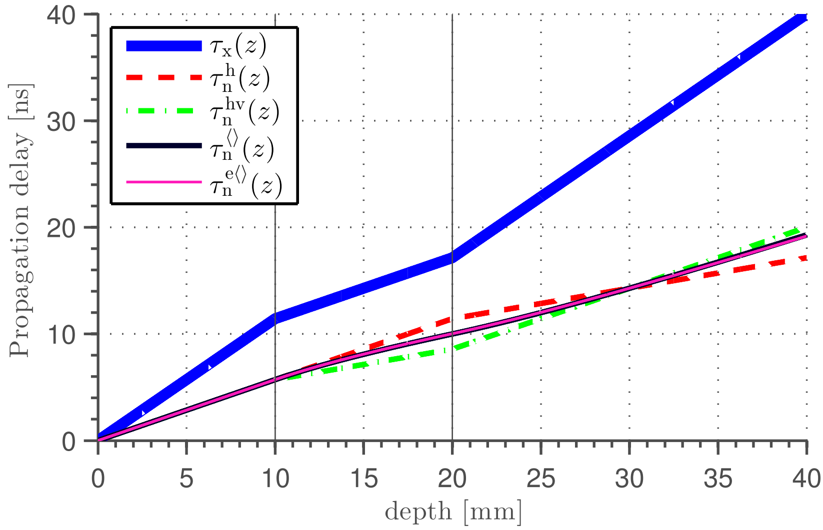

Figure 2.15: Comparison of different estimators for the reverberation delay τ_n. The effect of a blood vessel in surrounding fatty tissue is modeled by lowering the gradient of the propagation delay by 50 % between 10 and 20 mm. Note how $\tau_{np}^{\langle\rangle}(z)$ and $\tau_{np}^{e\langle\rangle}(z)$ are almost indistinguishable.

However, looking at the statistics of many ultrasound images a trend is found. Assuming equal probability for scatterers at any depth the mean based estimators will be more correct on average as their bias is zero. Following Eq. (2.73) $\tau_{np}^{h}(z)$ then leads to an overestimate while $\tau_{np}^{hv}(z)$ leads to an underestimate. Including nonlinear attenuation will lower the reverberation delay magnitude as scattering at shallow depths are weighted more. However, to be able to say something general about this case concerning the under or over estimate of the τ_{np}^{h} and τ_{np}^{hv} estimators a more in depth mathematical study is required.

How typical are concave or convex first order delays? In paper B a first order propagation delay piecewise linear with a reduction of the delay gradient of 50 % in a set interval is studied. This is to emulate the change in propagation delay when a blood vessel is present in the medium. Looking at the absolute value of the propagation delay (τ_{x-} or $|\tau_{x+}|$), τ_x is convex up to the end of the blood vessel. Figure 2.15 shows a similar example where the blood vessel is moved from what is used in paper B. The first order delay, $\tau_{x-}(z)$, is convex up to the end of the blood vessel inserted between 10 and 20 mm. Up to this point it is also shown that Eq. (2.73) holds as $\tau_{np}^{h} > \tau_{np}^{\langle\rangle} > \tau_{np}^{hv}$. This relation further holds down to 30 mm. The graph is no longer strict convex but a visual observation aids in the proof of Eq. (2.73). At 30 mm the mean gradient between 0 and $z/2 = 15$ mm and between

$z/2$ and $z = 30$ mm is equal as a line from $(0,0)$ to $(30, \tau_{\mathrm{x}}(30)$ passes through the point $(15, \tau_{\mathrm{x}}(15)$. Beyond this point the inequalities of Eq. (2.73) are switched, as is also observed in Fig. 2.15

Some methods for estimating the first order delay may automatically lead to a convex τ_{x}. An example is the estimation outlined in Sec. 2.5, and by Rau.[1] Shortly repeated here, the method in question finds the shortest path above the estimated total delay, $\tau_{\mathrm{y}}(z)$, from the point $\tau_{\mathrm{x}}(0) = 0$ to the max imaging depth $\tau_{\mathrm{y}}(z_{\max}) = \textit{some value}$. It should be evident upon inspection that this results in a convex function. For this estimation Eq. (2.73) will therefore always hold. As the actual first order delay is not known one should thread lightly when making generalizations on which estimator will work best in any setting. However, what *can* be said is that using this estimation scheme for the first order propagation delay will always lead to $\tau_{\mathrm{n}p}^{\mathrm{h}} \geq \tau_{\mathrm{n}p}^{\langle\rangle} \geq \tau_{\mathrm{n}p}^{\mathrm{hv}}$.

2.11.5 Difference between phaser means $\tau_{\mathrm{n}p}^{\langle\rangle}$ and $\tau_{\mathrm{n}p}^{\mathrm{e}\langle\rangle}$

As is seen from Fig. 2.15 the difference between the running mean of the first order delay with ($\tau_{\mathrm{n}p}^{\mathrm{e}\langle\rangle}$) or without ($\tau_{\mathrm{n}p}^{\langle\rangle}$) a complex phase in the calculation is very small. Just how small can be seen in Fig. 2.16 where $\tau_{\mathrm{n}p}^{\langle\rangle} - \tau_{\mathrm{n}p}^{\mathrm{e}\langle\rangle}$ is plotted. The plot shows a difference at most 0.1 ns for the case discussed in the previous section.

The effect of a 0.1 ns error can be extracted from Fig. A.4 in paper A. It shows that the effect of an increased error in the estimated delay is lower for higher errors. In other words, an addition of a 0.1 ns error in the reverberation delay estimation is only significant when the initial value is close to correct. With an error of 0.5 ns on the estimated delay, an addition of another 0.1 ns only reduces the increased SRR by 2 dB.

2.12 Pulse simulations and difference between the model in paper A and B

2.12.1 Setting up the pulse simulations

To create the full rf-signal for the processing in paper A and B one first need to simulate the required pulses. To generate the first order signal the pulses needs to be propagated nonlinearly out to the first scatterer and then linearly back to the transducer. Since all the scatterers are assumed to be planes, which does not modify the shape of the pulse, some shortcuts are possible. First, a start pulse is simulated out to the maximum depth of 40 mm where the simulations are stored for every mm. This leads to 40 pulses. Each of the stored pulses is then simulated linearly back to the transducer and saved to disc (or RAM). This procedure corresponds to step (1) and (2) of Fig. 2.17. The pulses are beamformed to generate pulses used for generation of the first order rf-signal.

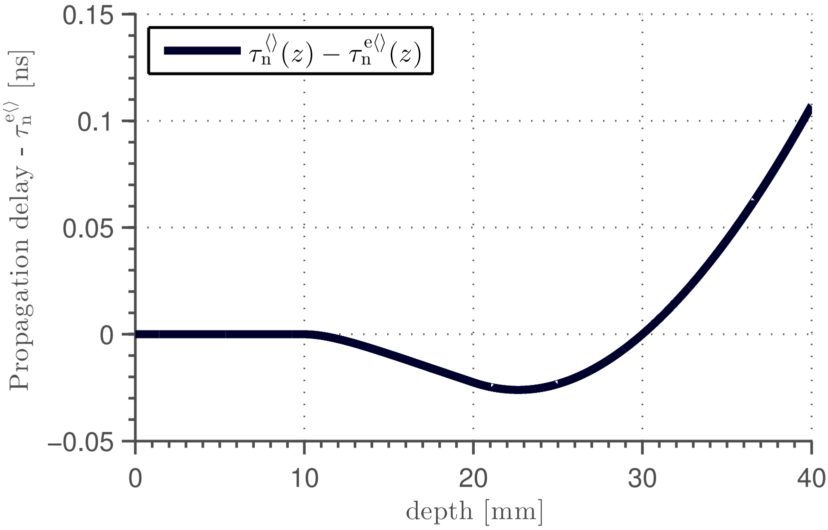

Figure 2.16: Deviation of $\tau_{\mathrm{n}p}^{\langle\rangle}$ compared to $\tau_{\mathrm{n}p}^{\mathrm{e}\langle\rangle}$ in ns.

The reverberation pulses are not only dependent on the total propagation path but also of the position of the first scattering event. To generate these pulses, the non-beamformed first order pulses can be utilized in order to save simulation time. A first order pulse is the same as the first propagation path of either Class Ia or Class Ib reverberation where the pulse is first propagated out to a scatterer and then returned to the transducer before it propagates another time out into the medium. The first order signal pulses are propagated in steps of 2 mm and then immediately beamformed and stored to disc (or RAM) until the total propagation path is twice the needed maximum imaging depth (here 80 mm). This corresponds to step (3) in Fig. 2.17. This procedure is the repeated for each z_1 until a complete set of pulses are generated (crosses in Fig. 2.17). As the second scatterer does not change the pulse in any way there is no distinction of whether the pulse is propagated towards or away from the transducer. The only important factor is the position of the first scatterer and the total propagation path.

2.12.2 Difference between simulation model in paper A and paper B

There is a slight difference between the algorithms to generate rf signals from pulses in paper A and B. Since paper B was written first the algorithm here is the original while the algorithm in paper A is an extension. The change lies in how the NPDs are handled. In paper B the NPDs are contained in the pulses. By convolving a time-shifted pulse with a set of scatterers an rf-signal is obtained with the same time-shift as in the pulse used. In paper A, however, the time-shift

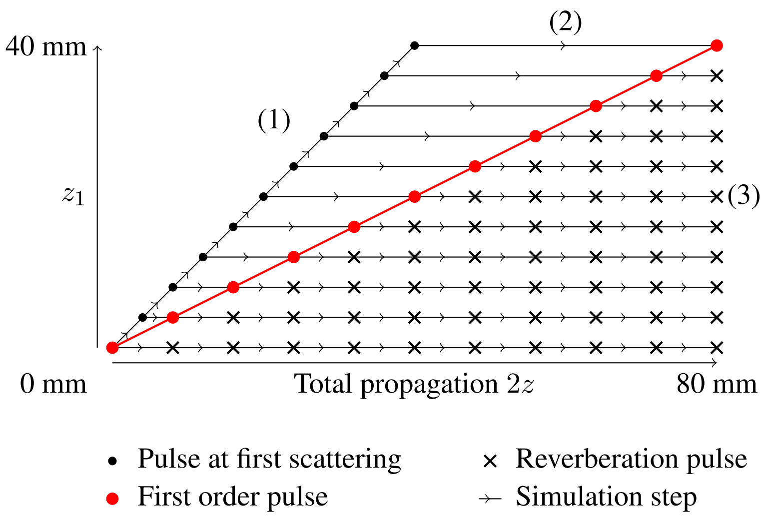

Figure 2.17: Simulation scheme. (1) Nonlinear simulation of pulses up to the first scatterer at z_1. (2) Linear simulation from first scatterer back to transducer. First order signal pulses are stored. (3) First order pulses are propagated further linearly to generate reverberation pulses. Last step is beamforming of first order and reverberation pulses based on total propagation length $2z$. Only pulses for each 4 mm is shown to make the figure less cluttered.

(NPD) is removed from the pulse. It is upsampled between pulses to match the sampling frequency of the scatterers and then applied to the scattering vector. The un-shifted pulses are then convolved with a set of time-shifted scatterers to obtain a time-shifted rf-signal. In both algorithms rf-signals from different set of pulses, representing different depths, are meshed together to create a full rf-signal over the whole depth-range of interest.

For one pulse and one constant delay there are no difference between the algorithms of paper A and B (y is the rf-signal, R is the set of scatterers, u is the pulse, and τ is the delay in time),

$$y(t+\tau) = \int_{-\infty}^{\infty} R(\xi+\tau)u(t-\xi)\,\mathrm{d}\xi, \qquad \text{(2.78a, paper A)}$$

$$= \int_{-\infty}^{\infty} R(\xi)u(t+\tau-\xi)\,\mathrm{d}\xi. \qquad \text{(2.78b, paper B)}$$

Where the equations are made equal by the redefinition $\xi \to \xi + \tau$.

In reality a pulse does not change only at each mm propagated. It changes continuously. The idea behind the change in the model from paper B to A was to extract one feature of the pulses, the NPD, upsample it to be continuous and then apply it directly on the scatterers to make this feature of the nonlinear propagation evolve continuously with depth. Ideally, upsampling could be done between the full pulses to give exact pulses at each specific depth, not just each whole mm. However, this would demand a lot of computer resources.

2.13 Combating ghost corrections through an iterative scheme

As discussed in paper B the adaptive reverberation delay estimation method, $\tau_{\mathrm{n}}^{\mathrm{RR}}$, uses a noisy signal as basis and the result can be a specific estimated reverberation delay at a certain depth to correct for a strong reverberation noise not actually present in the observed signal. It is postulated in the same paper that an iterative scheme can be applied to combat this weakness in the estimation scheme.

Iteration is done by doing a new reverberation delay estimation after DCS correction, and using the estimated first order signal for R in the equation for $\tau_{\mathrm{n}}^{\mathrm{RR}}$. Call this "second iteration" delay $\tau_{\mathrm{n},2}^{\mathrm{RR}}$. To summarize, the first and second iterations give delays from the equations

$$\tau_{\mathrm{n}}^{\mathrm{RR}}(z) = \frac{-1}{\omega_{\mathrm{c}}}\angle \int_0^z \mathrm{d}z_1 \,\mathrm{env}\,\{y(z_1)\}^\gamma \,\mathrm{env}\,\{y(z-z_1)\}^\gamma \,\alpha^{z_1} \mathrm{e}^{-i\omega_{\mathrm{c}}\tau_{\mathrm{x}}(z_1)}, \quad (2.79)$$

$$\tau_{\mathrm{n},2}^{\mathrm{RR}}(z) = \frac{-1}{\omega_{\mathrm{c}}}\angle \int_0^z \mathrm{d}z_1 \,\mathrm{env}\,\{\hat{x}(z_1)\}^\gamma \,\mathrm{env}\,\{\hat{x}(z-z_1\}^\gamma \,\alpha^{z_1} \mathrm{e}^{-i\omega_{\mathrm{c}}\tau_{\mathrm{x}}(z_1)}. \quad (2.80)$$

To ease notation the signals have been indexed with depth following $z = c_0 t/2$.

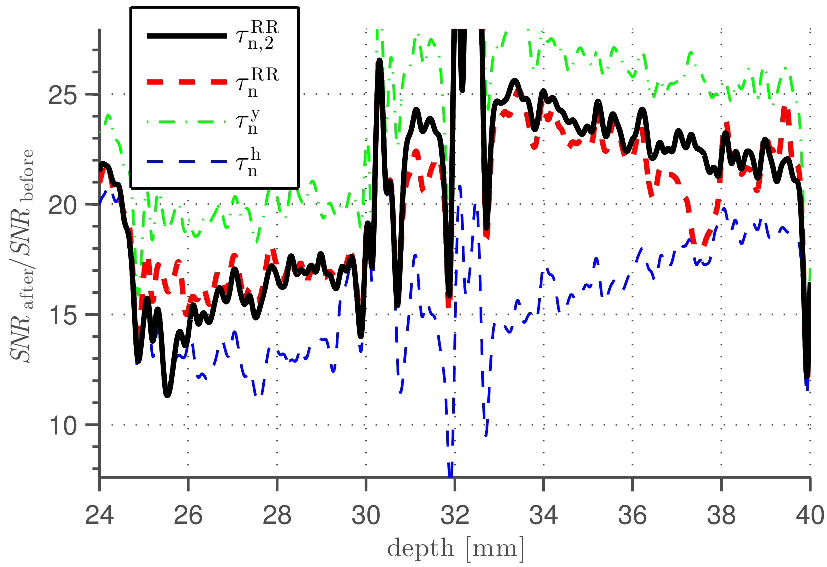

Figure 2.18: Zoomed in version of Fig. B.7 from paper B, where in addition a correction has been done with an iterative method $\tau_{\mathrm{n},2}^{\mathrm{RR}}$

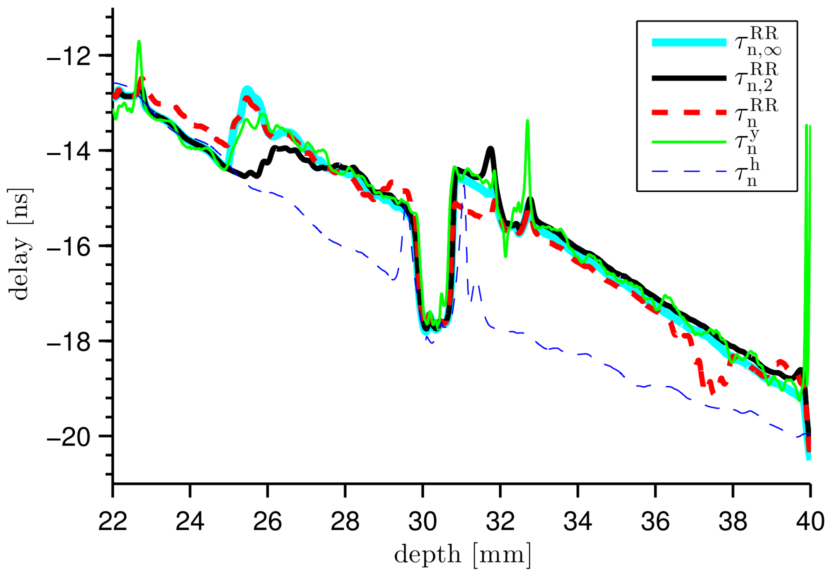

Figure 2.19: Reverberation delays used in correction from Fig. 2.18. Additionally the adaptive reverberation delay based on the true first order signal is shown, written as $\tau_{\mathrm{n},\infty}^{\mathrm{RR}}$. All delays in the plot are about equal up to this depth, with a linear development with depth.

Figure 2.18 shows the SRR improvement using $\tau_{\mathrm{n},2}^{\mathrm{RR}}$ compared to the corrections in Fig. B.7 in paper B. The iterative method shows to combat the ghost correction at 37 mm as expected. A rather unexpected result is a worse SRR improvement around 25 mm right after the synthetic blood vessel (15 mm to 25 mm). This reduction in SRR increase compared to the first iteration can also be inferred by looking at a plot of the estimated reverberation delays, see Fig. 2.19. Here, there is a discrepancy between the true reverberation delay $\tau_{\mathrm{n}}^{\mathrm{y}}$ and the second iteration estimation $\tau_{\mathrm{n},2}^{\mathrm{RR}}$ around 25 mm. The first iteration and reverberation delay based on the true first order signal, $\tau_{\mathrm{n},\infty}^{\mathrm{RR}}$, shows to follow the true delay well at this depth (and rather, all other depths). Simulated, but not plotted here, is the next iteration of the reverberation delay estimation. It shows that this next iteration also fails to get a correct reverberation delay estimation at 25 mm. Without doing further simulations the author is inclined to assume that even further iteration steps do not remedy this issue. The result raises questions of the usefulness of an iterative scheme. The effects of ghost corrections are reduced, but the introduction of new, not fully understood, errors could potentially result in a end signal with more reverberation noise after iterations than after one pass of the algorithm.

2.14 Properties of Class II scattering

Class II reverberations were introduced in Sec. 1.3 and consists of sets of three scatterers where none are the transducer-body interface. As with Class I reverberations, Class II is also divided into a type “a” and “b” (see Fig. 1.2 from the introduction for a refresher). Class II reverberations were assumed to be low compared to Class I as the transducer-body interface is believed to be a strong scatterer such that noise with this interface as a second scatterer would dominate in the image. However, in this section the Class II reverberations are given some thought and the NPD of this class is worked out in the simplest case of a linear first order NPD and uniform scatterers.

2.14.1 Scatterer combinations

An estimate for the reverberation strength, independent of the pulse, can be created by summing over all possible reverberation combinations. For the Class I noise a corresponding formula was worked out in paper B,

$$RR(z) = R_{\mathrm{transducer}} \int_0^z R(z_1) R(z - z_1)\, \mathrm{d}z_1. \tag{2.81}$$

For Class II reverberations the formula becomes more complicated. Given first scattering at z_1 and second scattering at $z_2 < z_1$ the third scatterer needs to be positioned at $z_3 = z - z_1 + z_2$ given resulting noise at a depth z. The resulting formula for the reverberation strength now closely resembles that of Eq. (2.81) save for an extra integral over all possible z_2 depths,

$$RRR(z) = \int_0^z \mathrm{d}z_2\, R(z_2) \int_{z_2}^z R(z_1) R(z - z_1 + z_2)\, \mathrm{d}z_1. \tag{2.82}$$

Note how the lower limit for z_1 is z_2. The second scatterer always needs to be lower than the first scatterer. This is also true for the third scatterer, $z_2 < z_3$. By defining $z_3 = z - z_1 + z_2$ this is always satisfied when $z_1 > z_2$. The lowest z_3 is when z_1 is at its maximum $z_1 = z$. This reduces to $z_3 = z_2$.

The most evident result from Eq. (2.82) is that there are many more possible combinations of scatterers that generate Class II reverberation noise than Class I noise. It is also noted that the complexity of calculating the assumed reverberation strength from a set of scatterers $R(z)$ is higher for Class II as the positions of the three scatterers can vary more for reverberations combining to noise at a given depth z.

2.14.2 Estimating the Class II delay

Equation (2.82) can lead to an estimated reverberation delay for the Class II noise. Inserting a phaser in Eq. (2.82) and proceeding as with the $\tau_{\mathrm{n}}^{\mathrm{RR}}$ estimation from paper B yields

$$\begin{aligned}\tau_{\mathrm{n,II}}^{\mathrm{RR}} = & \frac{-1}{\omega_{\mathrm{c}}} \angle \Bigg\{ \int_0^z \mathrm{d}z_2\, R^\gamma(z_2) \\ & \cdot \int_{z_2}^z \mathrm{d}z_1\, R^\gamma(z_1) \alpha^{z_1} R^\gamma(z - z_1 + z_2) \mathrm{e}^{-i\omega_{\mathrm{c}}\tau_{\mathrm{x}}(z_1)} \Bigg\}.\end{aligned} \tag{2.83}$$

This might be a fine result, but it is not very informative. To make sense of the equation and to get a feel for the result some simplifications and assumptions can be made. Let $\gamma = 1$, $\alpha = 1$, and assume that the first order NPD is linear, $\tau_{\mathrm{x}}(z) = \nu z$. A coordinate substitution is also used,

$$\tilde{z}_1 = z_1 - z_2, \tag{2.84a}$$

$$\tilde{z}_3 = z_3 - z_2, \tag{2.84b}$$

$$\tilde{z} = z - z_2. \tag{2.84c}$$

The definition

$$\tilde{R}(z) = R(z + z_2), \tag{2.85}$$

makes it possible to rewrite Eq. (2.83) to

$$\tau_{\mathrm{n,II}}^{\mathrm{RR}} = \frac{-1}{\omega_{\mathrm{c}}} \angle \Big\{ \int_0^z \mathrm{d}z_2 R(z_2) \int_0^{\tilde{z}} \mathrm{d}\tilde{z}_1 R(z_1 - z_2 + z_2) \cdot R\left((z - z_2) - (z_1 - z_2) + z_2\right) \mathrm{e}^{-i\omega_{\mathrm{c}}\nu((z_1 - z_2) + z_2)} \Big\}, \tag{2.86}$$

$$= \frac{-1}{\omega_{\mathrm{c}}} \angle \Big\{ \int_0^z \mathrm{d}z_2 R(z_2) \mathrm{e}^{-i\omega_{\mathrm{c}}\nu z_2} \cdot \underbrace{\int_0^{\tilde{z}} \mathrm{d}\tilde{z}_1 \tilde{R}(\tilde{z}_1) \tilde{R}(\tilde{z} - \tilde{z}_1) \mathrm{e}^{-i\omega_{\mathrm{c}}\nu\tilde{z}_1}}_{\widetilde{CI}} \Big\}. \tag{2.87}$$

The last integral is equal to the case of Class I save for the coordinate substitution. Call this integral $\widetilde{CI}$. The phase component of the integral can be extracted by rewriting to

$$\widetilde{CI}(\tilde{z}) = \int_0^{\tilde{z}/2} \mathrm{d}\tilde{z}_1 \ \tilde{R}(\tilde{z}_1) R(\tilde{z} - \tilde{z}_1) \left(\mathrm{e}^{i\omega_{\mathrm{c}}\nu\tilde{z}_1} + \mathrm{e}^{i\omega_{\mathrm{c}}\nu(\tilde{z} - \tilde{z}_1)} \right) \tag{2.88}$$

$$= \mathrm{e}^{i\omega_{\mathrm{c}} z/2} \int_0^{\tilde{z}/2} \mathrm{d}\tilde{z}_1 \ \tilde{R}(\tilde{z}_1) \tilde{R}(\tilde{z} - \tilde{z}_1) 2\cos\left(\omega_{\mathrm{c}}\nu \frac{2\tilde{z}_1 - \tilde{z}}{2} \right) \tag{2.89}$$

$$= \mathrm{e}^{i\omega_{\mathrm{c}}\tilde{z}/2} |\widetilde{CI}(\tilde{z})| \tag{2.90}$$

Inserting this result in Eq. (2.87) yields

$$\tau_{\mathrm{n,II}}^{\mathrm{RR}} = \frac{-1}{\omega_{\mathrm{c}}} \angle \left\{ \int_0^z \mathrm{d}z_2 \ R(z_2) |\widetilde{CI}(\tilde{z})| \mathrm{e}^{-i\omega_{\mathrm{c}}\nu\left(\frac{z - z_2}{2} + z_2\right)} \right\} \tag{2.91}$$

$$= \frac{-1}{\omega_{\mathrm{c}}} \angle \left\{ \mathrm{e}^{-i\omega_{\mathrm{c}}\nu\frac{z}{2}} \int_0^z \mathrm{d}z_2 \ R(z_2) |\widetilde{CI}(\tilde{z})| \mathrm{e}^{-i\omega_{\mathrm{c}}\nu\frac{z_2}{2}} \right\} \tag{2.92}$$

If now it is assumed that the scatterer distribution is uniform, the integral can be solved by simply letting $R(z) = 1$. Then ignoring the modulus of the integral a naive estimation of the Class II reverberation delay can be made, $\tau_{\mathrm{n,II}}^{\mathrm{RR}} \to \tau_{\mathrm{n,II}}^{\mathrm{e}\langle\rangle}$.

Write,

$$\tau_{\mathrm{n,II}}^{\mathrm{e}\langle\rangle} = \frac{-1}{\omega_{\mathrm{c}}} \angle \left\{ \mathrm{e}^{-i\omega_{\mathrm{c}}\nu\frac{z}{2}} \int_0^z \mathrm{d}z_2\, \mathrm{e}^{-i\omega_{\mathrm{c}}\nu\frac{z_2}{2}} \right\} \tag{2.93}$$

$$= \frac{-1}{\omega_{\mathrm{c}}} \angle \left\{ \mathrm{e}^{-i\omega_{\mathrm{c}}\nu\frac{z}{2}} \frac{2i}{\omega_{\mathrm{c}}\nu} \left[\mathrm{e}^{-i\omega_{\mathrm{c}}\nu\frac{z_2}{2}} \right]_0^z \right\} \tag{2.94}$$

$$= \frac{-1}{\omega_{\mathrm{c}}} \angle \left\{ \mathrm{e}^{-i\omega_{\mathrm{c}}\nu\frac{z}{2}} \frac{2i}{\omega_{\mathrm{c}}\nu} \mathrm{e}^{-i\omega_{\mathrm{c}}\nu\frac{z}{4}} \left(\mathrm{e}^{-i\omega_{\mathrm{c}}\nu\frac{z}{4}} - \mathrm{e}^{+i\omega_{\mathrm{c}}\nu\frac{z}{4}} \right) \right\} \tag{2.95}$$

$$= \frac{-1}{\omega_{\mathrm{c}}} \angle \left\{ \frac{-4}{\omega_{\mathrm{c}}\nu} \sin\left(\omega_{\mathrm{c}}\nu\frac{z}{4} \right) \mathrm{e}^{i\omega_{\mathrm{c}}\nu\frac{z}{4}} \mathrm{e}^{-i\omega_{\mathrm{c}}\nu\frac{z}{2}} \right\} \tag{2.96}$$

$$= \nu\frac{3z}{4} = \tau_{\mathrm{x}}\left(\frac{3z}{4}\right). \tag{2.97}$$

Note how the estimated delay lies between the first order delay $\tau_{\mathrm{x}}(z)$ and the simple $\tau_{\mathrm{n}}^{\mathrm{h}}(z) = \tau_{\mathrm{x}}(z/2)$ estimate. This could be arrived at simply by noting how increasing z_2 from 0 to z moves the mean delay from Class a and b from $\tau_{\mathrm{x}}(z/2)$ to $\tau_{\mathrm{x}}(z)$. With uniform weighting this leads to the result $(\tau_{\mathrm{x}}(z/2) + \tau_{\mathrm{x}}(z))/2 = \tau_{\mathrm{x}}(3z/4)$ in the case of a linear first order delay.

2.14.3 Why Class II can be difficult to suppress

As noted from Sec. 2.14.2 the Class II noise has a NPD closer to the first order NPD than Class I noise. This smaller delay variation in effect makes it closer to the first order signal and thus harder to suppress through DCS. This problem persists with Class III reverberation briefly mentioned in the introduction of this thesis. Here all three scatterers are close to the imaging depth and the NPD of the reverberation signal is very close to the NPD of the first order signal.

Another aspect is the appearance of the speckle when changing polarity of the transmitted pulse complex. When CIa≠CIb it was seen from Fig. 1.4 in Sec. 1.3 that an inversion of the NPDs caused the Class Ia and Ib reverberation components to switch sides in the resulting reverberation noise. The result was speckle variations in the reverberation noise between the plus and minus polarity signals. When Class Ia and Ib are equal this switching of which comes first plays no role. A similar effect may, however, occur even if Class a and b reverberations are equal when Class II noise is introduced. Class II noise is closer in delay to the first order signal than Class I. Flipping of the polarity of the transmitted pulse complex and reversing the sign of the NPDs therefore also results in a switch in which of the Class I and Class II noise comes first back to the transducer. This speckle difference in the reverberation noise between the two received signals can therefore be damaging for DCS based reverberation suppression even with equal Class a and b reverberations.

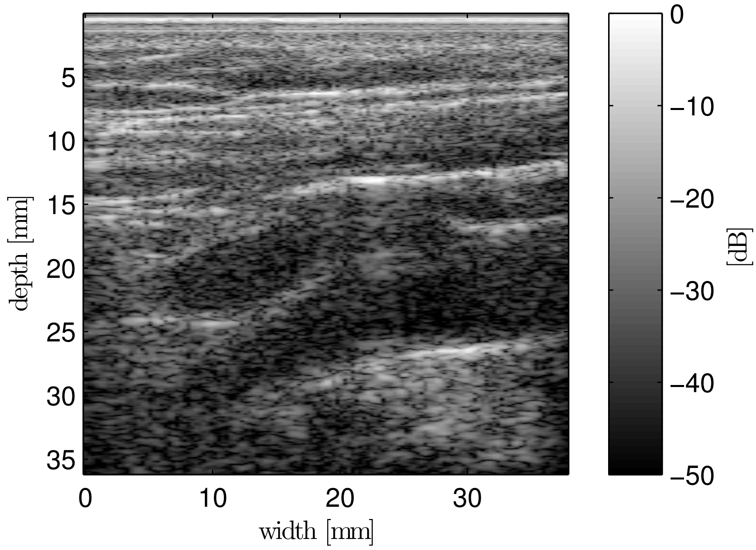

(a) No SURF processing.

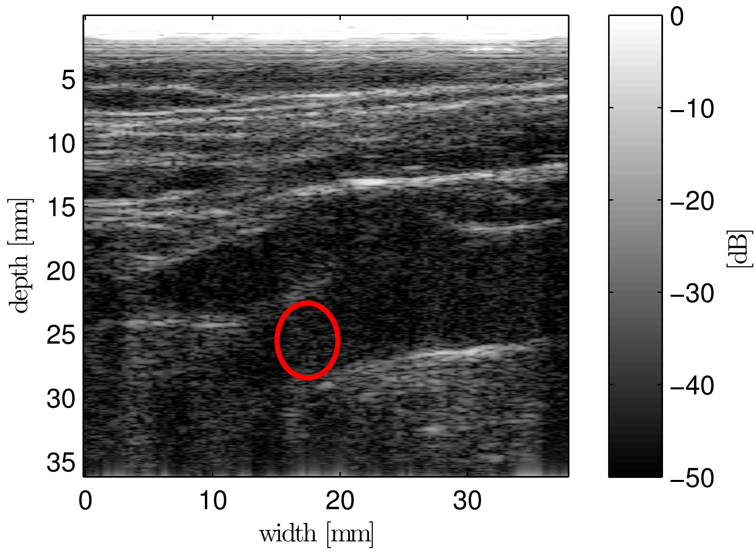

(b) SURF processed B-mode image. Reverberation noise remaining after processing highlighted by a red circle. Parameters: $\gamma = 1$, $\alpha = 3.75$ dB at 40 mm.

Figure 2.20: B-mode images. Without (a) and with (b) reverberation suppression.

2.14.4 Class II reverberations in vivo?

Figure 2.20 shows the result of SURF processing on a B-mode image of the bifurcation of the common carotid artery in a volunteer. A red circle in Fig. 2.20(b) shows an area with sub-optimal reverberation suppression as one would expect from the rest of the image that this area should be a part of the artery and thus result in a lower signal strength. As there are many layered structures above the highlighted area, one hypothesis is that this diffuse remaining noise is due to the presence of Class II reverberations. To study this hypothesis further one might look at the NPDs in this region. Class II reverberations are, as mentioned in the previous section, said to have a higher reverberation delay than Class I. Figure 2.21 shows the NPDs at 16.5 mm laterally, which is in the middle of the marked area from Fig. 2.20(b). Comparing to the blood vessel above, at around 15 to 20 mm depth, one could argue that the total NPD, τ_{y}, seems to vary more slowly between the first order NPD and the reverberation NPD when moving into the blood vessel. However, it seems difficult to draw any real conclusion from the plot as the total NPD has a negative spike around 25 mm where the value of τ_{y} is lower than the reverberation NPD τ_{n}. The opposite effect of what Class II reverberations would result in.

The “take home” message from the study of Figs. 2.20 and 2.21 can be that detection of Class II noise is difficult in vivo. Poor reverberation suppression could be due to numerous factors. A too high or too low estimation of the reverberation NPD, or large variance of the reverberation NPD all contribute to poor suppression. It is also possible that what one believe to be reverberation noise is in fact first order signals. To better understand Class II reverberation the author would suggest studies in ultrasound phantoms or by more complex computer simulations than the ones used here.

Figure 2.21: Nonlinear propagation delay at the lateral position of 16.5 mm from the image in Fig. 2.20. Vertical lines mark out the start and end depth of the circle in Fig. 2.20(b).

2.15 Estimation of nonlinear scatterers

The presence of nonlinear scatterer components in a received ultrasound signal is mentioned in both paper A and B but are not given further thought. Work has been done earlier by Svein-Erik Måsøy, Rune Hansen *et al.* where DBI was used to highlight microbubbles in vivo.[8] The idea was that the LF wave altered the size of the microbubble as observed by the HF pulse and resulted in different images for different polarities of the LF wave. By comparing these two images a contrast-enhanced image could be formed.

In this section a three pulse-complex transmit to both suppress reverberations and enhance ultrasound contrast agents at the same time is presented. The mathematical signal model extension is based on Eq. (B.4) from paper B and written

$$Y_p(\omega) = V_p(\omega)\left(X_{\mathrm{l}0}(\omega) + pX_{\mathrm{n}}(\omega)\right) + L_p(\omega)N_0(\omega). \tag{2.98}$$

Here the index, i, denoting an interval has been dropped and the first order signal has been substituted for two components, one representing linear scattering ($X_{\mathrm{l}0}$) and one representing nonlinear scattering (pX_{n}),

$$X_0(\omega) = X_{\mathrm{l}0}(\omega) + pX_{\mathrm{n}}(\omega). \tag{2.99}$$

Written out for three polarities the equation transforms to

$$Y_+(\omega) = V_+(\omega)\left(X_{\mathrm{l}0}(\omega) + X_{\mathrm{n}}(\omega)\right) + L_+(\omega)N_0(\omega), \tag{2.100a}$$
$$Y_0(\omega) = X_{\mathrm{l}0}(\omega) + N_0(\omega), \tag{2.100b}$$
$$Y_-(\omega) = V_-(\omega)\left(X_{\mathrm{l}0}(\omega) - X_{\mathrm{n}}(\omega)\right) + L_-(\omega)N_0(\omega). \tag{2.100c}$$

The equations can be written in matrix form as

$$\begin{pmatrix} Y_+ \\ Y_0 \\ Y_- \end{pmatrix} = \begin{pmatrix} V_+ & V_+ & L_+ \\ 1 & 0 & 1 \\ V_- & -V_- & L_- \end{pmatrix} \cdot \begin{pmatrix} X_{\mathrm{l}0} \\ X_{\mathrm{n}} \\ N_0 \end{pmatrix}, \tag{2.101}$$

where the frequency dependence has been omitted in the notation. The equation can be solved for any of the signal components. Here the interest lies in the nonlinear scattering component, X_{n}, and the solution is

$$\hat{X}_{\mathrm{n}} = \frac{(V_- - L_-)Y_+ + (V_+L_- - L_+V_-)Y_0 - (V_+ - L_+)V_-}{2V_+V_- - V_+L_- - L_+V_-}. \tag{2.102}$$

A time varying signal is found by taking the inverse Fourier transform, $\hat{x}_{\mathrm{n}}$. In a similar way an equation for the linear component can be derived,

$$\hat{X}_{\mathrm{l}} = \frac{-V_-Y_+ + (V_+L_- - L_+V_-)Y_0 + V_+V_-}{2V_+V_- - V_+L_- - L_+V_-}. \tag{2.103}$$

And the time dependent variant is written, $\hat{x}_{\mathrm{l}}$. The conventional estimation of the first order signal is further written $\hat{x}_0$.

Table 2.2: Scatterer positions and relative strength in estimated signal components ($\hat{x}$). Values taken from Fig. 2.22.

First order	R	$\hat{x}_{\mathrm{n}}$ [dB]	$\hat{x}_{\mathrm{l}}$ [dB]	$\hat{x}_0$ [dB]	Type
5	0.10	-23	**-10**	-0.2	Linear
12	0.05	**-5**	-16	-2	Nonlinear
15	0.10	-14	**0**	0	Linear
22	0.05	**0**	-14	-7	Nonlinear

Table 2.3: Reverberation positions and relative strength in estimated signal components ($\hat{x}$). Values taken from Fig. 2.22.

Depth [mm]	$\{z_1, z_3\}$	$\hat{x}_{\mathrm{n}}$ [dB]	$\hat{x}_{\mathrm{l}}$ [dB]	$\hat{x}_0$ [dB]	Type
10	5,5	-37	-29	-26	Linear
17	5,12	-28	-15	-18	Combination
20	5,15	-15	-16	-25	Linear
24	12,12	-29	-21	-25	Nonlinear
27	12,15	-10	-14	-26	Combination
30	15,15	-24	-21	-27	Linear
34	12,22	-30	-35	-48	Nonlinear
37	15,22	-21	-19	-27	Combination

2.15.1 Simulation setup and results

To test the effectiveness of Sec. 2.15 a simulation was done with scatterers similar to those of Case I from paper B. A total of 128 simulation runs were conducted in the same manner as in paper A where the pulses were simulated with nonlinearity given by $\beta_{\mathrm{n}}\kappa = 2 \cdot 10^{-9}$, and HF and LF amplitudes of 0.5 MPa. Strong linear scatterers were introduced at depths of 5 and 15 mm, and strong nonlinear scatterers were introduced at 12 and 22 mm. The reflection coefficients of the linear scatterers were 0.1 and 0.05 for the nonlinear. For the nonlinear scatterer strength note how a different sign between the plus and minus polarity would result in a scatterer strength difference equal to that of the linear scatterers. The mean background scatterer strength was 0.03. A low echogene area was inserted between 30 and 35 mm where the background scatterers were reduced to 1 %. See Table 2.2 for an overview of the scatterers and Table 2.3 for an overview of the resulting reverberations.

The first and main hypothesis to test is whether the nonlinear scatterer estimation of Sec. 2.15, highlights the signals from nonlinear scatterers more than the signals from the linear scatterers. The secondary hypothesis is whether the $\hat{x}_{\mathrm{n}}$ estimation also suppresses the reverberation noise in the same way as the con-

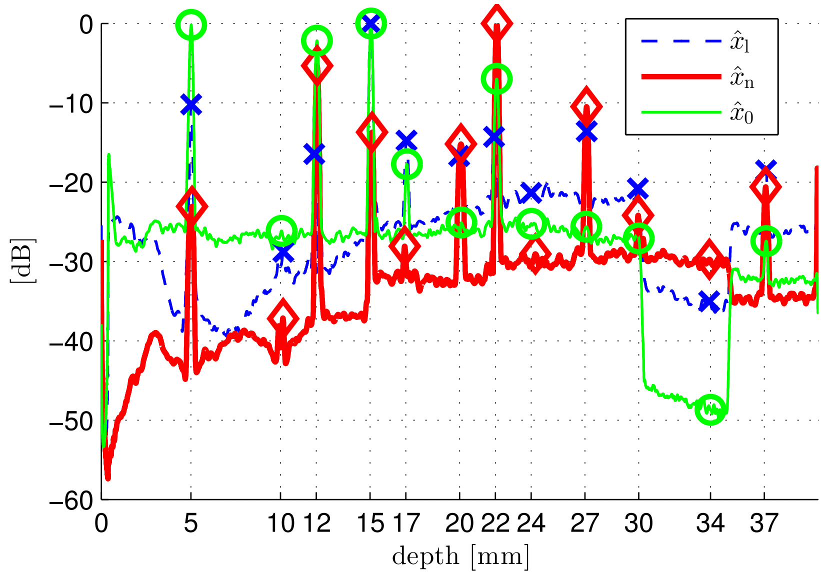

Figure 2.22: Relative mean signal strength for estimators of first order signal ($\hat{x}_0$), linear first order signal ($\hat{x}_\mathrm{l}$), and nonlinear first order signal ($\hat{x}_\mathrm{n}$). Estimation of nonlinear scatterers is relatively stronger at 12 and 22 mm where nonlinear scatterers are present than at locations 5 and 15 mm where linear scatterers are present.

ventional estimation of $\hat{x}_0$. A third hypothesis is whether the estimation of linear signal components suppresses the nonlinear scatterers and highlights the first order linear signal.

Figure 2.22 shows the mean envelope of all 128 runs for the three estimators: $\hat{x}_\mathrm{n}$, $\hat{x}_\mathrm{l}$, and $\hat{x}_0$. The data is plotted in dB and is normalized to the maximum value for each estimator. Values at the interesting areas with strong scatterers or strong reverberations are marked. The same values are also plotted in Tables 2.2 and 2.3 for the first order and reverberation positions respectively. The figure (and Table 2.2) shows that the nonlinear scatterers are the strongest components in the $\hat{x}_\mathrm{n}$ signal. The highest point is the nonlinear scatterer at 22 mm while the one at 12 mm is 5 dB lower. The next component is the linear scatterer at 15 mm which is 9 dB further down. The result supports the first hypothesis, and the $\hat{x}_\mathrm{n}$ estimation does indeed seem to favor the nonlinear components of the signal.

The reverberation noise in the low echogene region from 30 to 35 mm is highest for the nonlinear signal estimator. The second hypothesis can therefore not be confirmed by this result. Better reverberation suppression is achieved by the conventional $\hat{x}_0$ estimator which give a reverberation strength in the same region at almost 20 dB lower. The third and last hypothesis is studied in the same way as the first hypothesis. The strongest components of the linear signal $\hat{x}_1$ is the scattering of the linear scatters. The scatterer at 15 mm is strongest followed by the linear scatterer at 5 mm with 10 dB lower signal strength.

As an additional note, the conventional estimator $\hat{x}_0$ yields around the same signal strength for both the linear and nonlinear strong first order scatterings.

2.15.2 Reverberation suppression

It is difficult to draw any general conclusion from the reverberation peaks in Table 2.3. The conventional method is better on 6 of the reverberations peaks, the nonlinear scatterer estimator best in 3 cases, and the linear estimation in none. Although the conventional estimator shows better suppression in the low echogene area the results for the strong peaks vary too much for the present author to dare a conclusion. One interesting point, however, can be made from the theory of the reverberation suppression. According to paper B it is better to use signals of opposite polarity in reverberation suppression as these have the more similar speckle in the reverberations compared to correction with the zero-polarity signal and a non-zero polarity signal (Sec. B.3). Then with the nonlinear signal estimation also utilizing the zero-polarity signal the reverberation contribution from this signal will be hard to suppress. This can be an explanation for the elevated reverberation noise floor in the low echogene area from 30 to 35 mm. One would, however, also expect better suppression of the strong reverberation peaks compared to the nonlinear signal estimator at all depths which is not the case.

2.15.3 Conclusion

The estimation scheme for nonlinear scatterers does favor signals from nonlinear scatterers in a simulated medium. Reverberation suppression is lower than the conventional method and the author therefore proposes that future work should be done on creating a better estimation scheme. Theoretical reverberation models as presented in paper B give a theoretical backing for the breakdown of the reverberation suppression. The author further proposes study with varying nonlinear scatterer strengths to evaluate the sensitivity of the estimation scheme. It is, however, the author's opinion that these initial findings are promising for nonlinear scattering estimation from dual band signals.

Bibliography

[1] Jochen Matthias Rau. *Dual frequency band ultrasound for suppression of multiple scattering*. PhD thesis, NTNU, 2013.

[2] Rune Hansen and Bjørn. A. J. Angelsen. SURF imaging for contrast agent detection. *IEEE Trans. Ultrason., Ferroelect., Freq. Control*, 56(2):280–290, February 2009.

[3] Bjørn A. J. Angelsen. *Ultrasound imaging : waves, signals, and signal processing*, volume I. Emantec, 2000.

[4] Thomas Szabo. *Diagnostic Ultrasound Imaging: Inside Out (Biomedical Engineering)*. Academic Press Inc, 2004.

[5] Øyvind Standal, Bjørn A. J. Angelsen, and Thor Andreas Tangen. A phase based approach for estimation and tracking of locally variable delays. In *IEEE Ultrason. Symp.*, pages 1583–1585, October 2007.

[6] Francis A. Duck. *Physical Properties of Tissue*. Academic Press, 1990.

[7] Tonni F. Johansen. *Xtrans; Transducer simulation software*. Matlab code.

[8] Svein-Eirik Måsøy, Øvind Standal, Sven Peter Näsholm, Tonni F. Johansen, Bjørn Angelsen, and Rune Hansen. SURF imaging: In vivo demonstration of an ultrasound contrast agent detection technique. *IEEE Trans. Ultrason., Ferroelect., Freq. Control*, 55(5):1112–1121, May 2008.

Chapter 3

Conclusion

3.1 Summary of the work

The work in this thesis builds upon earlier work within the SURF research group. Especially the work by, Jochen Rau, Sven Peter Näsholm, Rune Hansen, Halvard Høilund-Kaupang, and Bjørn Angelsen. Special focus is on the work by Rau[1] which most recently got his PhD from the work within the same general topic as this thesis. The goal in this thesis was to gain a deeper understanding of the behavior of reverberation noise and utilize this knowledge to improve reverberation suppression under dual band imaging. A continuation of the theory is included in paper A while extensions on reverberation suppression through improved estimation is included in paper B. The signal model was also extended to take nonlinear scatterers into account, as first proposed by Hansen *et al.* [2]

The work on the theory behind reverberation in DBI showed that the statistics of the contributing scatterers in a reverberation pulse is important for the possible suppression. Where many scatterers combine to give reverberations at the same depth the variance in the different components makes it difficult to correct for the sum of them. Call this speckle differences. Various factors were determined to affect this result. The presence of nonlinear attenuation for instance, was found to give a scatterer dependent reverberation delay. A larger effect is the tissue dependent gradient of the first order NPD as determined by changing nonlinearity parameters with depth. To combat these effects an adaptive reverberation NPD estimation technique was developed.

3.2 Concluding remarks

The main results of this thesis are the extended theory around reverberation noise in dual band imaging as well as a new estimator for the nonlinear propagation delay of the reverberation noise. This work is included in two papers with additional discussions moved to an additional chapter. A chapter with discussions around estimation of the first order NPD is also included and contains a method to keep the estimation robust without requiring user input. The signal model was extended to include nonlinear scatterers and an estimation scheme was developed to extract the nonlinear signal components while trying to at the same time suppress reverberation noise.

3.3 Overview of publications

The listed papers are part of this thesis. The presentations and posters represent work done while writing the thesis, but are not submitted as being part of the thesis.

Papers

1. **Ole Martin Brende** and Bjørn Angelsen, "Limiting factors in reverberation suppression through delay corrected subtraction methods in dual band ultrasound imaging", undergoing second stage of review by *IEEE Transactions on Ultrasonics, Ferroelectrics and Frequency Control*.

2. **Ole Martin Brende** and Bjørn Angelsen, "Adaptive reverberation noise delay estimation for reverberation suppression in dual band ultrasound imaging", published by *the Journal of the Acoustical Society of America*, 25. November 2015. `http://dx.doi.org/10.1121/1.4935555`

Presentations

1. Bjørn Angelsen and **Ole Martin Brende**, "SURF Ultrasound Imaging: A new Method of Improved Imaging", *NOCOGO*, Billund, Denmark, October, 2012.

2. **Ole Martin Brende** and Bjørn Angelsen, "Reverberation suppression through dual-band ultrasound imaging", *Artimino*, Lake Rosseau, Ontario, Canada, June, 2013.

Posters

1. **Ole Martin Brende**, Catharina De Lange Davies and Bjørn Angelsen, "Multifunction nanoparticles and multifrequency ultrasound", *MedIm*, Trondheim, Norway, October, 2012.

2. Johannes Kvam, Bjørn Angelsen, **Ole Martin Brende** and Anne C. Elster, "GPGPU Accelerated Solution of Nonlinear Wave Propagation and Heat Diffusion", *Super Computing*, Boston, USA, October, 2013

Bibliography

[1] Jochen Matthias Rau. *Dual frequency band ultrasound for suppression of multiple scattering*. PhD thesis, NTNU, 2013.

[2] Rune Hansen and Bjørn. A. J. Angelsen. SURF imaging for contrast agent detection. *IEEE Trans. Ultrason., Ferroelect., Freq. Control*, 56(2):280–290, February 2009.

Part II

Papers

Paper A

Limiting factors in reverberation suppression through delay corrected subtraction methods in dual band ultrasound imaging

Ole Martin Brende and Bjørn Angelsen
Department of Circulation and Medical Imaging
Norwegian University of Science and Technology
N 7489 Trondheim, Norway

Running title: Reverberation suppression in dual band imaging

Submitted to IEEE Transactions on Ultrasonics, Ferroelectrics and Frequency Control

The paper presents a study of suppression of third order planar reverberations. The underlying method is delay corrected subtraction of two signals generated with transmit of a dual band pulse-complex. The lower frequency wave is changed between transmissions of multiple pulse-complexes. This has a different effect on the first order- and reverberation components of the total signal, and leads to the possible extraction of the first order signal. Damaging effects to the reverberation suppression studied here include: nonlinear self-distortion; distortion of the reverberation components by the low-frequency wave; the statistics of the scatterers; heterogeneity of the medium with depth; and error in the delay used for delay corrected subtraction. The main result of the theoretical and simulations based study is that increased material heterogeneity creating larger statistical variance of the reverberation noise is the most damaging effect to the presented reverberation suppression scheme. The next limiting factor is the distortion of the high-frequency imaging pulse created by the low-frequency wave. This effect is reduced by reducing the frequency of the low-frequency wave compared the pulse length of the high-frequency pulse.

Nomenclature

β_{n}	Nonlinearity parameter.
DBI	Dual Band Imaging.
DCS	Delay Corrected Subtraction.
HF	High Frequency (pulse).
κ	Compressibility.
$L_{ip}(\omega)^*$	Reverberation filter.
LF	Low Frequency (wave).
$N_{ip}(\omega)^*$, $n_{ip}(t)^*$	Reverberation signal.
ND, $\widetilde{L}_{ip}(\omega)^*$	Noise Distortion (reverberations).
NPD	Nonlinear Propagation Delay.
NSD	Nonlinear Self Distortion.
p	LF-wave configuration (polarity).
PFD, $\widetilde{V}_{ip}(\omega)^*$	Pulse Form Distortion.
SRR	Signal to Rev. noise Ratio.
$\tau_{\mathrm{n}p}{}^*$, $\tau_{\mathrm{x}p}{}^*$	Rev. and first order NPD.
$V_{ip}(\omega)^*$	First order filter.
$X_{ip}(\omega)^*$, $x_{ip}(t)^*$	First order signal.
$Y_{ip}(\omega)^*$, $y_{ip}(t)^*$	Total signal.

$^*p$ indicating the polarity of the LF wave and i indicating an interval.

A.1 Introduction

ANY received ultrasound signal can be divided into three parts: 1) linear first order scattering; 2) nonlinear first order scattering, eg. from microbubbles; and 3) multiple scattering, or reverberation-, noise. The linear first order part of the signal can be directly related to structural features of the medium under study. The reverberations are considered noise as their relation to the tissue is more complex and not converted correctly to anatomical structures through the time of flight estimation of depth, z, used by the scanner, $z = c_0 t/2$, where t is time of flight, and c_0 is the speed of sound. The goal should therefore be to extract the first order signal and suppress the reverberation noise. The nonlinear first order scattering signal component is not considered in this paper.

In dual band imaging (DBI) the conventional high-frequency imaging pulse (HF) is modified through nonlinear propagation effects by a co-propagating low-frequency wave (LF). The LF wave is called as such, and not as a pulse, as it has a longer temporal duration than the imaging pulse. The HF and LF combination is called a *pulse-complex*. By comparing different received imaging pulses transmitted with different underlaying LF manipulation waves it has been observed that the reverberation noise behaves differently than the first order signal (which will become evident in this paper). This information is used to extract the first order signal. This procedure, with reverberation processing under dual band transmits, is commonly called SURF (Second order UltRasound Field) imaging[1, 2]. In this paper the limitations of SURF imaging is discussed when a method called delay corrected subtraction (DCS) is utilized to remove the reverberation noise. Focus is on how nonlinear propagation of the pulses and varying tissue properties is damaging to the reverberation suppression scheme.

Reverberation noise is here limited to maximum three scattering events. As the pulse amplitude drops significantly after each scattering this turns the focus of this study to the most dominant reverberation noise. The authors' research has been most geared toward the carotid artery where the tissue is most dominantly layered orthogonal to the beam direction. This has prompted the study of how reverberations of such layers damage the contrast resolution in the image. This thus ignores second order reverberations as scattering of orthogonal planes create a complete reversal of the beam direction which means that second order reverberations does not return to the transducer. Further, the scattering off of the transducer surface is considered significantly stronger than inter-media scattering, which limits the study to reverberations where the second scatterer is the transducer-body interface.

There are other methods than those utilizing DBI that aim to reduce reverberation noise. Maybe the most widespread is the use of harmonic imaging. Harmonic imaging was first utilized to view the nonlinear first order scattering from microbubbles. [3] However, in the 1990's it was noticed that the imaging modality also gave enhanced images when microbubbles were not present. [4] By looking at the second harmonics, rather than an image created from the frequency band centered around the transmit frequency, one now had an image of the nonlinear forward propagation of the wave. [5] It was discovered that the received harmonics were generated by the tissue and not transmitted by the transducer and the modality was thus called tissue harmonic imaging. An effect of this imaging modality was reduced reverberation noise. [6]

The paper is structured as follows. First, a general introduction to nonlinear propagation and how this affects the first order signal as well as the reverberation noise. Then, the method of delay corrected subtraction (DCS) for reverberation suppression, which hinges on the presented theory, is laid out. A section follows with theoretical discussion of how the presented theory is damaging to the reverberation suppression under DCS. This is the main matter of this paper. Further, nonlinear pulse simulations are carried out to corroborate the theoretical discussion. This is facilitated by creating an idealized simulation framework where the different nonlinear effects can be isolated and studied. Results of the simulations and theoretical work are then discussed in lieu of the model.

A.2 Initial theory

A.2.1 Nonlinear media and dual band imaging

Nonlinear propagation occurs when there is a nonlinear relation between an applied pressure and the volume compression of a small volume. [7, eq. (4)] Allowing up to second order modification of this relation results in the following formula for the modified propagation speed

$$c_1 = \frac{c_0}{\sqrt{1 - 2\beta_{\mathrm{n}}\kappa p_{\mathrm{LF}}}} \approx \frac{c_0}{1 - \beta_{\mathrm{n}}\kappa p_{\mathrm{LF}}}, \tag{A.1}$$

where c_0 is the non-modified linear propagation velocity, p_{LF} is the pressure of the pulse, κ is the material compressibility, and β_{n} is the nonlinearity parameter.[1] [7], [8, p. 12.21] The result is that the peaks of a pulse travel faster than the troughs. The waveform is distorted as harmonic components are generated. This is called nonlinear self-distortion (NSD). The loss of the energy in the harmonic bands when the received pulse is bandpass filtered is called nonlinear attenuation. For the discussion in this paper this understanding of nonlinear propagation is sufficient. For a more thorough introduction the authors can recommend other literature. See for instance [1, 8] or [7].

[1] In other literature often written out as $\beta_{\mathrm{n}} = 1 + B/2A$. Where A and B are the first- and second-order term of the Taylor expansion of the pressure as a function of density.

In DBI a low-frequency (LF) wave is used to modify the propagation of a high-frequency (HF) pulse. By placing the HF pulse on the top of the LF wave the increased pressure across the HF pulse introduces an increased propagation speed. The opposite is the case when the polarity of the LF wave is switched (it is inverted). The effect of the LF wave can be broken down into two parts. The first is the nonlinear propagation delay (NPD) introduced by the higher propagation speed. The second is an additional pulse form distortion (PFD) of the HF pulse caused by variations of the LF wave across the HF pulse, and the increased nonlinear self-distortion (NSD) due to increased overall pressure.

A.2.2 Nonlinear propagation delay

The nonlinear propagation delay (NPD) can be calculated from the increased propagation speed up to a depth z. At z the pulse-complex is scattered and the reduced amplitude of the LF wave means that nonlinear propagation effects can be neglected on the propagation back to the transducer. The NPD becomes

$$\tau_{\mathrm{x}p}(z) = \int_0^z \frac{\mathrm{d}s}{c_1} - \int_0^z \frac{\mathrm{d}s}{c_0}, \tag{A.2}$$

$$\approx -\int_0^z \frac{\mathrm{d}s}{c_0}\beta_{\mathrm{n}}(s)\kappa(s)\left(p \cdot p_{\mathrm{ref}}(s)\right). \tag{A.3}$$

The subscript “x” indicates that this is the delay on the first order scattered signal as “X” later is used to denote the first order signal. The amplitude of the LF wave is defined through a reference pressure, p_{ref}, and a unitless amplitude and polarity parameter p, such that $p_{\mathrm{LF}} = p \cdot p_{\mathrm{ref}}$. The parameter p is henceforth referred to as the *polarity* of the pulse-complex (HF and LF combined), as it in this paper only takes the values, $p \in \{+1, 0, -1\}$.

This delay is referred to as the *first order NPD*, or the *first order delay*, and it has some interesting properties. Note that as long as the reference pressure does not change sign the sign of the integrand is also unchanged and the NPD is monotonically increasing or decreasing with depth. The shape of the NPD with depth becomes important later in the paper. A linear gradient of the first order NPD, referred to later as *linear NPD*, means that the value of the integrand is constant throughout the area of interest. In general, by varying the material parameters β_{n} or κ, the shape of the NPD becomes nonlinear with depth. In other words when the tissue is composed of different materials the gradient of the NPD varies. In Section A.3.4 it is discussed why this change in gradient is destructive to reverberation suppression through DCS. Note that the word *nonlinear* in *nonlinear propagation delay* refers to the nonlinear propagation, and not to the shape of the delay when plotted against depth (or time).

The propagation delay is only due to the amplitude of the manipulating LF wave at the center of the HF pulse. After the first scattering event, the drop in the

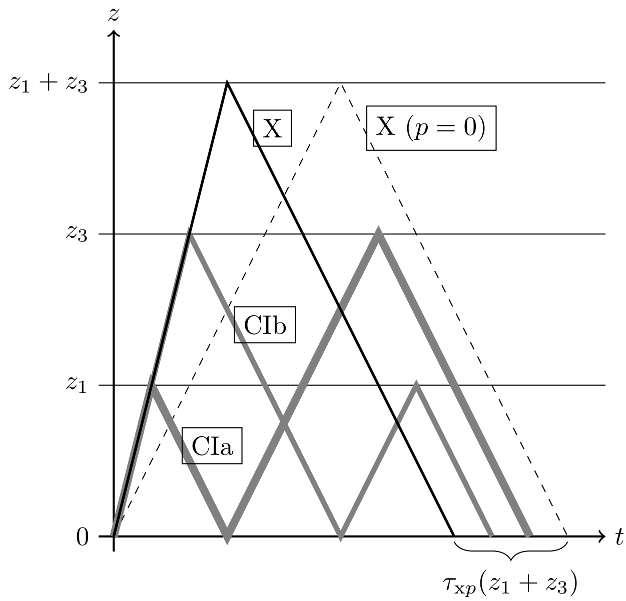

Figure A.1: Third order reverberation classification scheme with the transducer as a second reflector. Thinner lines have more nonlinear propagation. Dotted line is reference first order signal where there is no LF wave. First order propagation is marked by an X. Modifying LF wave gives a higher propagation velocity up to the first scattering event, highly exaggerated here.

LF amplitude will make the wave propagate with the non-modified propagation speed c_0. By looking at the accumulated time delay (NPD) between the received signals with and without a modifying LF wave, it is therefore possible, when knowing the nonlinearity parameters of the medium, to know how long the dual band pulse propagated before it was scattered first. In other words, when c_0, c_1 and τ_{xp} is known one can solve (A.2) for z. For the first order signal (without transmission of an LF wave) this information is also given by the time of flight of the pulse, $t(z) = 2z/c_0$.

Reverberation noise is generated by multiple scattering of the transmitted pulse. The time of flight of this noise is determined by the total propagation path, while the NPD is determined by the depth of the first scatterer. For the reverberation component of the total signal there is therefore a discrepancy between the time of flight and the NPD. This can be used to isolate the reverberation component from the total signal through delay corrected subtraction. The reverberation components are delayed with the estimated NPD of the reverberation components and then subtracted away. This is explained in detail in Section A.2.5.

A.2.3 Nonlinear distortion effects

The pulse form distortion (PFD) of the received signal does not seem to follow a simple mathematical expression as is the case with the NPD. However, it can be related to the change in the HF pulse with a co-propagating LF wave compared to a pure HF transmit with no co-propagating LF wave. With the bandwidth of the HF sufficiently high and the separation in frequency between the HF and LF large enough, the sum and difference spectra of the HF and LF generated due to nonlinear propagation will overlap. This makes it possible to model the effect of the modifying LF wave by a filter. Let $X_{ip}(\omega)$ be the Fourier transform of an interval, with a certain length given the label i, of the received first order linear signal with the LF configuration determined by the parameter p. The relation to the frequency spectrum of a pure HF transmit ($p = 0$) of the same area is given through the filter $V_{ip}(\omega)$ with ω as the temporal angular frequency,

$$X_{ip}(\omega) = V_{ip}(\omega) X_{i0}(\omega). \tag{A.4}$$

This filter also contains the NPD. Extracting this delay and the remainder is the PFD,

$$V_{ip}(\omega) = \mathrm{e}^{-i\omega\tau_{\mathrm{x}ip}} \widetilde{V}_{ip}(\omega). \tag{A.5}$$

Here the NPD ($\tau_{\mathrm{x}ip}$) is assumed constant in the interval i.

A.2.4 Reverberation model

In a similar way to first order scattering, a modifying LF wave also introduces changes to the reverberation signal. A main difference between first order and reverberation signals is that there can be many different components of the reverberation signal giving signal at a certain perceived depth. To better be able to discuss reverberation noise a classification scheme for the possible reverberation components needs to be introduced.

As mentioned in the introduction, this paper handles third order reverberations where the scatterers are planes and the transducer is the second scatterer. It has been shown that scatterers of this type (or any third order reverberation) always appear in pairs. [9, Paper D],[10, Paper D] Here, the two components of such a reverberation pair is denoted Class Ia and Ib. The "I" indicates that the second scatterer is the transducer while the "a" and "b" distinguishes between two possible propagation paths. Considering a scatterer at z_1 and one at z_3, two possible third order reverberation propagation paths are possible (see Fig. A.1): 1) propagation to z_1, back to the transducer, out to z_3, and back to the transducer again. This is Class Ia (or CIa); and 2) the opposite direction, Class Ib (or CIb).

Considering transmit of only a HF pulse the time of flight of the reverberation pairs need to follow

$$\frac{2(z_1 + z_3)}{c_0} = \frac{2z}{c_0}, \quad \text{or} \tag{A.6}$$

$$z_1 + z_3 = z, \tag{A.7}$$

to give reverberation noise at z as interpreted by the ultrasound imaging software. The same equation is modified when introducing an altered propagation speed up to the first scatterer. Class Ia and Ib reverberations now give rise to noise at slightly different depths

$$\frac{z_1}{c_1} + \frac{z_1 + 2z_3}{c_0} = \tau_{\mathrm{x}}(z_1) + \frac{2z}{c_0}, \quad \text{CIa}, \tag{A.8}$$

$$\frac{z_3}{c_1} + \frac{2z_1 + z_3}{c_0} = \tau_{\mathrm{x}}(z_3) + \frac{2z}{c_0}, \quad \text{CIb}. \tag{A.9}$$

Note that the pulse length is not taken into consideration in this mathematical description. As the pulse has a non-zero length the signal at a specific depth z will consists of contributions of an interval of scatterers contributing such that the resulting pulse overlaps with z. This effect is studied later in this paper, but is not important for the current discussion. The message here is that the NPD of a reverberation signal depends on the position of the first scattering event.

Assuming a fatty tissue $\left(\beta_{\mathrm{n}}\kappa \approx 3 \cdot 10^{-9}\ \mathrm{Pa}^{-1}\right)$[11], $c_0 = 1440\ \mathrm{m/s}$ and $p_{\mathrm{LF}} = 0.5\ \mathrm{MPa}$ in (A.3) yields a linear first order NPD (τ_{x}) of 1.04 ns/mm. Comparatively the temporal period of the HF oscillations is $T_{\mathrm{HF}} = 1/(8\ \mathrm{MHz}) = 125$ ns. For imaging up to 40 mm the NPD is then below one third of a HF pulse oscillation. This relatively low value, coupled with a HF pulse length of 2.5 oscillations used here, allows for the consideration of the NPD as an intrinsic property of the reverberation noise at a given depth. The average reverberation delay of Class Ia and Ib, $(\tau_{\mathrm{x}}(z_1) + \tau_{\mathrm{x}}(z_3))\,/2$, can be viewed as a property of the combined reverberation noise from that pair at z. When many reverberation pairs contribute to noise at a certain depth the total reverberation delay at that depth is a weighted average of the delays of all the pairs. Call this average reverberation delay $\tau_{\mathrm{n}}(z)$.

In the same way as with the first order component, where the change in the pulse shape due to a modifying LF wave was modeled through a filter containing the PFD and the first order NPD, a filter containing the Noise Distortion (ND) and reverberation NPD can be used to model the change in the reverberation component, $N_{i0}(\omega)$, of the total signal.

$$N_{ip}(\omega) = L_{ip}(\omega) N_{i0}(\omega), \quad \text{where} \tag{A.10}$$

$$L_{ip}(\omega) = \mathrm{e}^{-i\omega\tau_{\mathrm{n}ip}} \widetilde{L}_{ip}(\omega). \tag{A.11}$$

and where $\widetilde{L}_{ip}(\omega)$ represents the ND.

The reverberation model can be combined with the model for the first order signal to give a total signal model for DBI. Still working in Fourier space on small intervals, the total signal $Y_{i0}(\omega)$ is the sum of the first order and reverberation components at the same interval,

$$Y_{i0}(\omega) = X_{i0}(\omega) + N_{i0}(\omega). \tag{A.12}$$

Equations (A.4) and (A.10) can be utilized to give the corresponding total signal with a modifying LF wave present in the propagation,

$$Y_{ip}(\omega) = V_{ip}(\omega)X_{i0}(\omega) + L_{ip}(\omega)N_{i0}(\omega). \tag{A.13}$$

A.2.5 Reverberation suppression with DCS

In this section the delay corrected subtraction (DCS) method for reverberation suppression is explained. As input the method takes two received signals transmitted with a different configuration of the LF wave. Here, waves of opposite polarities are used, $p = +1$ referred to as the *positive* polarity, and $p = -1$ referred to as the *negative* polarity. Equation (A.13) is transformed into a set of equations,

$$\begin{pmatrix} Y_{i+} \\ Y_{i-} \end{pmatrix} = \begin{pmatrix} V_{i+} & L_{i+} \\ V_{i-} & L_{i-} \end{pmatrix} \begin{pmatrix} X_{i0} \\ N_{i0} \end{pmatrix}. \tag{A.14}$$

The equation can be solved for the first order component, X_{i0},

$$X_{i0} = \frac{Y_{i+}L_{i+}^{-1} - Y_{-}L_{i-}^{-1}}{V_{i+}L_{i+}^{-1} - V_{i-}L_{i-}^{-1}}. \tag{A.15}$$

The complex pulse distortions (PFD and ND) are not known and are difficult to estimate. However, other publications have shown that the NPD of the first order and reverberation components can be estimated. [12, 13] Assuming no PFD or ND ($\widetilde{V}_{ip} = \widetilde{L}_{ip} = 1$) yields an estimate for the first order signal (using (A.5) and (A.11)),

$$\hat{X}_{i0} = \frac{Y_{i+}\exp\left(i\omega\hat{\tau}_{\mathrm{n}i+}\right) - Y_{i-}\exp\left(i\omega\hat{\tau}_{\mathrm{n}i-}\right)}{\exp\left(i\omega(\hat{\tau}_{\mathrm{n}i+} - \hat{\tau}_{\mathrm{x}i+})\right) - \exp\left(i\omega(\hat{\tau}_{\mathrm{n}i-} - \hat{\tau}_{\mathrm{x}i-})\right)}. \tag{A.16}$$

The result can be transformed to the time domain by assuming a single frequency pulse at ω_{c} and ignoring the phase change introduced by the gain factor in the denominator,

$$\hat{x}_0 = \frac{y_+(t + \hat{\tau}_{\mathrm{n}+}) - y_-(t + \hat{\tau}_{\mathrm{n}-})}{2\sin\left\{\omega_{\mathrm{c}}\big((\hat{\tau}_{\mathrm{n}+} - \hat{\tau}_{\mathrm{x}+}) - (\hat{\tau}_{\mathrm{n}-} - \hat{\tau}_{\mathrm{x}-})\big)/2\right\}}. \tag{A.17}$$

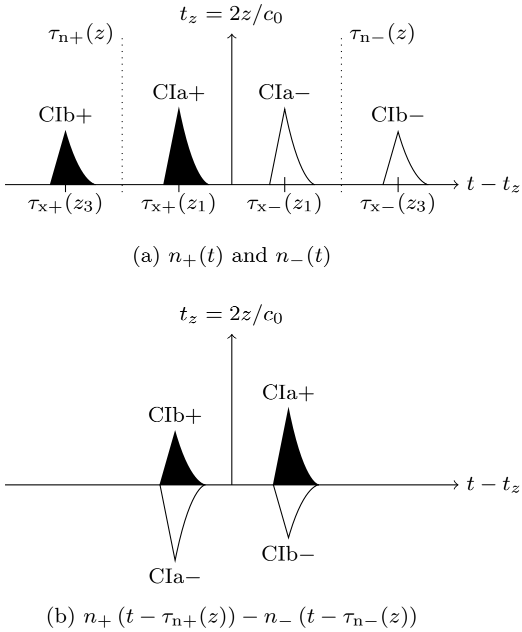

Figure A.2: Delay corrected subtraction (DCS) reverberation suppression method. (a) The reverberation noise for two pulse-complex transmits: a positive low-frequency peak (black) and negative low-frequency peak (white). (b) Alignment in time and subtraction of the reverberation components. The Class Ib reverberation from one polarity cancels out the Class Ia from the other. Note, however, that the Class Ib reverberation is lower in magnitude due to more nonlinear attenuation caused by loss of energy up to harmonic bands due to nonlinear propagation.

This delay corrected subtraction method works under the assumption that the only difference between the reverberation components of signals transmitted with different LF polarities is a time delay. The total signals are shifted in time such that the reverberation components are overlapped and then subtracted. This removes the reverberation noise but introduces a gain on the first order components. This gain is corrected for by the denominator in (A.17). See Fig. A.2 for a visual explanation on how the reverberation noise is suppressed with DCS.

As seen in Fig. A.2, the method requires that the Class Ia reverberation of one pulse-complex transmit is equal to the Class Ib reverberation component of another. And vice versa. This is a softer requirement than a pure delay difference between the reverberation signals, as a pure delay difference would exclude also speckle differences. As pulse form distortion and nonlinear propagation delays are inherently dependent on the position of the first scatterer, as discussed previously, this could make CIa and CIb different. Such effects are discussed in depth in

Section A.3.

A.2.6 Limitations on band separation

To minimize the PFD which is due to variations of the LF wave across the HF pulse (Section A.2.3), one needs to either: 1) lower the LF frequency; or 2) lower the length of the HF pulse. With the relation between bandwidth, B, and pulse length, T_p, given by $B = 2\pi/T_\mathrm{p}$, and the relation between period, T, and frequency, $\omega/2\pi$, given by $T = 2\pi/\omega$, it is possible to write a constraint on the bandwidth of the HF based on the frequency of the LF given that the pulse length of the HF, $T_\mathrm{p,HF}$, should be much smaller than the period of the LF, T_LF,

$$T_\mathrm{LF} \gg T_\mathrm{p,HF}, \quad \text{giving} \tag{A.18}$$

$$\omega_\mathrm{LF} \ll B_\mathrm{HF}. \tag{A.19}$$

The lower limit for the LF band is determined by the transducer hardware. When the goal is to have a uniform LF field as observed by the HF, one wants to minimize the effect of focusing. The HF pulse therefore needs to be in the near-field of the LF wave over the whole region of interest. The near-field region is limited by $D^2/2\lambda$ in each dimension. [14, pp. 1.10-1.11] Here D is the width of the transducer aperture. Increasing the LF wavelength thus results in the need for a higher LF aperture. In previous work a factor of ≈1:10 between HF and LF wavelengths has been used in DBI. This relation is also used here where the HF is at 8 MHz and the LF is at 0.78 MHz.

A.2.7 Tissue harmonic imaging

Tissue harmonic imaging (or simply *harmonic imaging*) is an alternate method for reducing reverberation noise in an image. A brief introduction is given here to get an overview of the method SURF imaging can be seen to compete with.

Tissue harmonic imaging utilizes the generation of second order harmonic components in the forward propagating signal. [5] If reverberation noise is said to originate from scatterers at much shallower depths than the imaging region of interest, then the first order component of the total signal should have a higher second order harmonic signal strength than the reverberation component. By imaging the second order harmonic, this would increase the signal to reverberation noise ratio (SRR). However, as is discussed in Section A.2.4, reverberation noise always act in pairs. And the statement about tissue harmonic imaging presented here only holds for *one* of the components in such a pair. The reverberation component scattered at shallow depths first, Class Ia. SURF imaging suppresses both components equally.

A.3 Destructive effects to DCS suppression

As explained above, the delay corrected subtraction method works by subtracting equal reverberation noise of two signals from each other. The reverberation noise is made equal by correcting for a difference in propagation delay in two signals. The first order and "true" signal components have another propagation delay difference and are thus kept in the subtraction. If the reverberation noise components are unequal after delay correction, the reverberation suppression is reduced.

As shown in Section A.2.4 the reverberation signal can be divided into a Class Ia and Ib. Further, Fig. A.2 illustrates that Class Ia from one signal is subtracted away by the Class Ib of the other signal and vice versa. Keeping this in mind the destructive effects to DCS suppression are here divided in to three parts.

1. Effects that make CIa and CIb unequal between two signals, described in Sections A.3.1 and A.3.2.

2. Effects that make the alignment of CIa of one signal and CIb of another difficult, described in Sections A.3.3 to A.3.5.

3. Delay estimation errors, described in Section A.3.6.

A.3.1 Nonlinear self-distortion (NSD) and nonlinear attenuation

As mentioned in Section A.2 nonlinear propagation up to the first scatterer is responsible for a scatterer specific propagation delay. Another effect of nonlinear propagation is nonlinear self-distortion of the imaging pulse. As the pulse propagates nonlinearly, energy from the main frequency band is moved up into harmonic bands and the pulse is distorted. Upon receive, the pulse-complex is bandpass filtered to remove the LF wave and the harmonic components. This means that the energy moved to the harmonic bands is lost. Call this loss *nonlinear attenuation*. As noted earlier the amplitude of the pulse-complex is reduced so much after scattering that further nonlinear propagation can be neglected. This means that the loss of energy up to harmonic bands is dependent on the depth of the first scatterer. Following this logic it means that the Class Ia reverberation component has less nonlinear attenuation than the Class Ib component as CIb has a longer propagation path up to the first scatterer. This difference in CIa and CIb is damaging for the delay corrected subtraction method as described in Section A.2.5 where it was noted that CIa of one pulse-complex transmit is subtracted by CIb of another (see Fig. A.2).

A.3.2 Pulse form distortion (PFD)

Pulse form distortion or PFD, as mentioned briefly in Section A.2, is the modification of the HF pulse form by the LF wave. Since the modifying LF waves are different for transmits of different polarities, the effects of PFD on the transmitted HF pulses will also be different. Transmitting a HF on top of an LF peak ($p = 1$, plus polarity) gives the center of the HF pulse higher propagation velocity than its edges. Placing the HF on the trough of an LF wave ($p = -1$, minus polarity) yields higher propagation speeds at the ends of the HF pulse compared to at its center.

Different PFD between different HF/LF pulse-complex configurations (polarities) leads to sub par correction in DCS as the goal is to subtract *equal* reverberation components from each other. The only correction done in DCS is adjusting for the difference in delay between different polarity signals.

A solution is to lower the LF frequency which would keep the induced propagation delay introduced by the amplitude, but minimize the effect of PFD (see Section A.2.6).

One consideration not taken into account here is the phase shift of the LF wave as it propagates to its focus. [8, pp. 12.99-100] This phase change alters the position of the HF on the LF. The HF also has a phase shift but this is negligible compared to that of the LF as the LF has a much lower frequency giving a bigger temporal effect of the same phase shift. Note how equal temporal shits of LF waves of opposite polarities would move the co-propagating HF pulses in the same direction on the LF waves. But since the sign of the underlying LF waves is different the introduced gradient of the LF pressure over the HF pulses would be of opposite sign. The phase shift of the LF therefore introduces different PFD of HF pulses in different polarity pulse-complexes. One polarity transmit would result in a stretching of the HF pulse as effect of the LF pressure gradient over the HF pulse. This would move the HF band down in frequency. For the opposite LF polarity the HF pulse would experience a contraction resulting in moving the HF band up in frequency. The increased frequency would result in a higher absorption of this transmitted pulse-complex as absorption in tissue increases with frequency. [15]

It seems reasonable to the authors that it is possible to minimize the PFD by finding an optimum position of the HF on the LF at the start of the transmit such as to keep it on top of the LF up to the depth of interest. The authors would suggest this as a future study. Here, the HF pulse is positioned directly on top of the LF at transmit.

A.3.3 Propagation delay differences between polarities

The theory behind DCS as explained in Section A.2.5 assumes that the only difference between reverberation noise for different polarities at a given depth is a nonlinear propagation delay, τ_{np}. In reality, as illustrated in Fig. A.2 there is not *one* reverberation noise component with *one* varying delay for each polarity. The correction delay applied in DCS is a mean between Class Ia and Ib components. In addition there are multiple Class Ia and Ib pairs around a single depth which may have different mean delays. As illustrated in Fig. A.2, the correction is possible by subtracting the mean delay between corresponding reverberation pairs at different polarities and subtracting them from one another. It is assumed that all reverberation pairs at a given depth have the same mean delay. This may not be the case as is discussed further in Section A.3.4. It is not directly assumed that the mean reverberation delay is equal in magnitude for signals of opposite polarities, $\tau_{\mathrm{n}+} \neq -\tau_{\mathrm{n}-}$, but it *is* assumed that the distance between Class Ia and Ib reverberation pairs are equal. If this distance is unequal it is not possible to align the reverberation pairs on top of each other as in (b) in Fig. A.2 and optimal correction is not possible.

Demanding that the distance between CIa and CIb is constant between polarities (ignoring different strengths of CIa and CIb) yields

$$\begin{aligned} &\tau_{\mathrm{n}+}(z-z_1) - \tau_{\mathrm{n}+}(z_1) = \\ &\qquad -\big(\tau_{\mathrm{n}-}(z-z_1) - \tau_{\mathrm{n}-}(z_1)\big)\ \forall z > 0. \end{aligned} \tag{A.20}$$

This can be rewritten to the definition of the derivative around $z/2$ with step-size $\Delta z = (z - 2z_1)/2$,

$$\begin{aligned} &\tau_{\mathrm{n}+}(z/2+\Delta z) - \tau_{\mathrm{n}+}(z/2-\Delta z) = \\ &\qquad -\big(\tau_{\mathrm{n}-}(z/2+\Delta z) - \tau_{\mathrm{n}-}(z/2-\Delta z)\big)\ \forall z > 0. \end{aligned} \tag{A.21}$$

This shows that the mean gradient of the first order NPD from z_1 to $z_3 = z - z_1$ needs to have opposite sign between opposite polarities. If this relation is to hold for all z the mean gradient needs to be equal for all depths. In addition demanding $\tau_{\mathrm{n}+}(0) = \tau_{\mathrm{n}-}(0) = 0$ then results in $\tau_{\mathrm{n}+}(z) = -\tau_{\mathrm{n}-}(z)$. It has not been assumed that Δz can take any value, meaning that the equation should hold for any scattering combination. The equation only needs to hold when comparing different polarity signals of the same underlying scatterers. If the equation is to hold for any z_1 (or Δz) the result would be a reverberation delay independent of the position of the scatterers. Equation (A.21) leads to $\tau_{\mathrm{n}+}$ and $\tau_{\mathrm{n}-}$ being point symmetric around the corresponding function values at $z/2$. If this is to hold for all depths z, the shape of $\tau_{\mathrm{n}+}(z)$ and $\tau_{\mathrm{n}-}(z)$ would need to be linear.

Going back to the more general case where it is demanded that $\mathrm{d}\tau_{\mathrm{n}+}/\mathrm{d}z = -\mathrm{d}\tau_{\mathrm{n}-}/\mathrm{d}z$, (A.3) shows that for (A.20) to hold it is required that the observed LF pressure peak is of equal magnitude between transmits of opposite polarity. In other words the propagation of the positive and negative polarity LF wave needs to have equal, but opposite sign, pressures across the co-propagating HF pulse. If this is not the case the DCS correction suffers. Nonlinear distortion has the effect of making the peaks higher than the troughs which would give this effect. [8, pp. 12.99-100]

A.3.4 Scatterer statistics and scatterer dependent delay

As noted briefly in Section A.3.3 many reverberation pairs contribute to noise at a given depth. The reverberation delay used in the DCS correction is a mean of the delays of all the reverberation pairs. If the variance of the delay between different pairs is small, the mean delay will give a good estimation for all pairs and the DCS method will be able to suppress many reverberation pairs well. If the variance is high, the delay used for correction may only be good for a small portion of the reverberation pairs, and the error present in the other pairs will result in a poor reverberation suppression overall in the final image.

So when is the total reverberation delay close to the same value for all reverberation pairs at a given depth? Considering collections of reverberation pairs alone, and not individual scattering cases this is synonymous to that the mean delay of a Class Ia and Ib pair being independent of the depth of the first and third scatterer. $\tau_{\mathrm{n}}(z;z_1,z_3) = (\tau_{\mathrm{x}}(z_1) + \tau_{\mathrm{x}}(z_3))/2 \to \tau_{\mathrm{n}}(z)$. This is the case when the first order propagation delay increases linearly with depth (see Section A.3.3). When the mean delay of a reverberation pair depends heavily on the position of the scatterers the resulting reverberation noise at a given depth will have high variance as typically many possible scattering pairs give noise at a certain depth.

There are multiple effects that would make the propagation delay nonlinear. From (A.3) it is seen that with either a depth variable nonlinearity parameter β_{n}, or compressibility κ, of the medium the shape of the first order NPD, $\tau_{\mathrm{x}}(z)$, is not linear. Focusing, or de-focusing of the LF wave would also alter the pressure observed by the HF pulse. Movement of the HF relative to the top of the LF wave would also alter the observed pressure and generate a nonlinear-with-depth NPD. Typically one transmits a focused HF pulse on top of an unfocused LF wave. The focusing delays of the HF will then make the HF be positioned on different points on the LF on the periphery as compared to at the center channel. The alteration of the received pulse this generates is rather complex as it results in a combination of pulses from different parts of the transducer which exhibit not only different propagation delays but also different pulse form distortion. However, it is reasonable to assume that it has an effect on the linearity of the first order propagation delay. Applying a focusing lens in elevation on the probe which is typically done in linear array transducers to get a more narrow HF focus, would also give focusing of the LF wave.

Another effect that yields a scatterer dependent reverberation delay is nonlinear

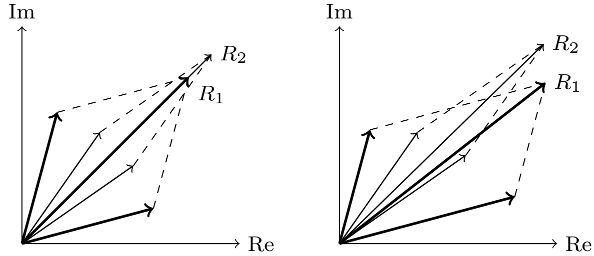

(a) No nonlinear attenuation. (b) With nonlinear attenuation.

Figure A.3: Effect of nonlinear attenuation on the scatterer position dependence on the combined reverberation delay of a reverberation pair at a given depth. A single third order scattering event is modeled by $\alpha(z_1)\mathrm{e}^{i\omega\tau_{\mathrm{x}}(z_1)}$, where α represents the nonlinear attenuation and τ_{x} is the first order delay. Two such events combine to a pair R with a resulting delay (phase). (a) No nonlinear attenuation and no scatterer dependence on the delay (phase) of the combined reverberation. Two reverberation pairs R_1 and R_2 have the same phase independent of the depth of the scatterers. (b) Nonlinear attenuation yields a delay (phase) dependent on the scatterer depths which combine to the reverberation pairs R_1 and R_2.

attenuation, as discussed in Section A.3.1. This is the removal of energy from the base band up to higher harmonics during nonlinear propagation. This effect makes Class Ib noise lower in magnitude compared to Class Ia as Class Ib has a bigger portion of nonlinear propagation compared to Class Ia (see Fig. A.3). The mean reverberation delay is then weighted more towards the Class Ia reverberations than Class Ib as Class Ia is more prominent in the total signal.

In conclusion the first order propagation delay will typically not be perfectly linear even in a homogeneous material and there will be a scatterer combination dependence on the reverberation delay at a certain depth. This is further discussed by the authors in another paper. [13] The scatterer dependent propagation delay yields a variance in the reverberation delay of different pairs contributing to reverberation noise at a given depth. This lowers the effectiveness of the DCS suppression method as it is not possible to apply a single delay (τ_{n}) that can align up all the CIa and CIb components as described in Fig. A.2 of Section A.2.5. This is studied later in simulations in Section A.5.2.

A.3.5 HF pulse length

A long pulse leads to poorer depth resolution. Defining the retarded time at the center of the pulse when doing the conversion from time of flight to depth makes thin scatterers stretch out both above and below the actual depth. Analogous to this is what happens to the propagation delay as a pulse-complex hits a thin scatterer in a low echogene region. The propagation delay is related to the depth, or time of flight, of the pulse before it hits the first scatterer. As different parts of the same pulse hits the scatterer at different times they will result in converted signals representing scatterers at slightly different depths, but the propagation delay will be the same as the total path propagated by different parts of the pulse is the same.

Consider two strong scatterers closer than one HF pulse length from each other. As they are at different depths, pulses scattered off of each of them will have different propagation delays. As the scatterers are closer than a pulse length, the received signals from the two will interfere. The NPD in the area between the two scatterers will be a weighted mean of the NPDs of each of the two scatterers.

For reverberation suppression by delay corrected subtraction this becomes a problem. The DCS algorithm needs to know the exact delay between the reverberation components of the two signals used. When scatterers representing different NPDs overlap it is difficult to apply a single delay to correct for the noise generated by both of them. This would indicate a dependence on the HF pulse length on the effectiveness of DCS. This is studied by simulations in Section A.5.4.

A.3.6 Error in estimated nonlinear propagation delays

The effect of an error in the estimated reverberation delay, $\hat{\tau}_\mathrm{n}$, can be estimated mathematically through a simple assumption of single band pulses without distortion. The DCS correction can be written (based on (A.13) and (A.15)),

$$\begin{aligned}\hat{X}_0 = \quad & X_0 \frac{\mathrm{e}^{i\omega(\tau_\mathrm{x}-\hat{\tau}_\mathrm{n})} - \mathrm{e}^{-i\omega(\tau_\mathrm{x}-\hat{\tau}_\mathrm{n})}}{\mathrm{e}^{i\omega(\hat{\tau}_\mathrm{x}-\hat{\tau}_\mathrm{n})} - \mathrm{e}^{-i\omega(\hat{\tau}_\mathrm{x}-\hat{\tau}_\mathrm{n})}} \\ & + N_0 \frac{\mathrm{e}^{i\omega(\tau_\mathrm{n}-\hat{\tau}_\mathrm{n})} - \mathrm{e}^{-i\omega(\tau_\mathrm{n}-\hat{\tau}_\mathrm{n})}}{\mathrm{e}^{i\omega(\hat{\tau}_\mathrm{x}-\hat{\tau}_\mathrm{n})} - \mathrm{e}^{-i\omega(\hat{\tau}_\mathrm{x}-\hat{\tau}_\mathrm{n})}},\end{aligned} \tag{A.22}$$

$$\begin{aligned}\hat{X}_0 = \quad & X_0 \frac{\sin\left(\omega(\tau_\mathrm{x}-\hat{\tau}_\mathrm{n})\right)}{\sin\left(\omega(\hat{\tau}_\mathrm{x}-\hat{\tau}_\mathrm{n})\right)} \\ & + N_0 \frac{\sin\left(\omega\delta\tau_\mathrm{n}\right)}{\sin\left(\omega(\hat{\tau}_\mathrm{x}-\hat{\tau}_\mathrm{n})\right)},\end{aligned} \tag{A.23}$$

where $\delta\tau_\mathrm{n} = \tau_\mathrm{n} - \hat{\tau}_\mathrm{n}$, is the error in the estimated reverberation noise delay, and $\tau_\mathrm{n} = \tau_{\mathrm{n}-} = -\tau_{\mathrm{n}+}$ and the same relation for τ_x with the same assumption for the estimated delays. The estimated first order NPD is written $\hat{\tau}_\mathrm{x}$. Calculating the SRR increase yields

$$\mathrm{SRR}_\mathrm{increase} = \frac{\mathrm{SRR}_\mathrm{after}}{\mathrm{SRR}_\mathrm{before}}, \tag{A.24}$$

$$= \frac{\sin\left(\omega(\tau_\mathrm{x}-\hat{\tau}_\mathrm{n})\right)}{\sin\left(\omega\delta\tau_\mathrm{n}\right)}. \tag{A.25}$$

Note how this result is independent of the estimation of the first order NPD. Setting $\tau_\mathrm{x} = 40$ ns and $\tau_\mathrm{n} = \tau_\mathrm{x}/2 = 20$ ns, with a center frequency of 8 MHz results in the

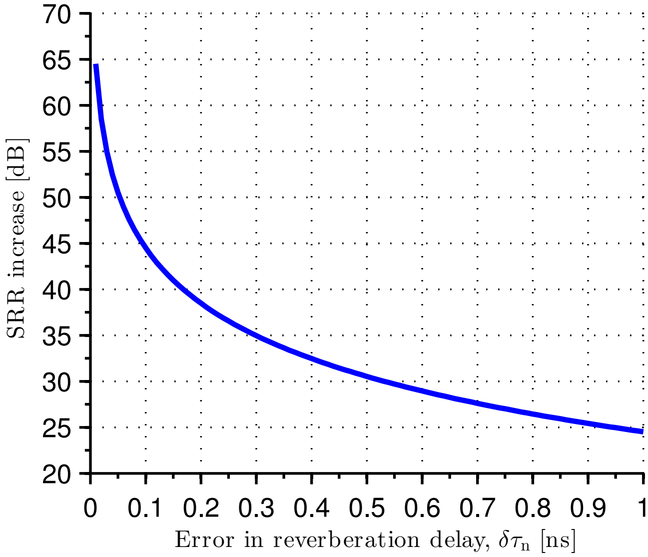

Figure A.4: Effect of an error in the estimated reverberation delay as applied in delay corrected subtraction. Decibel plot of (A.25).

curve shown in Fig. A.4. A relatively small error quickly reduces the possible SRR increase achievable through DCS. With different reverberation pairs having different delays at the same depth, the different reverberation pairs will be suppressed with different effectiveness given one delay. To get a best possible suppression of the noise it is therefore necessary to not only apply a correct delay in DCS but also that all reverberation pairs have the same delay at a certain depth.

A.4 Numerical simulation setup

Pulses are simulated through an in-house program based on Abersim. [16] The Abersim computer package is a simulation tool for the nonlinear propagation of forward propagating waves from arbitrary geometries. Linear and nonlinear propagation is computed separately by using an operator splitting approach. The linear propagation is solved for by using an angular spectrum method. Nonlinearity is accounted for through pressure dependent perturbation of the linearly propagated field using the method of characteristics. Abersim allows for accurate and fast nonlinear simulation of forward propagating waves and was therefore ideal for this study.

Setup for the simulations are found in tables A.1 and A.2. The pulse-complexes are simulated in steps of 1 mm in a three dimensional homogeneous medium and then beamformed. To generate an rf-signal from the simulated pulses, the pulses

Table A.1: Simulation parameters

Parameter	Value	Unit
Samples in azimuth	64	-
Samples in elevation	64	-
Propagation depth	40	mm
Step size depth	1	mm
Step size azimuth	0.3	mm
Step size elevation	0.3	mm
Sampling frequency	200	MHz
Non-linearity parameter, β_p	$2.0 \cdot 10^{-9*}$	Pa^{-1}
Wave propagation speed, c_0	1540	m/s

*Varied in Fig. A.6

Table A.2: Pulse setup parameters

Parameter	HF	LF	Unit
Transmit pressure	0.5	0.5	MPa
Center frequency	8	0.78	MHz
Focus azimuth	22	∞	mm
Focus elevation	22	22*	mm
Pulse oscillations	2.5	2.5	-
Aperture azimuth	7.3	11	mm
Aperture elevation	4.3	8	mm
Shape	Gaussian	Gaussian	-

*Lens focus over HF aperture.

are first stripped of their NPD. A synthetic NPD is applied to a set of scatterers which is then convolved with the pulses. Overlapping squared sinusoidal windows are utilized to get a smooth transition between pulses. The procedure is equal to one published previously[13] and is therefore only briefly described here. The difference is that here, the NPD is extracted from the pulses and applied directly on the scatterers.

The procedure is similar for generating reverberation signals. Here the simulated pulses are dependent on the depth of the first scatterer and on the total propagation depth. The meshing of pulses and scatterers is therefore a little more complicated. Reverberation noise for a 2 mm interval at depth z is generated by first convolving a 1 mm square window at z_1 of the stretched scatterers (as used for generating the first order rf-signal), with an un-streched version of the same scatterers with a corresponding 1 mm square window around z_3. The result is a triangular window of length 2 mm around depth $z = z_1 + z_3$. This resulting *reverberation scatterer* is then convolved with a pulse simulated nonlinearly to z_1 and linearly the remaining distance $z_1 + 2z_3$. The process is repeated for all combinations of z_1 and z_3 for all depths z and summed to get a total reverberation signal. As the scatterers in this study are planar, a scattering is a complete mirroring of the pulse-complex. This means that to simulate a reverberated pulse-complex, one propagates nonlinearly up to a depth z_1 and then linearly the remaining distance $2z - z_1$. The second and third scatterer (the transducer and another scatterer in the tissue) is not explicitly handled in the pulse-complex simulation. Only in the *reverberation scatterer* with which the received pulse-complex is later convolved.

Using a synthetic delay on the scatterers achieves two things: 1) complete control of the NPD, allowing the investigation of this effect isolated; and 2) a continuously developing NPD. Having the NPD on the pulses would result in areas of constant NPD meshed together. This would not produce speckle differences between different polarities of the LF wave. Which is of interest in this study.

To study the signal to reverberation noise ratio (SRR), the simulated pulses are combined with 300 sets of scatterers to generate 300 scan lines. One set of scatterers is sampled with $f_\mathrm{s} = 200$ MHz up to a total depth of 40 mm. The scatterers are random with a Gaussian distribution of strength and Poisson distribution in distance between each other. The mean distance between scatterers are 20 samples or $20c_0/2f_\mathrm{s} = 77$ µm.

A.5 Results of numerical study

The damaging effects to DCS suppression of reverberation noise is studied by how it alters the signal to reverberation noise ratio (SRR) after processing compared to with no processing. The DCS algorithm of (A.17) is applied to the first order signal and reverberation component of the total signal separately meaning that the

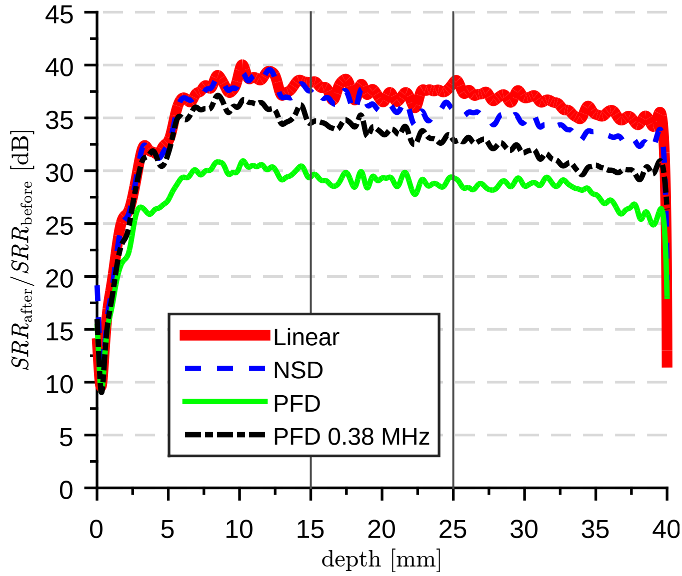

Figure A.5: SRR increase simulations with nonlinear self-distortion (NSD), full pulse form distortion (PFD), and a linear simulation. A linear propagation delay is applied synthetically and is equal for all scenarios. Vertical lines used in comparison with Fig. A.7.

SRR increase can be calculated. This procedure is identical to that presented in a previous paper by the authors. [13]

A.5.1 Effect of NSD and PFD

Applying a linear synthetic NPD on a linear simulation and applying DCS correction yields the top curve in Fig. A.5. The result is an increase in SRR between 35 and 40 dB between 5 mm and 40 mm depth compared to the unprocessed result. Simulating pure HF pulses nonlinearly and then applying a synthetic NPD gives rf-signals with NSD but no PFD. The result is an equal increase in the SRR increase up to around the focus at 22 mm. After this the SRR increase is around 2-3 dB less than the linear simulation without NSD.

The effect of PFD is studied by introducing an LF wave in the simulation. With the same linear synthetic first order NPD, the SRR increase is around 30 dB and between 5 and 10 dB lower than that of the linear simulation. The effect of the PFD is lowered when the LF frequency is halved, where at 10 mm the effect is a 6 dB improvement which drops linearly towards 30 mm. The near field constraint on the LF wave mentioned in Section A.2.6 is not maintained here and might explain the decline in SRR increase with depth.

The effect of the nonlinearity of the medium on the SRR increase is shown in Fig. A.6. The synthetic first order NPD is kept linear and equal such that the graph

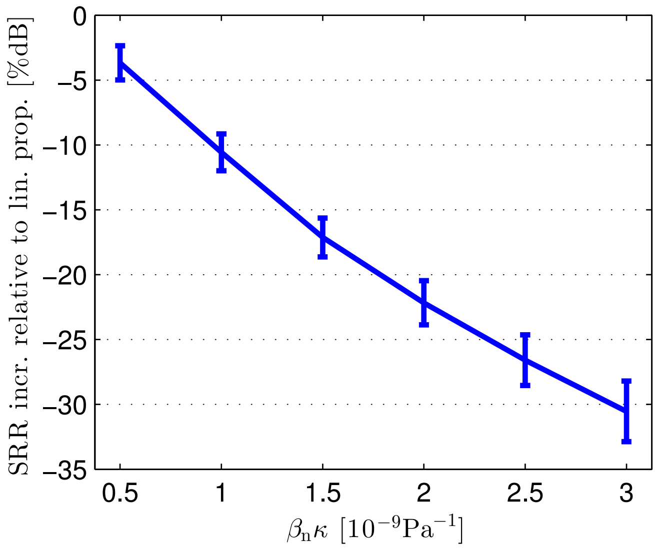

Figure A.6: Change in SRR increase after DCS correction in simulations with varying nonlinearity. Change is calculated relative to SRR increase in a linear simulation. The line thus shows the movement of the PFD line in Fig. A.5 with varying nonlinearity of the medium. SRR increase is averaged between 5 mm and 39 mm to disregard an almost equal increase up to 5 mm and uncertainties in the model at maximum depth. Errorbars show the standard deviation over the range used in computation of the average.

only should reflect changes in the PFD. The change in decibels increase of SRR is plotted in % relative to the top line in Fig. A.5 representing a pure linear simulation ($\beta_n\kappa = 0$, Linear). This method of displaying the result minimized the variance with depth. The result is a near linear dependence on $\beta_n\kappa$ from values ranging from 0 Pa^{-1} to $3 \cdot 10^{-9}$ Pa^{-1}. A rule of thumb can be extracted as a reduction of 10 %dB per $1 \cdot 10^{-9}$ Pa^{-1} increase of $\beta_n\kappa$. For comparison typical biological values range from (all in 10^{-9} Pa^{-1}): ≈ 1.59 for blood, through ≈ 1.78 for skeletal muscle and up to ≈ 3.20 for fat (based on numbers found in literature[11]). This indicates that higher nonlinearity gives lower effect of DCS suppression of noise in dual band imaging.

A.5.2 Shape of the delay curve

As postulated in Section A.3.4 the shape of the delay curve seems to have a large effect on the SRR increase. See Fig. A.7, compared to Fig. A.5. In Fig. A.7, the mean NPD is still 1 ns/mm, but it is 50 % lower between 15 and 25 mm compared to outside this interval. The effect is a gradient steeper than 1 ns/mm from 0 to 15 mm, and from 25 to 40 mm, and a lower gradient than 1 ns/mm between 15

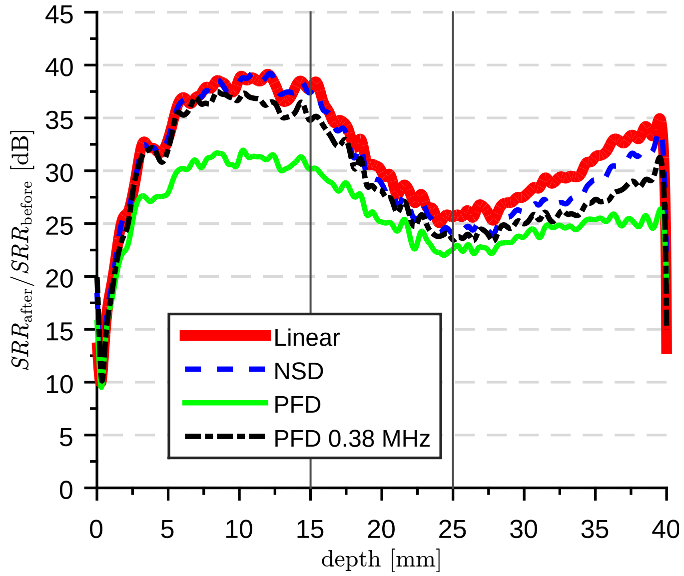

Figure A.7: SRR increase simulations with nonlinear self-distortion (NSD), full pulse form distortion (PFD), and a linear simulation. A piecewise linear propagation delay is applied synthetically and is equal for all scenarios in the figure. The gradient of the linear delay is reduced to 50 % between 15 and 25 mm compared to outside this region.

and 25 mm. In medical terms this would correspond to a fatty layer from 0 to 15 mm followed by blood between 15 and 25 mm, with another fatty layer down to 40 mm. The scatterer dependent reverberation delay this generates removes the 10 dB difference between the linear and full PFD simulation of Fig. A.5 and drops both down to around 25 dB at 25 mm. A reduction of around 12 dB for the linear simulation and around 6 dB for the simulations with full PFD. Note that the simulation with full PFD already has a scatterer dependent reverberation delay as this is introduced by the nonlinear attenuation as discussed in Section A.3.4 (see Fig. A.3).

A.5.3 Propagation delay differences between polarities

In Section A.3.3 it was indicated that a difference in the propagation delay between polarities also would lead to different reverberation components. This would reduce the effectiveness of the DCS algorithm. To isolate and study this effect, signals based on zero polarity pulses are applied with delays and examined. First: equal but opposite sign NPDs are applied to the plus and minus signals. The NPD is linear and the value of the gradient is varied between 0.25 and 1 ns/mm. Second: the NPD is fixed for the minus polarity signal at 1 ns/mm and varied between -0.25 and -1 ns/mm for the plus polarity signal. The SRR increase through DCS

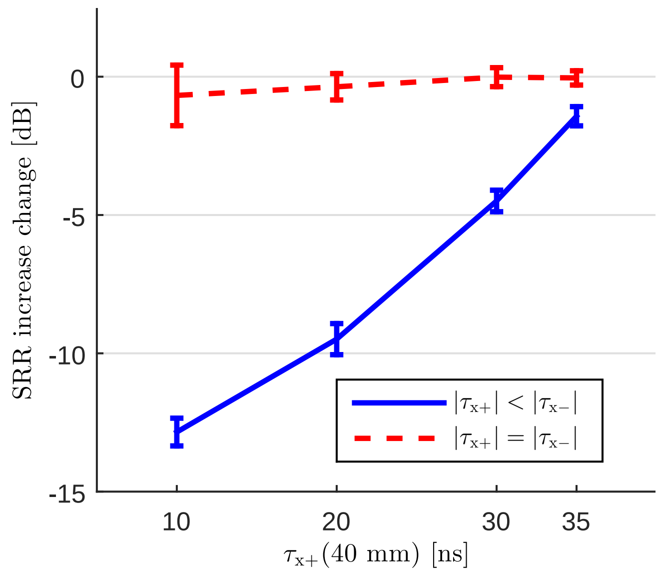

Figure A.8: Change in SRR increase when altering the maximum delay of a linear propagation delay development from 40 ns at 40 mm. Dashed line shows change when maximum delay is changed for the plus and minus polarity signals simultaneously. The full line shows the change in SRR increase when only the maximum delay of the plus polarity is changed and the maximum delay of the minus polarity is kept at 40 ns. The graph strengthens the theory laid out in Section A.3.3 and discussed in Section A.5.3. SRR increase is averaged between 25 and 39 mm and errorbars shows the standard deviation within this region. Signals based on pure nonlinear HF simulation with synthetic first order NPDs applied.

is then compared to the case when $|\tau_{x+}| = |\tau_{x-}| = 40$ ns at 40 mm (see Fig. A.8).

Fig. A.8 shows that the SRR increase is independent of the maximum of the linear propagation delay when it is equal between polarities. Some variation with depth is observed, but the variance between different runs of the simulations is too high to state a dependence. When changing the maximum propagation delay of the plus polarity there is a relatively large drop in the effectiveness of the DCS algorithm. This result supports the discussion in Section A.3.3 that the separation of CIa and CIb reverberation noise is increased and that this leads to a poorer result of the DCS method.

A.5.4 Pulse length

As outlined in Section A.3.5 the temporal length of the HF pulse sets a limit on the precision of the NPD as it varies with depth. Section A.2.6 also explains why a longer pulse length of the HF increases PFD. Fig. A.9 shows that by reducing the pulse length of the transmitted HF pulse from 2.5 to 1.5 oscillations gives an

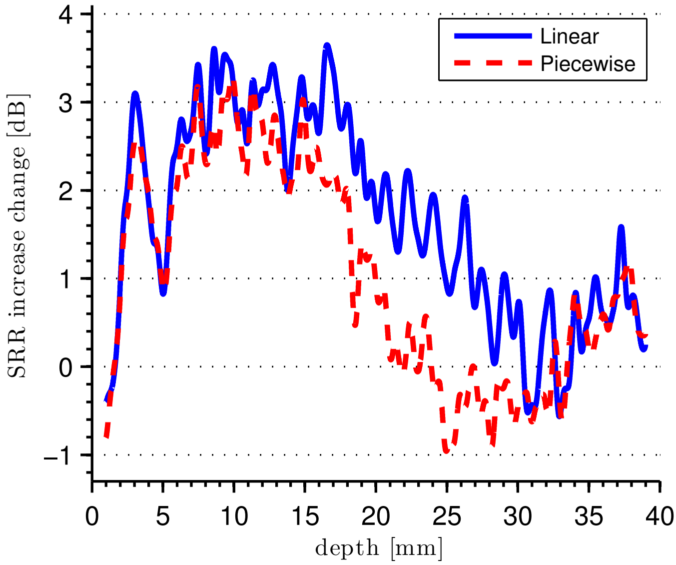

Figure A.9: Changing the pulse length of the HF from 2.5 to 1.5 yields a change shown here in the SRR increase through DCS. Signals based on nonlinear pulse simulations with synthetic first order delays. Whole line shows linear first order delay development while dashed line shows the situation with a piecewise linear first order delay curve, similar to the one used in Fig. A.7.

average increase of the SRR increase (nonlinear simulation with PFD). The gain by lowering the pulse length is greater when the first order NPD is linear as in Fig. A.5 with an increase of 2 to 3 dB before the focus at 22 mm. After the focus the gain is lowered to around 1 dB. For a piecewise linear first order NPD (Fig. A.7) the gain from lowering the HF length is about the same up to 15 mm and slightly lower and even negative around focus.

As illustrated by Fig. A.7 compared to Fig. A.5, the introduction of a piecewise linear first order NPD reduces the difference between a linear simulation and a simulation with full PFD. With a link between shorter HF pulse length and lower PFD this effect is also observed in Fig. A.9. For a piecewise linear first order NPD the reduction of PFD introduced by a shorter HF pulse is lower at the same depths as where the linear and full PFD simulations are similar in Fig. A.7, namely between 15 and 25 mm. Why a shorter pulse would give a lower SRR improvement around focus is not understood by the authors.

A.6 Further discussion

The results shown in Section A.5 gives an overview of how damaging the theoretical effects presented in Section A.3 are to reverberation suppression with the DCS algorithm. However, three topics need to be discussed explicitly: 1) The limits of reverberation suppression when there is no nonlinear propagation effects except for a linear delay; 2) The role of the shape of the nonlinear propagation delay curve; and 3) A decision as to what is the largest damaging effect to reverberation suppression. These are addressed in the subsequent sections.

A.6.1 Why does linear propagation not show infinite reverberation suppression?

As discussed in Section A.3.5 the length of the imaging HF pulse sets not only limitations on the spatial resolution, but also limitations on the accuracy of the propagation delay correction that can be used. When pulses scattered of different scatterers overlap, a mean correction delay must be used on the combined signal (as discussed in Section A.3.5). It is worth noting that this effect is quite small as the propagation delay does not change much over a pulse length. Assuming, as in Section A.2.4, $\mathrm{d}\tau_{\mathrm{n}p}/\mathrm{d}z \approx 1$ ns/mm, a center frequency of 8 MHz, and a pulse length of 2.5 oscillations, leads to a variation of $\tau_{\mathrm{n}p}$ over the pulse length to $1\,\text{ns/mm}\cdot 1540\,\text{m/s}\cdot 2.5/8\,\text{MHz} = 0.481$ ns. Reading from Fig. A.4 with an error of $0.481/2$ ns the best case SRR increase is ≈ 36 dB. This result can explain why not an infinite SRR increase is observed for the linear simulation in Fig. A.5. Doing the same calculation for a shorter pulse with 1.5 oscillations yields a maximum of ≈ 40 dB. This calculated increase corresponds to the 3-4 dB increase shown in Fig. A.9.

A second contributor to sub-par SRR increase for a linear simulation is speckle variations between reverberations of different polarities. A negative NPD effectively moves the scatterers further apart while a positive NPD moves them closer together. The result is different signal when convolved with the imaging pulse.

A.6.2 Gradient, value or shape of delay giving reduced suppression?

Introducing a piecewise linear shape of the NPD of the first order signal as in Fig. A.7 compared to a fully linear delay as in Fig. A.5 shows a lower SRR improvement after DCS processing. As the maximum value of the delay is constant and set to 40 ns at 40 mm, there are two possible reasons for this change in SRR increase. Either the suppression is better with a higher gradient of the propagation delay as is the case from 15 to 25 mm in Fig. A.5, or it is the shape of the whole curve that is important. Discussion of how reverberation components combine would suggest that it is the shape of the whole curve and not the gradient at a specific depth that is important. This is also reaffirmed by the observation that the SRR improvement is equal in the linear (Fig. A.5) and piecewise linear case (Fig. A.7) up to 15 mm, where the gradient is changed in the latter case.

However, to be sure that it is the shape of the delay curve that give rise to a lower SRR increase the case with piecewise linear delay was reexamined with an inverse change in the delay curve. Instead of halving the gradient from 15 to 25 mm it was doubled. The plot is not included here but displays a similar trend to what is shown in the inverse case as seen in Fig. A.7. The logical conclusion is thus that it is the shape of the delay curve up to the imaging depth and not the gradient at a specific depth that determines the level of reverberation suppression. Fig. A.8 also indicates that the maximum value of the delay plays no role. Note however that this is the conclusion looking at the NPDs alone. For instance increasing the nonlinearity of the medium, which would lead to an increase of the maximum value of the NPDs, would also lower the SRR increase due to an increase in PFD and NSD as shown in Fig. A.6.

To illustrate the importance of the shape of the delay curve the case of a piecewise linear delay as is used in Fig. A.7 can be discussed. Consider three scatterers which all generate reverberation noise at 25 mm. Scatterers at 0 mm and 25 mm, giving Class Ia and Ib reverberation noise.[2] And one single scatterer at 12.5 mm where CIa = CIb. Note how the scatterer at 25 mm also gives reverberations at 50 mm. This noise is not considered here. As in Fig. A.7 the mean gradient is 1 ns/mm from 0 to 40 mm with 50 % reduction between 15 to 25 mm compared to at other depths. It can be shown that this leads to a first order delay of $\tau_{\mathrm{x}}(12.5) = 14.29$ ns and $\tau_{\mathrm{x}}(25) = 22.86$ ns. The reverberation coming from the pair of scatterers at 0 and 25 mm gets a mean reverberation delay of $\tau_{\mathrm{n}}(\{0, 25\}) = (\tau_{\mathrm{x}}(0) + \tau_{\mathrm{x}}(25))/2 = 11.43$ ns. The pulse scattered twice of the scatterer at 12.5 mm gets a reverberation delay of $\tau_{\mathrm{n}}(\{12.5, 12.5\} = \tau_{\mathrm{x}}(12.5) = 14.29$ ns. The difference between these reverberation delays is 2.86 ns and by doing DCS with the mean of these two reverberation delays the error is 1.43 ns for both the pair and the single scatterer. Calculating the maximum SRR increase from (A.25) this gives 16.54 dB. When Fig. A.7 shows a higher SRR increase than 16.54 dB at 25 mm, this indicates that there are more or other scatterers combining to reverberation noise at that depth than those considered here. This example was designed to illustrate the worst case.

A.6.3 What is the biggest effect?

When one assumes that the NPDs are relatively equal in magnitude between polarities (Fig. A.8), the biggest inhibitor of a high SRR increase using DCS seems to be the effect of a nonlinear depth variation of the first order NPD as discussed in

[2] An observant reader could argue that this is simply a first order signal. Consider this instead as the maximum limit for separation of the CIa and CIb reverberation components.

Section A.6.2, and seen in Fig. A.7 compared to Fig. A.5. The scatterer dependent reverberation delay that this introduces (Section A.3.4) creates a variance between the delay of different reverberation pairs which makes it impossible to apply an optimal reverberation delay ($\hat{\tau}_{\mathrm{n}p}$) in the DCS method.

A.7 Conclusion

The effectiveness of the reverberation noise suppression is measured by the increase in the signal to reverberation noise ratio (SRR) after processing. The idealized theoretical framework presented here shows that the increase in SRR is 10 dB less when pulse form distortion (PFD) of the imaging pulse (HF) is present compared to when it is not. This indicates that an increased suppression of reverberation noise could be possible through the presented processing by methods which lower the PFD. It was found here that lowering the frequency of the modification pulse (LF) leads to less PFD and better reverberation reduction under delay corrected subtraction (DCS) suppression. In a medium with large changes in the nonlinearity with depth the destructive effects of PFD are negated by the increased complexity of reverberation noise which also reduces reverberation suppression. Optimizing transmitted pulses to reduce PFD therefore seems more important for mediums with low changes in the nonlinearity with depth.

Acknowledgment

The authors would like to thank J. Kvam for providing a pulse simulation framework and writing the text on Abersim, and O. F. Myhre for proof-reading and contributing in scientific discussions.

Bibliography

[1] R. Hansen and B. A. J. Angelsen, "SURF imaging for contrast agent detection," *IEEE Trans. Ultrason., Ferroelect., Freq. Control*, vol. 56, no. 2, pp. 280–290, February 2009.

[2] S.-E. Måsøy, Ø. Standal, S. P. Näsholm, T. F. Johansen, B. Angelsen, and R. Hansen, "SURF imaging: In vivo demonstration of an ultrasound contrast agent detection technique," *IEEE Trans. Ultrason., Ferroelect., Freq. Control*, vol. 55, no. 5, pp. 1112–1121, May 2008.

[3] D. L. Miller, "Ultrasonic detection of resonant cavitation bubbles in a flow tube by their second-harmonic emissions," *IEEE Ultrasonics Symposium*, pp. 217–224, September 1981.

[4] K. Caidahl, E. Kazzam, J. Lidberg, G. Neumann-Andersen, J. Nordanstig, S. Rantapaa Dahlqvist, A. Waldenström, and R. Wikh, "New concept in echo-

cardiography: harmonic imaging of tissue without use of contrast agent," *Lancet*, vol. 352, pp. 1264–1270, October 1998.

[5] M. A. Averkiou, D. N. Roundhill, and J. E. Powers, "A new imaging technique based on the nonlinear properties of tissues," *ULTRASON*, pp. 1561–1566, 1997.

[6] M. A. Averkiou, "Tissue harmonic imaging," *ULTRASON*, pp. 1563–1572, 2000.

[7] R. Hansen, S.-E. Måsøy, T. F. Johansen, and B. A. J. Angelsen, "Utilizing dual frequency band transmit pulse complexes in medical ultrasound imaging," *J. Acoust. Soc. Am.*, vol. 127, no. 1, pp. 579–587, January 2010.

[8] B. A. J. Angelsen, *Ultrasound imaging : waves, signals, and signal processing*. Emantec, 2000, vol. 2.

[9] J. M. Rau, "Dual frequency band ultrasound for suppression of multiple scattering," Ph.D. dissertation, NTNU, 2013.

[10] H. Høilund-Kaupang, "Models and methods for investigation of reverberations in nonlinear ultrasound imaging," Ph.D. dissertation, Norwegian University of Science and Technology, Department of Circulation and Medical Imaging, 2011.

[11] F. A. Duck, *Physical Properties of Tissue*. Academic Press, 1990.

[12] J. M. Rau, S.-E. Måsøy, R. Hansen, B. Angelsen, and T. A. Tangen, "Methods for reverberation suppression utilizing dual frequency band imaging," *J. Acoust. Soc. Am.*, vol. 134, no. 3, pp. 2313–2325, 2013.

[13] O. M. Brende and B. Angelsen, "Adaptive reverberation noise delay estimation for reverberation suppression in dual band ultrasound imaging," *J. Acoust. Soc. Am.*, vol. 138, no. 5, pp. 3341–3351, nov 2015. [Online]. Available: http://dx.doi.org/10.1121/1.4935555

[14] B. A. J. Angelsen, *Ultrasound imaging : waves, signals, and signal processing*. Emantec, 2000, vol. 1.

[15] T. Szabo, *Diagnostic Ultrasound Imaging: Inside Out (Biomedical Engineering)*. Academic Press Inc, 2004.

[16] M. Frijlink, H. Kaupang, T. Varslot, and S. E. Måsøy, "Abersim: a simulation program for 3d nonlinear acoustic wave propagation for arbitrary pulses and arbitrary transducer geometries," *IEEE Ultrasonics Symposium*, pp. 1282–1285, 2008.

Ole Martin Brende was born in Ålesund, Norway, in 1987. He received the M.Sc.(tech.) degree in Applied Physics in 2011 from the Norwegian University on Science and Technology. He started the Ph.D. at the Department of Circulation and Medical Imaging at the same university later that year. His Ph.D. work is on reverberation suppression in dual band imaging in medical ultrasound under guidance by Bjørn Angelsen.
He is currently a Research and Development Engineer at SURF Technology AS, Trondheim, Norway.

Bjørn Angelsen (M'79–SM'82) was born in Vestvågøy, Norway, in 1946. He received the M.E.E. degree in 1971 from the Norwegian University of Science and Technology, Trondheim, and the Ph.D. from the same University in 1977. His Ph.D. work was on Doppler ultrasound measurement of blood velocities and flow in the heart and the large arteries. He has been a professor of Medical Imaging at the same university since 1983.
In 1977 and 1978 he was a visiting Post-Doc at the University of California, Berkeley, and Stanford Research Institute, Palo Alto. He has been strongly involved in the development of cardiac ultrasound imaging instruments in collaboration with Vingmed Ultrasound, now GE Vingmed Ultrasound. He has written textbooks on ultrasound cardiac Doppler measurements and theoretical ultrasound acoustics, and holds several patents in the field of ultrasound imaging.

Paper B

Adaptive reverberation noise delay estimation for reverberation suppression in dual band ultrasound imaging

Ole Martin Brende[1] and Bjørn Angelsen
Department of Circulation and Medical Imaging
Norwegian University of Science and Technology
N 7489 Trondheim, Norway

Running title: Reverberation suppression in dual band imaging

Accepted for publication by the Journal of the Acoustical Society of America

The behavior of the propagation delays introduced in dual frequency band ultrasound imaging is discussed. In particular, the delay of reverberation noise components is examined. Using a delay corrected subtraction (DCS) method it is possible to suppress the reverberation noise if the behavior of the propagation delays is known. Here, a signal adaptive estimation for the reverberation delay is introduced and applied through DCS to suppress reverberation noise in a numerically simulated signal. The reverberation reduction is compared to DCS suppression using a simpler delay estimation and shows that a signal based adaptive estimation yields a improved suppression of reverberation noise. The study indicates that the advantage of the adaptive estimation is highest when the medium has changing nonlinearity with depth.

[1]Author to whom correspondence should be addressed. Electronic mail: ole.m.brende@ntnu.no

B.1 Introduction

Research in the field of ultrasound imaging has observed an increased focus on nonlinear imaging over the past 25 years. Notable are the study and clinical use of tissue harmonic imaging[1, 2], the use of nonlinear effects in ultrasound contrast imaging using microbubbles[3–5], pulse inversion[6, 7], and amplitude modulation[8, 9]. Another use, further studied here, is the use of a dual frequency band pulse called dual band imaging (DBI), also known as Second order UltRasound Field (SURF) imaging[10, 11], to reduce reverberation noise. A dual frequency band pulse has a high frequency ($\sim$8 MHz) pulse superimposed on a low frequency ($\sim$0.8 MHz) pulse. DBI has also been used in conjunction with contrast agent imaging.[4, 12]

A received ultrasound signal can be broken down into three components, ignoring electrical noise. The first, and often most interesting is linear first order scattering. This component is used to image density variations in the medium. The second is nonlinear first order scattering, e.g. scattering from microbubbles[3]. Here the scattering strength depends nonlinearly on the pressure amplitude and frequency.[3] For instance, imaging at the resonance frequency of a bubble gives a stronger rf-signal back compared to imaging at other frequencies. This component is further neglected in this study. The last is multiple scattering noise. Multiple scatterings at shallow depths create ghost signals deeper in the medium which can hide weak first order scattering signals. In this paper the use of DBI to suppress multiple scattering, or reverberation, -noise is studied. The main concept behind the suppression technique is that DBI introduces propagation delays which are different for the first order scattering and multiple scatterer components of the total signal. By transmitting two pulses designed to give different propagation delays, and knowing how these delays behave, it is possible to mathematically solve for the first order signal. Here, a signal adaptive method to estimate the propagation delays of the reverberation components is introduced. The method uses an estimation for the reverberation noise strength to adaptively estimate the resulting delay of the reverberation noise components. This differs from earlier work where a fixed relation between the first order and reverberation delay was used.[13, 14]

Reverberation noise can be damaging to studies where information in low echogene structures is required. Reverberation noise originating from strong scatterers at shallow depths can create image artifacts in the region of interest deeper in the tissue. Examples include imaging of tumors or arthereosclerotic lesions where fatty layers above the blood vessel combine with the vessel wall and create reverberation noise in the blood vessel.

Effects of nonlinear propagation increase with propagation distance which is utilized in harmonic imaging to reduce reverberation noise. The forward propagating pulse generates harmonic frequencies as it propagates but after the first scattering event the amplitude of the wave is reduced such that further propagation can be considered linear. By bandpass filtering over the 2nd harmonic band of the returned pulse it is therefore possible to suppress reverberation noise originating from structures that scatter the pulse at shallow depths as these signals have a smaller harmonic component. However, 3rd order reverberation noise always acts in pairs.[15] Consider two scatterers; one close to the transducer, and another closer to the imaging depth. A third order scattering combination can take two paths. One path is to scatter off the shallow scatterer first, then the transducer, and lastly the deep scatterer. This is denoted Class Ia (or CIa). The alternative route is the reverse, with scattering off the deep scatterer first, then the transducer, and lastly the shallow scatterer. This path results in Class Ib (or CIb) noise (see Fig. B.1 from the discussion in Sec. B.2.1). Where harmonic imaging only suppresses reverberation noise generated by scattering of the shallow scatterer (CIa), DBI, or SURF, makes it possible to suppress both at the same time. This theoretical advantage makes it interesting to study DBI even if the hardware needed to transmit a dual band pulse is more complex.

Previous work with DBI-based reverberation suppression is based on assumptions of equality of the reverberation noise pairs.[14] This paper tests this hypothesis further backed by computer simulations. A new type of estimation of the behavior of the reverberation components is derived based on the presented theory and tested on simulated data to show an improvement of the Signal to Reverberation noise Ratio (SRR).

When implemented, the suggested improvements to DCS processing would allow for a more direct suppression of reverberation noise leading to higher contrast resolution in B-mode ultrasound images damaged by reverberation noise. This could potentially allow for easier medical diagnosis.

B.2 Theory

B.2.1 Dual band imaging

This section provides a short introduction to DBI, for a thorough review the authors suggests earlier work.[10, 11, 13] DBI consists of adding a low frequency (LF) manipulation pulse to a conventional high frequency (HF) imaging pulse. By changing the amplitude or polarity of the LF pulse the propagation of the HF pulse is altered. By placing the HF pulse on a positive swing of the LF pulse, thus increasing the observed pressure in the tissue, the HF pulse achieves a higher propagation velocity. A change in the polarity of the LF pulse results in a negative pressure which in a similar way give a lower effective propagation speed. With a varying LF pressure over the HF, the different parts of the HF pulse have different propagation speeds and the result is a Pulse Form Distortion (PFD). A lower LF frequency results in a slower variation in the LF pressure across the HF pulse and thus less PFD.

The change in effective propagation velocity has been shown to follow[11]

$$c \approx \frac{c_0}{1 - \beta_{\rm n} \kappa p_{\rm LF}} \approx c_0(1 + \beta_{\rm n} \kappa p_{\rm LF}). \tag{B.1}$$

Here c_0 is the speed of sound in the medium without a modifying LF pulse, $\beta_{\rm n}$ is the nonlinearity parameter of the medium, κ is the compressibility, and $p_{\rm LF}$ is the mean LF pressure over the HF pulse. The change in propagation speed leads to a Nonlinear Propagation Delay (NPD) along the propagation path of the forward propagating pulse relative to propagation without a manipulating LF pulse,

$$\tau_{{\rm x}p}(z) = -\int_0^z \frac{{\rm d}s}{c_0(s)} \beta_{\rm n}(s) \kappa(s) p_{\rm LF}(s). \tag{B.2}$$

The subscript x indicates that this is a delay on the first order component. The second subscript, p, indicates that the delay is dependent on the LF pulse. It can be omitted for a simpler notation, as is done in the figures and tables in this paper.

Typically one transits multiple times per imaging line, keeping the HF constant and altering the amplitude and/or polarity of the LF with each transmit. The parameter p is used to keep track of each of the LF amplitudes and polarities. A HF positioned on top of a LF peak corresponds to $p = +1$, while changing the sign of the LF the polarity gives $p = -1$. Transmitting with a pure HF pulse is equivalent to $p = 0$. These three configurations are the only ones used in this study, although it is possible to also transmit with $p = \pm 1/2$, reducing the LF amplitude by a factor 2. The formalism is identical to defining the pressure through a reference pressure multiplied by p, or $p_{\rm LF} = p \cdot p_{\rm LF}^{\rm ref}$. Henceforth different LF configurations will be referred to as different polarities as the reference amplitude is considered fixed, for instance, a *zero polarity transmit* corresponds to $p = 0$, or a pure HF transmit.

The first order and multiple scattering noise behave differently depending on the polarity (and amplitude) of the LF. By creating a model for the difference in the behavior it is shown here that the first order scattering component can be extracted from the received total signals. The result is a signal with less reverberation noise than one generated by a pure HF transmit, as with conventional imaging.

The ratio between the LF and HF center frequencies typically vary from 1:5 to 1:20 depending on the implementation. The LF is unfocused and the HF is focused. A lowest possible LF frequency gives less variation of the LF pressure across the HF pulse. However, the lowest possible LF frequency is limited by the transducer aperture and frequencies. It is ideal that the imaging region is in the near-field region of the LF pulse to keep the LF pressure peak relatively constant. This puts a limit on the transducer aperture as the near field region is defined as

Table B.1: Pulse setup parameters

Parameter	HF	LF	Unit
Transmit pressure	0.5	0.5	MPa
Center frequency	8	0.78	MHz
Focus azimuth	22	∞	mm
Focus elevation	22	22	mm
Pulse oscillations	1.5	2.5	-
Aperture azimuth	7.3	11	mm
Aperture elevation	4.3	8	mm

$z < 2a^2/\lambda$. Where the transducer width is $2a$ and λ is the wavelength of the LF.[16] In this work a LF pulse at 0.78 MHz is used along a HF at 8 MHz. See Table B.1 for a full overview of the pulse setup.

B.2.2 Signal components

Ignoring nonlinear scattering and electric noise, a received ultrasound signal can be divided into two parts, first order scattering, $x(t)$, and reverberation scattering, $n(t)$.

The total signal can be divided up in a set of depth regions with index i, and Fourier transformed

$$Y_{ip}(\omega) = X_{ip}(\omega) + N_{ip}(\omega). \tag{B.3}$$

A received $p \neq 0$ first order scattering signal component can be modeled through the $p = 0$ first order scattering signal through a filter $V_{ip}(\omega)$, which includes the changes to the signal introduced by a nonzero modifying LF wave. Correspondingly for the reverberation components through, $L_{ip}(\omega)$.

$$Y_{ip}(\omega) = V_{ip}(\omega)X_{i0}(\omega) + L_{ip}(\omega)N_{i0}(\omega). \tag{B.4}$$

The filter on the first order scattering components contains the nonlinear propagation delay (see Eq. (B.2)) due to the magnitude of the manipulation pressure, and the pulse form distortion due to nonlinear effects and uneven manipulation pressure across the HF pulse.

The NPD $\tau_{\mathrm{x}ip}$ represents a time shift between the first order components. This time shift, or delay, is called the first order delay for short and corresponds to the linear phase of $V_{ip}(\omega)$,

$$V_{ip}(\omega) = \mathrm{e}^{-i\omega\tau_{\mathrm{x}ip}}\widetilde{V}_{ip}(\omega). \tag{B.5}$$

Here $\widetilde{V}_{ip}(\omega)$ is the PFD filter.

The total manipulation of the reverberation noise is a sum of all the pulse distortions to the pulses that contribute to reverberation noise at the given depth. Similarly to the first order scattering component, the difference between the reverberation noise of different polarities is modeled through a Noise Distortion (ND) filter with a corresponding NPD. The relationship of these to $L_{ip}(\omega)$ is similar to the relationship of the PFD and first order delay to $V_{ip}(\omega)$ (Eq. (B.5)).

$$L_{ip}(\omega) = \mathrm{e}^{-i\omega\tau_{\mathrm{n}ip}}\widetilde{L}_{ip}(\omega). \tag{B.6}$$

Where $\widetilde{L}_{ip}(\omega)$ is the ND filter and $\tau_{\mathrm{n}ip}$ is the mean NPD of the reverberation components that contribute to reverberation noise in interval i. In the same way that the first order scattering signal component is delayed $\tau_{\mathrm{x}ip}$, the reverberation components are delayed $\tau_{\mathrm{n}ip}$. This NPD of the reverberation signal is called the reverberation delay. Note how there can be many different combinations of scatterers that generate reverberation noise at a certain depth, and it is therefore necessary to talk about a *mean* reverberation delay.

The first order delay $\tau_{\mathrm{x}ip}$ and reverberation delay $\tau_{\mathrm{n}ip}$ generally vary with depth. Neglecting the distortion of the pulses for different polarities, $V_{ip} = L_{ip} = 1$, and only looking at the delay difference, Eq. (B.3) can be rewritten to the time domain with only a delay variance between the signal components.

$$y_p(t) = x_0\left(t - \tau_{\mathrm{x}p}(t)\right) + n_0\left(t - \tau_{\mathrm{n}p}(t)\right) \tag{B.7}$$

Here the NPDs are continuous with time instead of constant within a small interval i. Given two received signals based on different LF pulses following the model in Eq. (B.7), Sec. B.3 shows how the first order component $x_0(t)$ can be extracted given estimated values for the delays, $\tau_{\mathrm{x}p}(t)$ and $\tau_{\mathrm{n}p}(t)$. The delays can be estimated by comparing the $p \neq 0$ signals to a reference $p = 0$ signal as explained in Sec. B.4.

B.2.3 Behaviour of the delays

By assuming that the amplitude drop at the 1st scattering is so large that the nonlinear effects can be neglected and noting that the propagation delay is a cumulative effect, the propagation delay can be directly related to the depth of the first scattering event. This assumes a monotonically increasing (or decreasing) propagation delay which is the case if the sign on the LF pressure observed by the HF pulse is constant throughout the propagation. This is always the case in this study.

The first order delay stems from the propagation delay at the imaging depth while the delay from a reverberation component contributing to noise at the same depth has the first scattering at a shallower position. Since the magnitude of the propagation delay increases with depth, the delay of the reverberation component will always be lower in magnitude compared to the first order component. The

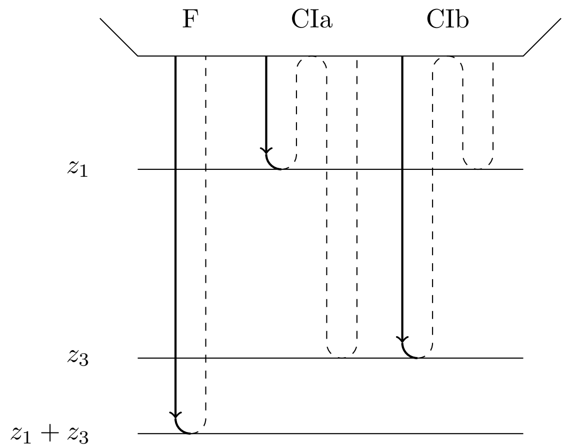

Figure B.1: Classification of reverberation noise. The 2nd scatterer is limited to the transducer ($z_2 = 0$) which is denoted by "I" in the notation. Dotted lines represent linear propagation while solid lines represent nonlinear propagation.

classification scheme for reverberation components, as briefly mentioned in the introduction, is shown in Fig. B.1. With planar scatterers at z_1 and z_3 the result is reverberation noise at $z = z_1 + z_3$. The CIa component scatters of the plane at z_1 first, and the CIb component scatterers of z_3 first. The "I" in the notation indicates that the second scatterer is the transducer surface as is the case for all reverberation considered in the paper.

In a heterogeneous medium there are multiple pairs of scatterers contributing to noise at a given depth. Since they always appear in pairs and the generated signals can be added linearly, generality is not lost by studying such pairs of scatterers instead of the "a" and "b" reverberation components individually. The total reverberation delay from the combined Class Ia and Ib reverberation pair can be calculated through the phase of the combined signal. Assuming delta scatterers and infinitely long pulses this results in a delay on the form

$$\begin{aligned}\tau_{\mathrm{n}p}(z;z_1,\omega_{\mathrm{c}})\\ &= \frac{-1}{\omega_{\mathrm{c}}}\angle\left(Q\mathrm{e}^{-i\omega_{\mathrm{c}}\tau_{\mathrm{x}p}(z_1)} + \mathrm{e}^{-i\omega_{\mathrm{c}}\tau_{\mathrm{x}p}(z-z_1)}\right). \end{aligned} \tag{B.8}$$

The operator $\angle\{\cdot\}$ extracts the phase of the complex number. The factor Q allows for effects such as unequal transmit and receive beams, and non-linear attenuation that make the amplitudes of the reverberation components different. Assuming equal transmit and receive beams and only considering plane scatterers, as is done throughout this paper, and for now assuming no nonlinear attenuation a simple delay estimation can be calculated by setting $Q = 1$,

$$\begin{aligned}\tau_{\mathrm{n}p}(z; z_1, \omega_{\mathrm{c}}) =& \frac{-1}{\omega_{\mathrm{c}}} \angle \Bigg\{ \mathrm{e}^{-i\omega_{\mathrm{c}} \dfrac{\tau_{\mathrm{x}p}(z_1) + \tau_{\mathrm{x}p}(z - z_1)}{2}} \\ & \cdot 2\cos\left(\omega_{\mathrm{c}} \frac{\tau_{\mathrm{x}p}(z_1) - \tau_{\mathrm{x}p}(z - z_1)}{2} \right) \Bigg\} \\ =& \frac{\tau_{\mathrm{x}p}(z_1) + \tau_{\mathrm{x}p}(z - z_1)}{2}. \end{aligned} \tag{B.9}$$

With a linear delay, $\tau_{\mathrm{x}p} \propto z$, the noise delay becomes $\tau_{\mathrm{n}p}(z) = \tau_{\mathrm{x}p}((z_1+z_3)/2) = \tau_{\mathrm{x}p}(z/2)$. Independent of the position of the first and third scatterers. This result is therefore valid for all the scatterer pairs that contribute to noise at depth z. The difference from this result introduced by nonlinear attenuation through Q is studied through simulations in Sec. B.6.1.

Assuming $\tau_{\mathrm{n}p}(z) = \tau_{\mathrm{x}p}(z/2)$ in a very non-linear medium shows not to be ideal. With changing non-linearity through the medium the propagation delay is also not linear which adds another error to the simple $\tau_{\mathrm{n}p}(z) = \tau_{\mathrm{x}p}(z/2)$ estimate. Denote this simple reverberation delay estimate $\tau^{\mathrm{h}}_{\mathrm{n}p}$, where the h indicates value at *half* depth,

$$\tau^{\mathrm{h}}_{\mathrm{n}p}(z) \triangleq \tau_{\mathrm{x}p}(z/2). \tag{B.10}$$

In this paper a new delay estimate is introduced which circumvents the problems with different CIa/CIb strength and non-linear first order NPD, $\tau_{\mathrm{x}p}(t)$, in the estimation of the reverberation delay, $\tau_{\mathrm{n}p}(t)$.

B.3 Suppression method

The aim is to solve for the first order signal from a set of equations on the form of Eq. (B.7). In this section the received signal from transmit of two identical HF pulses with opposite LF polarity is studied. The parameter p takes the values ± 1. In general p could take any value and the method is valid for any combination of two pulse complexes. However, a special case is obtained when using opposite polarities of the LF pulses. Switching the sign of the LF pulse would according to Eq. (B.2) also result in a switch of the sign of the propagation delay. The cosine factor in Eq. (B.9), representing a speckle variation which is dependent on the propagation delay, is independent of the polarity of the delay and will hence remain unchanged after a change in sign of the LF pulse.

Returning to Eq. (B.7) with $p = \pm 1$ a set of two equations are obtained

$$\begin{aligned} y_+(t) &= x_+(t) + n_+(t), \\ &= x_0(t - \tau_{\mathrm{x}+}(t)) + n_0(t - \tau_{\mathrm{n}+}(t)), \qquad \text{(B.11a)} \\ y_-(t) &= x_-(t) + n_-(t), \\ &= x_0(t - \tau_{\mathrm{x}-}(t)) + n_0(t - \tau_{\mathrm{n}-}(t)). \qquad \text{(B.11b)} \end{aligned}$$

Applying an appropriate delay to each of the total signals and subtracting, the reverberation terms can be eliminated

$$\begin{aligned} y_+(t+&\tau_{\mathrm{n}+}(t)) - y_-(t + \tau_{\mathrm{n}-}(t)) \\ &= x_+(t + \tau_{\mathrm{n}+}(t)) - x_-(t + \tau_{\mathrm{n}-}(t)) \\ &= x_0(t - \tau_{\mathrm{x}+}(t) + \tau_{\mathrm{n}+}(t)) \\ &- x_0(t - \tau_{\mathrm{x}-}(t) + \tau_{\mathrm{n}-}(t)) \qquad \text{(B.12)} \end{aligned}$$

This is known as the Delay Corrected Subtraction (DCS) method.[14] The resulting signal has fully suppressed noise components under the given assumptions but a shift between the first order components. This time shift introduces a gain factor which is more easily calculated by studying the signal in the Fourier space. Equation (B.12) is rewritten to

$$\begin{aligned} &Y_{i+}(\omega)\mathrm{e}^{-i\omega\tau_{\mathrm{n}i+}} - Y_{i-}(\omega)\mathrm{e}^{i\omega\tau_{\mathrm{n}i-}} \\ &= X_{i0}(\omega)\left(\mathrm{e}^{i\omega(\tau_{\mathrm{x}i+}-\tau_{\mathrm{n}i+})} - \mathrm{e}^{i\omega(\tau_{\mathrm{x}i-}-\tau_{\mathrm{n}i-})}\right). \end{aligned}$$

Solving for the signal component, X_{i0}, assuming narrowband pulses and transforming to the time domain only taking care of the modulus for the gain factor, results in an estimated first order signal

$$\hat{x}_0(t) = \frac{y_+(t + \tau_{\mathrm{n}+}(t)) - y_-(t + \tau_{\mathrm{n}-}(t))}{\left|\mathrm{e}^{i\omega_c(\tau_{\mathrm{x}+}(t)-\tau_{\mathrm{n}+}(t))} - \mathrm{e}^{i\omega_c(\tau_{\mathrm{x}-}(t)-\tau_{\mathrm{n}-}(t))}\right|}. \qquad \text{(B.13)}$$

This correction can also be used where one of the transmitted pulses is a pure HF pulse by setting the first order and reverberation delay of the received $p = 0$ signal to zero.

Note again that the phase of the gain factor is excluded in the calculation. However, as it can be calculated this phase change poses no trouble for imaging modalities such as tissue elastography where phase information of the signal is required.

B.4 Delay estimation

To be able to use the DCS method outlined above, one needs to estimate the delays of the different components in the signal. The main scope of this paper is on acquiring well suited delays for this purpose. The focus is mainly on acquiring a good estimate of the reverberation delay, $\tau_{\mathrm{n}p}$.

Outside of computer simulations one cannot distinguish between the first order and reverberation components of the total signal. There is no direct access to the first order delay $\tau_{\mathrm{x}p}$, or the reverberation delay, $\tau_{\mathrm{n}p}$. What can be estimated is the total delay between the received total signals generated with different polarities of the LF pulse. Knowing how this total delay behaves it is possible to make an estimate for the first order and reverberation delays.

The total delay $\tau_{\mathrm{y}p}$ is found through an instantaneous phase method described by Standal *et al.*[17] In areas with strong first order signal (high SRR) this value approaches the first order delay. In areas with much stronger noise than first order signal (low SRR), this total delay approaches the delay of the reverberation components.[13] In practice there is always a mix between reverberation noise and first order signal, and a total delay between the first order delay and reverberation delay, $|\tau_{\mathrm{n}p}| < |\tau_{\mathrm{y}p}| < |\tau_{\mathrm{x}p}|$.

B.4.1 First order delay estimation

As the first order delay is always higher in magnitude than the reverberation delay, the first order delay can be estimated by looking at the maximum values of the total delay. Picking out the maximum values that show monotonic increase and interpolating linearly between these peaks, then gives an estimated curve for $\tau_{\mathrm{x}p}(t)$. A more robust estimation can be done by only selecting monotonically increasing peaks that minimize the gradient of $\tau_{\mathrm{x}p}$. This creates a shortest-path curve around the peaks of $\tau_{\mathrm{y}p}$ and avoids rapid fluctuations of the gradient.

Since this paper focuses on improving the estimation of the reverberation delay, the comparison of the different correction methods below therefore assumes that an ideal first order delay has been found. The first order delay is measured directly from the first order signal in the simulation. However, in a real experimental setup the true first order signal is not known. Only the total signal with noise.

B.4.2 Reverberation noise delay estimation

Earlier approaches to estimate the reverberation delay, $\tau_{\mathrm{n}p}$, assumed that the Class Ia and Ib noise were equal in strength and that the propagation delay development was linear. The result was the fixed relation from Eq. (B.10), $\tau_{\mathrm{n}p}(z) = \tau^{\mathrm{h}}_{\mathrm{n}p}(z) \triangleq \tau_{\mathrm{x}p}(z/2)$.

The aim here is to develop a robust and adaptive estimation of the reverberation delay without the assumptions of equal strengths for the Class Ia and Ib reverberation components, and a linear propagation delay development. To model the factor Q in Eq. (B.8) it is assumed that the only difference between CIa and CIb is due to nonlinear attenuation. Let the nonlinear attenuation to a depth z introduce an amplitude change α^z, this yields (from Eq. (B.8))

$$Q(z; z_1) = \alpha^{z_1}/\alpha^{z-z_1}. \tag{B.14}$$

With this definition a sum of all possible reverberation pairs resulting in noise at $z = z_1 + z_3$ can be constructed as

$$\sum_{z_1=0}^{z/2} \left\{ R(z_1)R(z-z_1)\left(\alpha^{z_1}\mathrm{e}^{-i\omega_\mathrm{c}\tau_{\mathrm{x}p}(z_1)} + \alpha^{z-z_1}\mathrm{e}^{-i\omega_\mathrm{c}\tau_{\mathrm{x}p}(z-z_1)} \right) \right\}. \tag{B.15}$$

Here, $R(z)$ is defined as the scatterer strength at depth z. The strength of a reverberation signal originating from scatterers at z_1 and $z - z_1$ is thus $R(z_1)R(z - z_1)$. Note that Eq. (B.15) does not correspond to the reverberation *signal*, but rather the *strength* and phase of the reverberation noise at a certain depth. An additional factor, describing the scatterer strength off the transducer could also be included. However, as only reverberation scattered off the transducer is studied here, and the factor is equal for all these components, it is omitted from the model as it would be canceled out in the SRR calculation. Equation (B.15) is used as a basis for an adaptive delay estimation by estimating the scattering strengths, $R(z)$, through the envelope of the received unprocessed signal, $\hat{R}(z) = \mathrm{env}\,\{y_0(2z/c)\}$. This estimation is based on both the first order signal and any reverberation noise. This might lead to an error in the estimation of the delay, discussed further in Sec. B.8.4.

Some scatterer combinations would create stronger reverberation noise than others. The contribution from these to the phase would therefore be of more importance than from diffuse weak scatterers. To highlight the stronger scatterers a parameter γ is introduced as a power for the estimated scatterer strength, $\hat{R} \to \hat{R}^\gamma$. As the interest lies only in the linear phase of the reverberation estimation (Eq. (B.15)), and not the absolute magnitude, this introduction of this parameter poses no further effects on the delay estimation save for the highlighting of strong scatterer combinations.

Realizing that the sum in Eq. (B.15) can be written as an integral, and changing the limits such that the integral sums Class Ia and Ib independently, an estimation model for the reverberation delay is achieved, call this $\tau_{\mathrm{n}p}^{\mathrm{RR}}$

$$\tau_{\mathrm{n}p}^{\mathrm{RR}}(z; \alpha, \omega_\mathrm{c}, \gamma) \triangleq \frac{-1}{\omega_\mathrm{c}} \angle \int_0^z \mathrm{d}z_1\; R^\gamma(z_1)\alpha^{z_1}\mathrm{e}^{-i\omega_\mathrm{c}\tau_{\mathrm{x}p}(z_1)} R^\gamma(z - z_1). \tag{B.16}$$

B.5 Simulation method

What makes the simulation used in this paper different from a full simulation is the separation of the pulse simulations and the scattering medium. The result is that computation heavy pulse simulations can be reused with different scattering sets and a faster computation time for a total problem is achieved. This is possible by considering a homogeneous medium with planar scatterers. The readers only interested in the main topic of this paper, the suppression results with an adaptive reverberation delay estimation, can skip directly to Sec. B.6 without lacking understanding when the results are discussed.

B.5.1 Simulation setup

The main assumption in this work is that the pulse amplitude drops so much after the first scattering event that the propagation further can be considered linear. To generate a first order received pulse from depth z, the simulation is nonlinear up to z and linear back to the transducer. The scatterers are assumed to be planes. To get the full signal, pulses were simulated in this manner for each whole millimeter up to a total depth of 40 mm. The reverberation components are simulated in a similar way, but the total propagation length is extended. As the scatterers were planar, a scattering would correspond to a mirroring of the pulse. By simulating pulses up to twice the maximum imaging depth of 40 mm with varying depth of nonlinear propagation both the first order and reverberation pulses could be calculated.

B.5.2 Incorporation of simulations in mathematical model

A set of simulated pulses are merged with a set of scatterers defined in $R(z) = \widetilde{R}(2z/c_0) = \widetilde{R}(t)$. In the frequency domain the final signal from a given depth is the Fourier transform of the scatterers multiplied by an imaging function, or point spread function.[16] The imaging function in this ultrasound system is the focused and beamformed pulses. The signal $x_i(t)$ at a given depth is then the convolution of the pulses and the scatterers at the same depth

$$x_i(t) = \int \mathrm{d}\xi \; u_i(\xi, z_i)\widetilde{R}(t-\xi). \tag{B.17}$$

The signal is only valid for the depth at which the pulse is simulated. To generate the total signal the computation in Eq. (B.17) must be done for each of the first order simulated pulses and merged. Each result, $x_i(t)$, is windowed by a square sinusoidal function centered around the valid depth, z_i, with width 2 mm. The results are then summed to generate the total signal.

Reverberation noise

Scatterers at z_1 and $z - z_1$ combine to give a reverberation signal at z, see Fig. B.1. By combining all possible scattering combinations a pseudo scatterer can be calculated

$$RR(z) = \int_0^z \mathrm{d}z_1 \, R(z_1)R(z - z_1), \tag{B.18}$$

$$= R(z) \otimes R(z). \tag{B.19}$$

For a linear simulation the reverberation signal would be the imaging pulse at z convolved with this combined pseudo scatterer. However, since the pulses are simulated linearly after the first scattering event (Born approximation), the reverberation pulses are dependent not only on the total propagation path, but also on this first scatterer position. When creating the final rf-signal care has to be taken to apply the simulated pulse with the correct scatterers corresponding to not only the total propagation path, but also on the position of the first scatterer. A simulated pulse with first scattering at $\tilde{z}_1$ and second scattering at $\tilde{z}_3$, written $u(t, \tilde{z}_1, \tilde{z}_3)$, should only interact with the combined scatterers based on $R(\tilde{z}_1)$ and $R(\tilde{z}_3)$. This is solved by applying a square window on $R(z)$ with width of one simulation step around $\tilde{z}$ and writing this as $R_\mathrm{w}(z; \tilde{z})$. The rf-signal based on a simulated pulse $u(t; \tilde{z}_1, \tilde{z}_3)$ can then be written as

$$n(t; \tilde{z}_1, \tilde{z}_3) = \int \mathrm{d}\xi \int_0^z \mathrm{d}z_1 \, u(\xi; \tilde{z}_1, \tilde{z}_3) \cdots$$
$$R_\mathrm{w}(z_1, \tilde{z_1}) R_\mathrm{w}(z - z_1 - c_0\xi/2; \tilde{z}_3) \tag{B.20}$$

The total reverberation signal is the combined signal from all components at all depths, written

$$n(t) = \sum_{\tilde{z}_1} \sum_{\tilde{z}_3} n(t; \tilde{z}_1, \tilde{z}_3). \tag{B.21}$$

A factor representing the scattering strength of the transducer should also be included, but is omitted here as it plays no role in the derivations and results described in this paper.

B.6 Initial simulation results

The aim in this paper is to reduce the reverberation noise in the combined rf-signal. However, as the simulation method first generates pure pulses independent of the scatterers in the medium, it is also possible to study the propagation effects on the pulses alone. This is done in this section, and related to the effect the pulses have on the reverberation noise in the combined rf-signal.

B.6.1 Variance in noise delay depending on first scatterer position

Combinations of CIa and CIb noise components give a total delay. As non-linear attenuation is different for the two components their weight will be different in

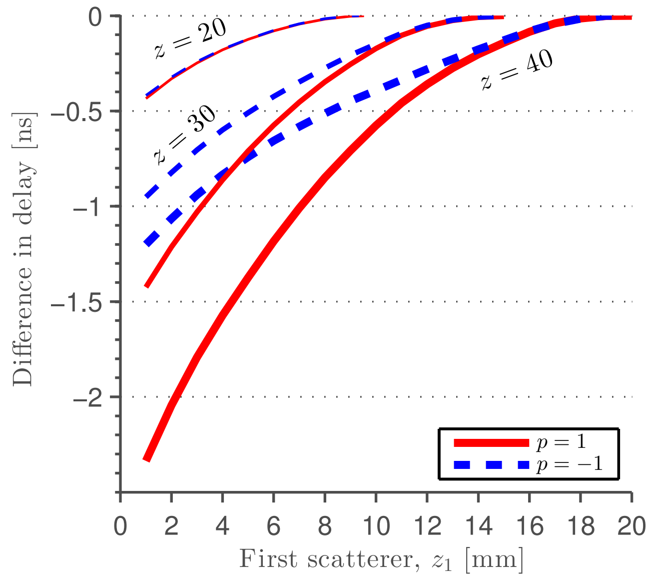

Figure B.2: The difference in the combined delay of CIa and CIb components for reverberation noise at three depths, 20, 30, and 40 mm, compared to the simple assumption of $\tau_n(z) = \tau_x(z/2)$. By varying the position of the first scatterer, z_1, a difference from the delay when CIa and CIb are equal is observed. The curves are symmetrical around $z_1 = z/2$, but this symmetry is omitted here for a clearer figure. The pulses were simulated with a constant nonlinear propagation delay gradient of 1 ns/mm. (Color online)

the resulting mean delay. The total reverberation noise delay will therefore be dependent on the position of the scatterers in the noise. This is supported by Fig. B.2 where there is a difference in the order of 1 ns between the CIa and CIb combinations with scattering at $z_1 = 1$ mm and $z_3 = 39$ mm, and the combination where $z_1 = z_3 = 20$ mm.

Note that this is an observed effect on a linear first order propagation delay curve. Making the first order propagation delay nonlinear would further create a dependency on the scattering positions for the combined CIa-CIb delay.

B.6.2 Nonlinear attenuation

As mentioned in Sec. B.2.2 nonlinear attenuation makes the magnitude of a CIa reverberation larger than for the corresponding CIb reverberation. This affects the mean reverberation delay of this reverberation pair.

To estimate the effect of nonlinear attenuation, pulses of equal total propagation distance with varying amount of nonlinear propagation is compared. The total energy is compared for a set range around the center frequency of the HF (4.3 MHz – 9.6 MHz).[18] Comparing pulses with 39 mm nonlinear propagation to 1 mm nonlinear propagation a relative drop of $Q \approx 3.2$ dB is found for the positive polarity and $Q \approx 1.8$ dB for the negative polarity pulses. Without any modifying LF pulse the drop is $Q \approx 2.6$ dB.

This result is inserted into Eq. (B.8) to calculate the resulting reverberation delay estimate. Assuming a constant first order propagation delay gradient of 1 ns/mm and measuring a center frequency shifted from 8 Mhz to 6.25 MHz at 40 mm the reverberation delay differs by -2.22 ns for the positive polarity and by -1.24 ns for the negative polarity compared to the simpler assumption that $\tau_{\mathrm{n}p}^{\mathrm{h}}(z = 40 \text{ mm}) = 20$ ns. This result fits within 0.1 ns of what is measured directly (see Fig. B.2.)

Figure B.2 shows that a larger separation of the scatterers giving reverberation noise at a certain depth yields a larger change in the mean nonlinear propagation delay of the reverberations compared to the fixed-relation estimation $\tau_{\mathrm{n}p}^{\mathrm{h}}$. A high separation between the scatterers along with a nonlinear attenuation makes the combined reverberation delay closer to that of the CIa component and thus lower in magnitude compared to the estimate from the fixed-relation equation (Eq. (B.10)).

B.7 Studying suppression

Since the first order and reverberation components are separated in the simulation, it is possible to calculate the SRR before the correction. And since the DCS correction method is linear, it is also possible to apply the correction algorithm to the first order- and reverberation signals alone and compute the SRR after correction. This makes it possible to study the SRR *increase* of different delay estimation algorithms through DCS correction.

B.7.1 Test method

The effect of the reverberation suppression methods are tested through five test cases, or *tissue models*. All five cases have a set of equal underlying background scatterers as basis. These have a Gaussian distributed amplitude and a Poisson distributed distance between them. A total of 300 realizations of the scatterer distributions are computed. These 300 realizations are then used as basis for each of the five test cases resulting in 300 simulations for each test case. The mean (and variance) of the Poisson distribution is $\lambda_{\mathrm{p}} = 20$ samples, corresponding to a spatial mean distance between scatterers as $\lambda_{\mathrm{p}} c_0 / 2 f_s = 77$ µm.

There are three factors that distinguish the tissue cases from each other. (1) The introduction of a low echogenic region from 15 mm to 25 mm. Reducing the scatterer strength of the Gaussian scatterers to 20 %. (Case III, IV and V.) (2) Manipulation of the first order delay to be either linear, or piecewise linear with a 50 % lower gradient between 15 mm to 25 mm. Both up to a maximum delay of ± 40 ns between the minus and zero, and plus and zero polarities. (Case II, IV, and

Table B.2: Changes applied to default tissue defined in Sec. B.7.1 used for studying SRR increase of different reverberation delay estimation methods. (Color online)

Case #	Delay shape	Scatterers
I	Linear	Homogeneous
II	Piecewise linear	Homogeneous
III	Linear	Low echogene insert
IV	Piecewise linear	Low echogene insert
V	Piecewise linear	Low echogene insert, strong scatter lines.

V being piecewise linear.) (3) Introduction of strong scatterers equal for each run of the test case at depths 7, 15 and 25 mm. This modification is only present in tissue case V. See Table B.2 for an overview of the tissue models.

Note that although the scatters are different between the tissue cases, and between different runs of each case, the same pulses are used in generating the received signal. Simulating the pulses in a pure homogeneous medium ignores aberration effects and ignores changes in the non-linearity of the propagation. Since the propagation delay varies proportionally with the non-linearity, $\beta_n \kappa$ (Sec. B.2.1), effects such as changes of the gradient in the first order delay curve is missed in the homogeneous simulation. This effect is reintroduced in tissue case II, IV, and V by manually altering the delay between the simulated pulses before the signal is generated. In the other cases the nonlinear delay of polarities $p \neq 0$ is removed and a linear delay is introduced.

The parameters for the pulse setup and simulation can be found in Table B.3. Note the non-linearity, $\beta_n \kappa = 2 \cdot 10^{-9}\mathrm{Pa}^{-1}$. For reference, typical values for tissue range from (all in 10^{-9} Pa^{-1}): ≈ 1.59 for blood, through ≈ 1.78 for skeletal muscle and up to ≈ 3.20 for fat.[19, 20]

B.7.2 Processing and results

The plots in Figs. B.3 to B.7 show the relative increase in signal to reverberation noise, SRR, for the DCS method outlined in Sec. B.3 using different delay estimations. All are based on a a posteriori direct measurement of the first order propagation delay. As this work is on estimating the reverberation delay, which is based on estimation of the first order delay, using a "perfect" first order delay gives a best case scenario for the reverberation delay estimation. The SRR plots (Figs. B.3 to B.7) show the increase in SRR for three different reverberation delays. (1) Using a direct measured reverberation delay representing the best case scenario with the suppression method, $\tau^{\mathrm{y}}_{\mathrm{n}p}(t)$. (2) The adaptive $\tau^{\mathrm{RR}}_{\mathrm{n}p}(t)$ estimated delay introduced in Sec. B.4.2 and (3) The fixed-relation $\tau^{\mathrm{h}}_{\mathrm{n}p}(t)$ estimation from Sec. B.2.3.

Table B.3: Simulation parameters

Parameter	Value	Unit
Samples in azimuth	64	-
Samples in elevation	64	-
Propagation depth	40	mm
Step size depth	1	mm
Step size azimuth	0.3	mm
Step size elevation	0.3	mm
Sampling frequency	200	MHz
Non-linearity parameter, β_p	$2.0 \cdot 10^{-9}$	Pa^{-1}
Wave propagation speed, c_0	1540	m/s

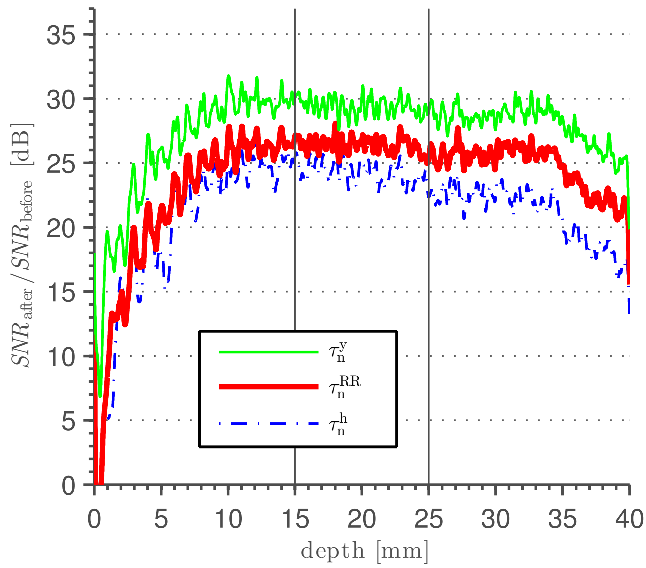

Figure B.3: Case I. Increase in SRR after correction based on different delay estimates. Linear first order propagation delay development (1 ns/mm) throughout plot. Delays used: best case, $\tau_{\mathrm{n}}^{\mathrm{y}}$, proposed method, $\tau_{\mathrm{n}}^{\mathrm{RR}}$, and earlier method, $\tau_{\mathrm{n}}^{\mathrm{h}}$. (Color online)

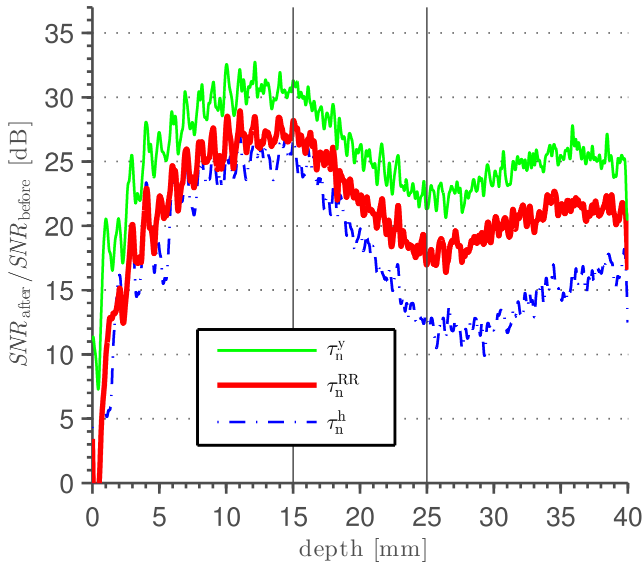

Figure B.4: Case II. Increase in SRR after correction based on different delay estimates. A decrease of 50 % in the gradient of the first order delay between 15 and 20 mm compared to other depths. Delays used: best case, τ_n^y, proposed method, τ_n^{RR}, and earlier method, τ_n^h. (Color online)

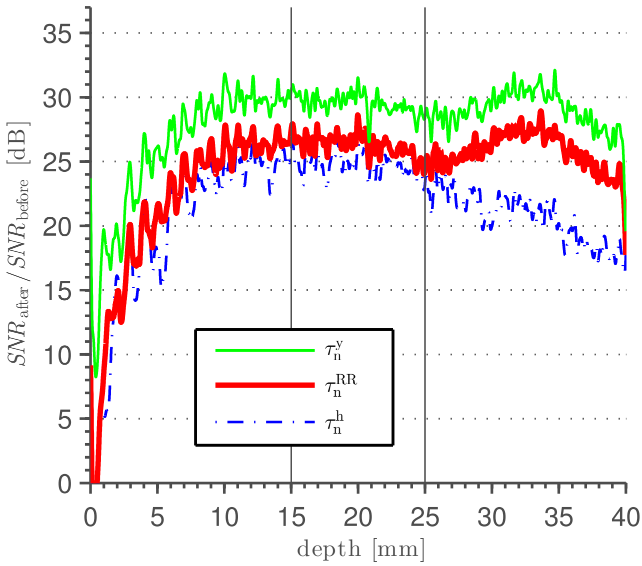

Figure B.5: Case III. Increase in SRR after correction based on different delay estimates. Linear propagation delay throughout plot. Scattering strength reduced to 20 % between 15 and 25 mm compared to case I scatterers (Fig. B.3). Delays used: best case, τ_n^y, proposed method, τ_n^{RR}, and earlier method, τ_n^h. (Color online)

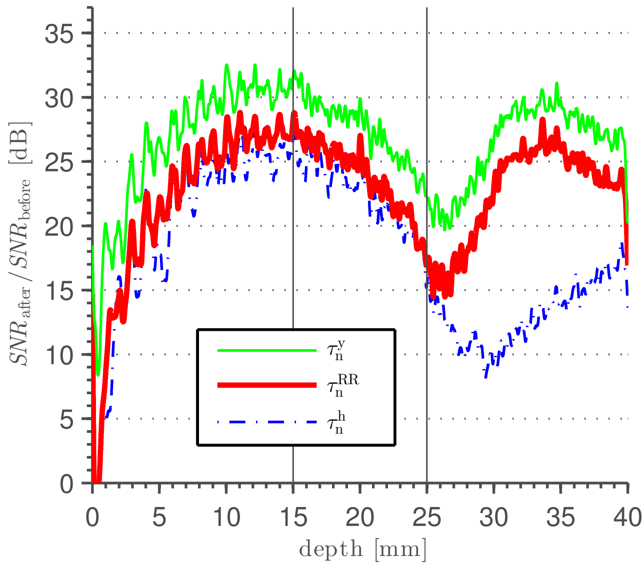

Figure B.6: Case IV. Increase in SRR after correction based on different delay estimates. A decrease of 50 % in the gradient of the linear delay and reduction of scattering strength to 20 % between 15 and 25 mm. A combination of case II (Fig. B.4) and III (Fig. B.5). Delays used: best case, τ_n^y, proposed method, τ_n^{RR}, and earlier method, τ_n^h. (Color online)

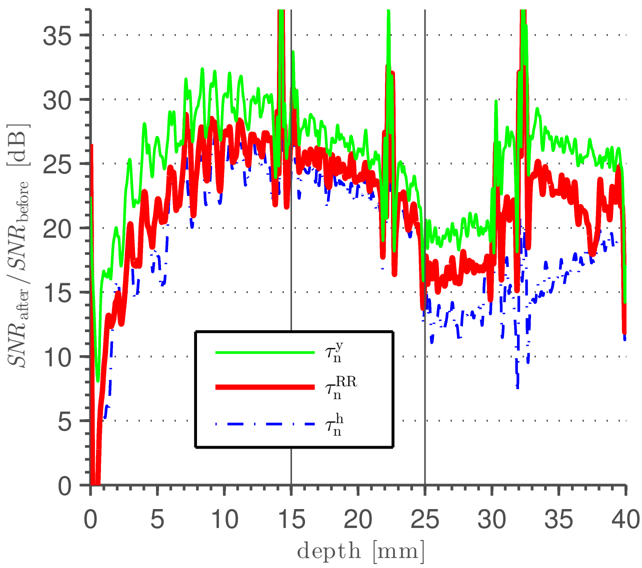

Figure B.7: Case V. Increase in SRR after correction based on different delay estimates. Decrease of 50 % in the gradient of the linear delay and reduction of scattering strength by 80 % between 15 and 25 mm. A combination of Case II (Fig. B.4) and III (Fig. B.5). In addition, strong scatterers is introduced at 7, 15 and 25 mm. Delays used: best case, τ_n^y, proposed method, τ_n^{RR}, and earlier method, τ_n^h. (Color online)

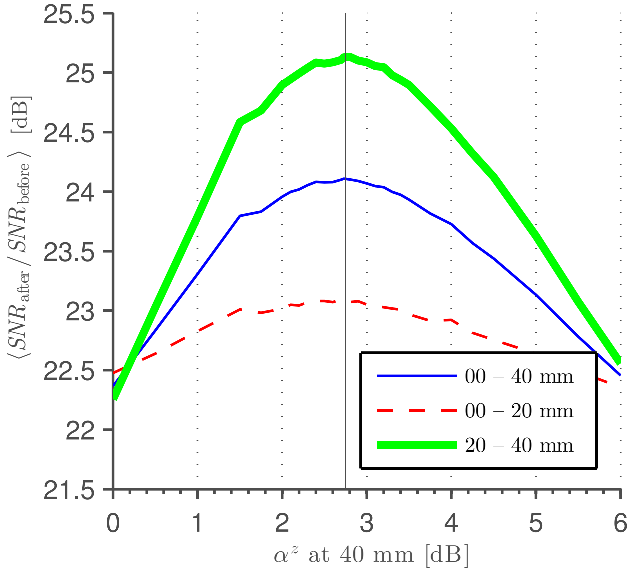

Figure B.8: Estimation of optimal nonlinear attenuation coefficient α for reverberation suppression. SRR increase (Eq. (B.22)) is compared for different values of α (in Eq. (B.16)) summed in dB over three depth ranges. Abscissa shows $\alpha^{z[\text{mm}]}$ in dB at 40 mm. The value for α^z used in this paper is marked as a vertical line in the figure. (Color online)

The SRR is calculated through the envelope of the signal components. The SRR after correction is averaged over all 300 runs and divided by the equally averaged SRR before any correction to give the SRR *increase*. To extract the general trend with depth and make a more readable plot the SRR increase is then subjected to a lowpass filter, $\mathcal{S}$ (Hamming, order 300, cutoff at 10 MHz), and plotted in decibels,

$$\mathrm{SRR} = 20 \cdot \log_{10} \mathcal{S} \left\{ \frac{\left\langle \dfrac{\mathrm{env}\{x_{\mathrm{after}}\}}{\mathrm{env}\{n_{\mathrm{after}}\}} \right\rangle_{\mathrm{runs}}}{\left\langle \dfrac{\mathrm{env}\{x_{\mathrm{before}}\}}{\mathrm{env}\{n_{\mathrm{before}}\}} \right\rangle_{\mathrm{runs}}} \right\}. \tag{B.22}$$

Section B.6.2 shows that there is a different nonlinear attenuation based on the LF polarity. This would indicate a different value for α in the adaptive reverberation delay estimation (Eq. (B.16)). However, to keep the model simple, a single *mean* value of α is used in this paper for both the plus and minus polarity reverberation delay estimation.

To find the α giving best SRR improvement, different values were tested on the case I tissue model, see Fig. B.8. An α corresponding to 2.75 dB loss over 40 mm was found to give the best SRR increase, and is therefore used further in this study. In addition, $\gamma = 3$ (from Eq. (B.16)) was set for all the test cases. A discussion of the value for γ is included in Sec. B.8.4.

In the tissue with linear propagation development, case I (Fig. B.3), the adaptive delay correction, $\tau_{\mathrm{n}p}^{\mathrm{RR}}$ gives an SRR improvement of about 25 dB around focus at 20 mm and is 2.5 dB poorer throughout the image than the best case suppression with a correction delay extracted directly from the reverberation components. The delay correction based on the fixed-relation $\tau_{\mathrm{n}}^{\mathrm{h}}$ is as good as the adaptive in the beginning but declines with depth to a maximum of 2.5 dB difference at 40 mm.

Introducing a piecewise first order NPD development, by keeping the average first order delay gradient between 0 and 40 mm as in case I, while lowering the gradient by 50 % between 15 and 25 mm (leading to an increase of the gradient at other depths), drops the SRR improvement of all three methods between 15 and 25 mm, case II (Fig. B.4). After 25 mm the difference between the adaptive correction and the simple is increased to 5 dB compared to the homogeneous case.

Keeping the same linear first order propagation delay as in case I, but reducing the scatterer strength to 20 % between 15 and 25 mm, case III Fig. B.5), does not significantly alter the difference in SRR increase up to 25 mm. After 25 mm the adaptive and true delay correction shows a small increase not observed for the correction with $\tau_{\mathrm{n}p}^{\mathrm{h}}$.

The effect of multiplying the scatterer strength between 15 and 25 mm by 0.2 and reducing the relative gradient in the same region by 50 % is best described as

Table B.4: SRR improvement at reverberation locations of strong scatterers, case V, with correction based on different estimations of the reverberation delay. First column shows scatterers that contribute to depth z (second column).

z_1,z_3 [mm]	z [mm]	$\tau_{\mathrm{n}}^{\mathrm{y}}$ [dB]	$\tau_{\mathrm{n}}^{\mathrm{h}}$ [dB]	$\tau_{\mathrm{n}}^{\mathrm{RR}}$ [dB]
{7,7}	14	43	41	36
{7,15}	22	37	33	30
{15,15}	30	30	27	26
{7,25}	32	41	38	21

a combination of the effects from case I and case III (case IV, Fig. B.6). There is a collective linear drop of the SRR increase from 15 to 25 mm followed by a rapid increase for the adaptive and true delay corrections and a weaker later improvement for the simple correction. From 30 to about 35 mm there is a separation of about 10 dB between the SRR increase of the adaptive correction compared to the simple correction.

Figure B.7 shows the SRR improvement from case V, where strong scatterers are superimposed on the medium from case IV. The strong scatterers are positioned at 7, 15 and 25 mm giving rise to reverberation noise at 14, 22, 30, and 32 mm (see Table B.4). The SRR improvement is similar to that from case IV (Fig. B.6) save for peaks at the reverberation locations. Peaks are observed for all correction methods at all peak positions except for at 32 mm for the fixed-relation $\tau_{\mathrm{n}p}^{\mathrm{h}}$ correction. A drop in the effectiveness of the adaptive correction is observed around 39 mm, where it equals the simple correction. As the numbers of the SRR improvement at the peaks can be hard to extract from the figure, they are also included in Table B.4.

B.8 Discussion

B.8.1 The general trend

A general trend in all the SRR-increase graphs (Figs. B.3 to B.6) is that the SRR improvement increases with depth up to about 10 mm. This can be explained by examining the components that make up the figure. Consider a medium with scatterers homogeneously distributed with depth (case I). Ignoring attenuation the signal amplitude from first order scattering will then be constant. The reverberation noise will increase linearly with depth as the number of possible combinations increase. The SRR for the unprocessed signal is then inversely proportional to the depth. Introducing a perfect correction removes the reverberations. One can assume a residual noise that is more or less constant with depth. For a sub-optimal correction assume that the residual noise increases with depth as there at higher depths are more components combining with different reverberation delays, thus

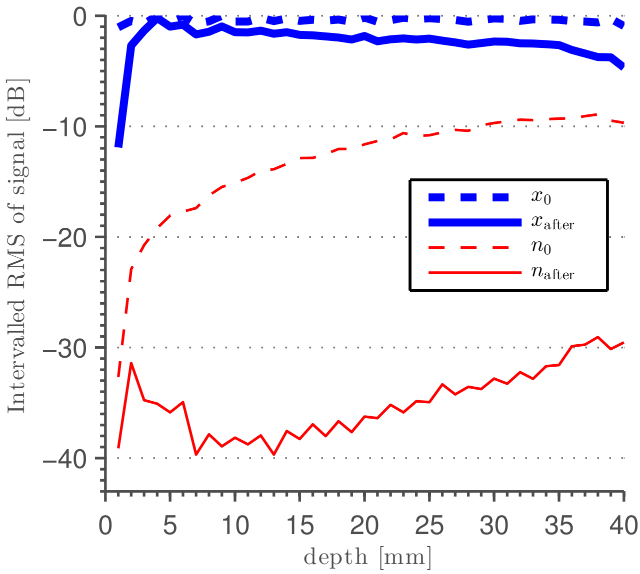

Figure B.9: Mean signal and noise component strengths before and after reverberation correction plotted with depth. The medium consists of Gaussian plane scatterers and a linear propagation delay (case I). (Color online)

making the correction delay more of an average than an accurate estimate. Calculating the SRR *increase* then leads to an increase with depth in the beginning, but as the correction becomes less precise the residual reverberation noise makes the SRR increase curve flatten out. This general trend is observed in the SRR plot for case I (Fig. B.3). In Fig. B.9 the strength of the signal and reverberation noise components are plotted before and after correction for case I. The figure shows that simulations agree with the discussion above.

Figure B.9 also shows that the signal strength of the first order component drops with depth after correction, meaning that the gain factor applied to the total signal is too low (denominator of Eq. (B.13)). A higher gain factor with depth would also further increase the noise level after correction. Regardless of this gain factor, or any Time Gain Compensation (TGC), the SRR plots remains unaffected as any gain is applied to both reverberation and first order components and do not show in the SRR result.

B.8.2 Effect of changes in nonlinearity

Figure B.4 shows that introducing a change in the nonlinearity of the medium in a region, emulated by altering the gradient of the first order NPD, lowers the achieved SRR increase. The SRR increase drops linearly as more and more reverberation components with different mean delays are introduced. With a nonlinear first order delay the total reverberation delay becomes more dependent on the scattering positions that contribute. As there are more and more components in the total signal that have a scattering position dependent delay, it is more difficult to find a suitable single reverberation delay to adequately correct for all the components as the variance in the reverberation delay between all the reverberation components increases. This hypothesis is strengthened by Fig. B.6 where there is a reduction to 20 % of the scatterer strength between 15 to 25 mm, meaning that the new, scattering position dependent, reverberation components have less strength than the other combinations coming from 0 to 15 mm where the delay is linear. This would explain the higher SRR increase in Fig. B.6 compared to Fig. B.4.

B.8.3 Understanding corrections at reverberation peaks

To understand the peak values in case V (Fig. B.7) it is necessary to study what scatterer combinations give rise to the different strong reverberations. Table B.4 shows that scatterers at 7 mm and 15 mm combined gives reverberation at 14, 22 and 30 mm. As the propagation delay is linear up to 15 mm, the propagation delay of these scatterer combinations would be well represented by the simple delay estimate (Eq. (B.10)). However, for the reverberation noise at 32 mm (from scatterers at 7 and 25 mm) the fixed-relation delay correction fails to suppress the noise as well as the adaptive correction. Table B.4 shows a suppression of 18.5 dB for the fixed-relation $\tau_{\mathrm{n}p}^{\mathrm{h}}$ based correction versus 35.5 dB suppression for the one based on the adaptive $\tau_{\mathrm{n}p}^{\mathrm{RR}}$ delay. The key behind this difference lies in the positions of the scatterer that combine to this reverberation noise, namely the scatterers at 7 and 25 mm. These do not have a linear first order delay of the form $\tau_{\mathrm{x}p} \propto z$ crossing through them and $\tau_{\mathrm{n}p}^{\mathrm{h}}$ (Eq. (B.10)) then fails to estimate the resulting reverberation delay. The adaptive delay, $\tau_{\mathrm{n}p}^{\mathrm{RR}}$, takes both the delay and the positions of the scatterers into account and is able to calculate a more accurate delay giving an SRR improvement more close to the best case correction.

B.8.4 Ghost corrections

A pitfall of the adaptive delay is that the scatterer estimate it takes as input, $\hat{R}(z)$, is based on the envelope of the total signal with reverberation noise, $\mathrm{env}\{x_0(t) + n_0(t)\}$. This can explain the failure of the adaptive method in case V (Fig. B.7) at around 38–39 mm where the correction is equal to that based on the $\tau_{\mathrm{n}p}^{\mathrm{h}}$ delay. As the envelope of the total signal also contains the strong reverberation at 14 mm caused by scattering of the 7 mm scatterer twice, a combination of this and the scatterer at 25 mm would yield an estimated strong scatterer at $14 + 25 = 39$ mm. The adaptive method would then calculate a specific correction delay for this depth based on a reverberation combination not actually realized by any scatterers in the true medium. This effect of specific correction based on false, *ghost*, scatterers is called *ghost corrections*.

As increasing γ in Eq. (B.16) increases the specificity of the $\tau_{\mathrm{n}p}^{\mathrm{RR}}$ estimate, increasing this parameter value also increase the effect of ghost corrections. Since increasing γ also increases the specificity towards true strong reverberation noise the result is a tradeoff between high specificity and robustness. By setting $\gamma = 1$ instead of 3, as used in Figs. B.3 to B.7, the correction of case V yields better correction at 39 mm, but poorer correction for the peaks at 14, 22 and 30 mm. At 22 and 30 mm the adaptive correction is poorer than the fixed-relation reverberation delay correction. This indicates that a $\gamma > 1$ is needed despite the higher chance of ghost corrections. The correction at 32 mm stays unaffected by the change in γ. The data showing this effect is for brevity not included in the paper

B.9 Conclusions

An adaptive estimation of the reverberation propagation delay is introduced and evaluated against five special tissue models to study its possible advantage compared to a more straightforward method. The estimation is adaptive in that it depends on the envelope of a received signal. Although it only proved minor improvements in the signal to reverberation noise ratio, SRR, for a simple medium with near uniformly distributed scatterers (Fig. B.3) in the order of 2 to 5 dB, it showed improvements in the order of 15 dB (Table B.4) when evaluated in situations for which it was designed. Namely mediums with a large change in the nonlinearity with depth and strong scatterers with large separation combining to generate reverberation noise. It is in this case that the increased complexity of the algorithm compared to a more simple approach can be justified.

This study has some limitations that might make the reported SRR increases both for the new and older correction methods hard to acquire in the lab on a real system. The system here consists of plane scatterers. The pulses used for generating the rf-signal were simulated in a homogeneous medium so there are no aberration effects. There is no electric noise or movement in the tissue between the transmit pulse complexes. However, these are effects that would affect both the adaptive and fixed-relation correction.

As this is a purely numerical study an obvious extension would be to take the method to the lab for an in vitro study. There are also possible mathematical extensions to the work. The DCS correction utilizes a constant, depth-independent, center frequency even though it is known that the center frequency drops with propagation due to frequency dependent absorption.[21] More extensive simulations could also be used to study the development of the nonlinear attenuation. A possible improvement is also to introduce an iteration scheme for estimation of the scatterers, R, used in the adaptive correction to remove the ghost correction artifacts discussed in Sec. B.8.4.

B.10 Acknowledgments

This work was supported through an "SO-stipend" by the Norwegian University of Science and Technology. The authors would like to thank Johannes Kvam for providing a pulse simulation framework and Ola Finneng Myhre for proof-reading and contributing in scientific discussions.

Bibliography

[1] K. Caidahl, E. Kazzam, J. Lidberg, G. Neumann-Andersen, J. Nordanstig, S. Rantapaa Dahlqvist, A. Waldenstrom, and R. Wikh, "New concept in echocardiography: harmonic imaging of tissue without use of contrast agent," Lancet **352**, 1264–1270 (1998).

[2] K. Spencer, J. Bednarz, P. Rafter, C. Korcarz, and R. Lang, "Use of Harmonic Imaging Without Echocardoigraphic Contrast to Improve Two-Dimensional Image Quality," Am. J. Cardiol. **82**, 794–799 (1998).

[3] E. Quaia, "Microbubble ultrasound contrast agents: an update," Eur. Radiol. **17**, 1995–2008 (2007).

[4] R. Hansen and B. A. J. Angelsen, "SURF imaging for contrast agent detection," IEEE Trans. Ultrason., Ferroelect., Freq. Control **56**, 280–290 (2009).

[5] R. Hansen and B. A. J. Angelsen, "Contrast Imaging by Non-Overlapping Dual Frequency Band Transmit Pulse Complexes," IEEE Trans. Ultrason., Ferroelect., Freq. Control **58**, 290 (2011).

[6] D. Simpson, C. T. Chin, and P. Burns, "Pulse inversion Doppler: a new method for detecting nonlinear echoes from microbubble contrast agents," IEEE Trans. Ultrason., Ferroelect., Freq. Control **46**, 372–382 (1999).

[7] P. N. Burns, S. R. Wilson, and D. H. Simpson, "Pulse inversion imaging of liver blood flow: improved method for characterizing focal masses with microbubble contrast," Invest. Radiol. **35**, 58–71 (2000).

[8] G. Brock-Fisher, M. Poland, and P. Rafter, "Means for increasing sensitivity in non-linear ultrasound imaging systems", U. S. Patent No: US5577505 A, (1996).

[9] V. Mor-Avi, E. G. Caiani, K. A. Collins, C. E. Korcarz, J. E. Bednarz, and R. M. Lang, "Combined Assessment of Myocardial Perfusion and Regional Left Ventricular Function by Analysis of Contrast-Enhanced Power Modulation Images," Circulation **104**, 352–357 (2001).

[10] R. Hansen, S.-E. Måsøy, T. F. Johansen, and B. A. J. Angelsen, "Utilizing dual frequency band transmit pulse complexes in medical ultrasound imaging," J. Acoust. Soc. Am. **127**, 579–587 (2010).

[11] R. Hansen, S.-E. Måsøy, T. A. Tangen, and B. A. J. Angelsen, "Nonlinear propagation delay and pulse distortion resulting from dual frequency band transmit pulse complexes," J. Acoust. Soc. Am. **129**, 1117–1127 (2011).

[12] S.-E. Måsøy, Ø. Standal, S. P. Näsholm, T. F. Johansen, B. Angelsen, and R. Hansen, "SURF Imaging: In Vivo Demonstration of an Ultrasound Contrast Agent Detection Technique," IEEE Trans. Ultrason., Ferroelect., Freq. Control **55**, 1112–1121 (2008).

[13] J. M. Rau, "Dual frequency band ultrasound for suppression of multiple scattering," (Ph.D. dissertation, Norwegian University of Science and Technology, Trondheim, Norway, 2013).

[14] J. M. Rau, S.-E. Måsøy, R. Hansen, B. Angelsen, and T. A. Tangen, "Methods for reverberation suppression utilizing dual frequency band imaging," J. Acoust. Soc. Am. **134**, 2313–2325 (2013).

[15] H. Høilund-Kaupang, "Models and Methods for Investigation of Reverberations in Nonlinear Ultrasound Imaging," (Ph.D. dissertation, Norwegian University of Science and Technology, Trondheim, Norway 2011).

[16] B. A. J. Angelsen, "Ultrasound imaging : waves, signals, and signal processing", vol. I (Emantec, Trondheim, Norway, 2000), pp. 1.10–1.11.

[17] Ø. Standal, B. A. J. Angelsen, and T. A. Tangen, "A phase based approach for estimation and tracking of locally variable delays", IEEE Ultrason. Symp., 1583–1585 (2007).

[18] This range was determined after visual inspection of the Fourier spectrum.

[19] F. A. Duck, "Physical Properties of Tissue" (Academic Press Inc, San Diego, CA, USA, 1990), p. 98.

[20] Values calculated from parameters found in the reference book by Duck[19]. Parameters are from a combination of studies. Temperatures and other properties of the tissue might not correspond between studies from which parameters to calculate the values was used.

[21] T. Szabo, "Diagnostic Ultrasound Imaging: Inside Out (Biomedical Engineering)" (Academic Press Inc, San Diego, CA, USA, 2004).

Part III

Complete index

List of Tables

List of Figures

Errata

Paper B

Corrections not present in included paper.
Section: B.3, **Page:** 113, **Comment:** Typo in equation.
Before:

$$\begin{aligned} &Y_{i+}(\omega)\mathrm{e}^{-i\omega\tau_{\mathrm{n}i+}} - Y_{i-}(\omega)\mathrm{e}^{i\omega\tau_{\mathrm{n}i-}} \\ &= X_{i0}(\omega)\left(\mathrm{e}^{i\omega(\tau_{\mathrm{x}i+}-\tau_{\mathrm{n}i+})} - \mathrm{e}^{i\omega(\tau_{\mathrm{x}i-}-\tau_{\mathrm{n}i-})}\right). \end{aligned}$$

Changed to:

$$\begin{aligned} &Y_{i+}(\omega)\mathrm{e}^{i\omega\tau_{\mathrm{n}i+}} - Y_{i-}(\omega)\mathrm{e}^{i\omega\tau_{\mathrm{n}i-}} \\ &= X_{i0}(\omega)\left(\mathrm{e}^{i\omega(\tau_{\mathrm{x}i+}-\tau_{\mathrm{n}i+})} - \mathrm{e}^{i\omega(\tau_{\mathrm{x}i-}-\tau_{\mathrm{n}i-})}\right). \end{aligned}$$

Section: Table B.4, **Page:** 128, **Comment:** Switched table headings. (Last two.)
Before:

z_1,z_3 [mm]	z [mm]	$\tau_\mathrm{n}^\mathrm{y}$ [dB]	$\tau_\mathrm{n}^\mathrm{h}$ [dB]	$\tau_\mathrm{n}^\mathrm{RR}$ [dB]
{7,7}	14	43	41	36
{7,15}	22	37	33	30
{15,15}	30	30	27	26
{7,25}	32	41	38	21

Changed to:

z_1,z_3 [mm]	z [mm]	$\tau_\mathrm{n}^\mathrm{y}$ [dB]	$\tau_\mathrm{n}^\mathrm{RR}$ [dB]	$\tau_\mathrm{n}^\mathrm{h}$ [dB]
{7,7}	14	43	41	36
{7,15}	22	37	33	30
{15,15}	30	30	27	26
{7,25}	32	41	38	21

Section: B.8.3, **Page:** 130, **Comment:** Updated figures from on old table.
Before:

Table B.4 shows a suppression of **18.5 dB** for the fixed-relation $\tau_{\mathrm{n}p}^{\mathrm{h}}$ based correction versus **35.5 dB** suppression for the one based on the adaptive $\tau_{\mathrm{n}p}^{\mathrm{RR}}$ delay.

Changed to:

Table B.4 shows a suppression of **21 dB** for the fixed-relation $\tau_{\mathrm{n}p}^{\mathrm{h}}$ based correction versus **38 dB** suppression for the one based on the adaptive $\tau_{\mathrm{n}p}^{\mathrm{RR}}$ delay.